UNIVERSITY OF BIRMINGHAM

CHARACTERZATION OF BRAIN TISSUE: DYNAMIC MECHANICAL TESTING AND VISCOELASTIC MODELLING

by

WEIQI LI

A thesis submitted to the

University of Birmingham for the degree of

DOCTOR OF PHILOSOPHY

School of Engineering

Department of Mechanical Engineering

University of Birmingham

March 2022

Abstract

Brain tissue is vulnerable and sensitive, predisposed to potential damage under various conditions of mechanical loading. The studies in this thesis aimed to investigate the viscoelastic properties of brain tissue under various loading conditions and develop viscoelastic models to capture the tissue behaviour.

The mechanical properties of brain tissue were quantified using dynamic mechanical analysis (DMA) where a sinusoidally varying displacement was applied to specimens and the viscoelastic properties were obtained under different testing protocols. The regional and directional properties of brain tissue were quantitatively measured at physiological and injurious loading conditions. The compressive properties of brain tissue were studied under time and frequency domains with the same physical conditions. The theory of viscoelasticity was applied to estimate the prediction of viscoelastic response through Finite Element models. Further, the effect of large strain to mechanical behaviour of brain tissue was investigated.

This thesis found brain tissue to have showed frequency dependent-viscoelastic properties. The compressive dynamic properties of brain tissue were heterogenous for regions and affected by indenter size and indentation depth. The results demonstrate the feasibility of deriving time-domain viscoelastic parameters from frequency-dependent compressive data for biological tissue. Applications of the brain viscoelastic properties presented in this thesis include the diagnosis of brain injury and fabrication of biomaterials to replicate brain tissue.

Acknowledgments

To my supervisors Professor Duncan Shepherd and Dr Daniel Espino for their supervision and providing me the opportunity to achieve the outcome presented in this thesis. Without their patience and support, the work would not have been possible.

To the mechanical engineering technical staff at University of Birmingham, Mr Lee Gauntlett and Mr Peter Thornton, for assistance in manufacturing of fixtures required for the experimental work in this thesis.

To the Biomedical Engineering Research Group of the Mechanical Engineering department at the University of Birmingham, for the exciting experience and support.

To Mom and Dad, thank you for your unconditional love and support in everything I have done throughout my doctorate.

To my wife, Huanyu Zhou, thank you for your love and constant presence.

Academic Output

Peer-reviewed publications

Weiqi Li, Duncan E.T. Shepherd, Daniel M. Espino, Frequency dependent viscoelastic properties of porcine brain tissue, Journal of the Mechanical Behavior of Biomedical Materials, Volume 102, 2020, 103460, ISSN 1751-6161.

Weiqi Li, Duncan E.T. Shepherd, Daniel M. Espino, Dynamic mechanical characterization and viscoelastic modeling of bovine brain tissue, Journal of the Mechanical Behavior of Biomedical Materials, Volume 114, 2021, 104204, ISSN 1751-6161.

Weiqi Li, Duncan E.T. Shepherd, Daniel M. Espino, Investigation of the compressive viscoelastic properties of brain tissue under time and frequency dependent loading conditions, Annals of Biomedical Engineering, 2021, DOI 10.1007/s10439-021-02866-0.

International Conference Presentations

Weiqi Li, Duncan E.T. Shepherd, Daniel M. Espino, 2019, Frequency dependent viscoelastic properties of porcine brain tissue, 25^{th} Congress of the European Society of Biomechanics, Vienna, Austria

Table of Contents

List of Figures

List of Tables

Acronyms

TBI ..... Traumatic Brain Injury

mTBI ..... Mild Traumatic Brain Injury

CSF ..... Cerebrospinal Fluid

DAI ..... Diffuse Axonal Injury

SBS ..... Shaken Baby Syndrome

CT ..... Computed Tomography

MRI ..... Magnetic Resonance Imaging

FE ..... Finite Element

DMA ..... Dynamic Mechanical Analysis

LVR ..... Linear Viscoelastic Region

QLV ..... Quasi-Linear Viscoelasticity

FFT ..... Fast Fourier Transform

MD ..... Mean Displacement

ANOVA ..... Analysis of Variance

1 Introduction

The brain is considered to be one of the most complex organs in the body and is responsible for a series of physical and mental tasks. Although the brain is well protected by the skull, it is still sensitive and vulnerable under potentially injurious loading conditions. Due to various external forces, traumatic brain injury (TBI) is a major cause of death and disability affecting millions of people (Taylor et al. 2017). According to the Centres for Disease Control, 2.53 million TBI-related emergency department visits were documented in 2014 and the TBI-related emergency department visits and deaths have increased steadily from 2006 to 2014 (Capizzi et al. 2020). Treatment modalities of brain injuries are categorized based on the severity of the injury ranging from mild to severe traumatic brain injury (Galgano et al. 2017). The focus of this thesis is on mild traumatic brain injuries which could be induced when oscillatory force is around 20 Hz (Laksari et al. 2015). In the subsequent chapters, the tested frequency range for dynamic mechanical experiments was up to 35 Hz to which the brain might be exposed during physiological and injury conditions (Rashid et al. 2013).

The aim of this thesis was to characterize the mechanical properties of brain tissue and develop viscoelastic models. The systematic characterization of brain tissue would provide essential information to the analysis of brain injuries in clinical treatments and lead to the development of computational simulations of head which can predict brain disease progression and develop smart protection systems. The specific objectives were to:

- Acquire the dynamic mechanical properties of brain tissue;

- Evaluate the effect of heterogeneous microstructure on mechanical properties of brain tissue and within the context of constitutive models;

- Investigate the time and frequency domain mechanical characterization of brain tissue.

The mechanical properties of brain tissue play an important role when head injuries are analysed. To obtain the mechanical properties of brain tissue, this thesis investigates animal brains extensively under various loading conditions. Characterization and quantification of these mechanical properties can be applied to models of brain disease via computational simulations. The effect of microstructural heterogeneity of brain tissue was identified for accurate prediction of injury across the brain structure. The measurements can provide a standard for clinical-grade biomaterials suitable for use in regenerative medicine (Bartlett et al. 2020). In addition, these mechanical properties can be used to determine a surrogate brain material for assessing the feasibility of head protection system (Zhang et al. 2019). The investigation of mechanical response under different loading environments (e.g. time and frequency domains) can contribute to a better understanding of the phenomenology of brain tissue and its constitutive modelling.

Chapter 2 presents the background information pertinent to this thesis. It includes an introduction to the brain system. Modelling and mechanical testing of brain tissue are discussed

under various testing conditions. Furthermore, the mechanics of these materials are analysed including viscoelastic and hyperelastic properties.

Chapter 3 describes a study on the general viscoelastic properties of porcine brain tissue. The variation of dynamic stiffness was assessed by comparing different indenter sizes and indentation depths. The viscoelastic moduli were also analysed over a range of loading frequencies. The chapter is based on the work published in the *Journal of the Mechanical Behaviour of Biomedical Materials* entitled 'Frequency dependent viscoelastic properties of porcine brain tissue'; 2020, volume 102, pages 103460. This work was also presented at the 25^{th} Congress of the European Society of Biomechanics, Vienna, Austria, 2019.

Chapter 4 details the analysis on the compressive frequency-dependent mechanical characterization of bovine brain tissue and identifies its viscoelastic modelling. In this chapter, the white and grey matter were investigated to determine the regional and directional properties of brain tissue. A frequency-dependent constitutive model was applied in the numeric simulation to capture the mechanical behaviour of brains. The work in this chapter is based on the work published in the *Journal of the Mechanical Behaviour of Biomedical Materials* entitled 'Dynamic mechanical characterization and viscoelastic modeling of bovine brain tissue'; 2021, volume 114, pages 104204.

Chapter 5 studies the viscoelastic properties of brain tissue under time and frequency dependent loading conditions. This chapter compares the frequency and time domain mechanical

characterization of brain tissue by converting its dynamic properties to enable mathematical modelling in the time domain. Further, the hyperelastic material model was used to investigate the large strain behaviour of brain tissue. The work in this chapter is based on the work published in the *Annals of Biomedical Engineering* entitled 'Investigation of the Compressive Viscoelastic Properties of Brain Tissue Under Time and Frequency Dependent Loading Conditions'; 2021, Volume 49, Pages 3737-3747.

Chapter 6 outlines the overall discussion, including the future work the findings presented in thesis could be applied to, and the final conclusions.

2 Background

2.1 Chapter Overview

This chapter provides the background information required to understand subsequent chapters in this thesis. To begin, a background is provided on skull and brain tissue in section 2.2. The discussion of the mechanics of materials applied in analysis of experimental results and simulations is outlined in section 2.3. Following this, literature on modelling and mechanical testing of brain tissue is critically analysed in section 2.4 under various testing conditions. Finally, section 2.5 summarizes the background chapter.

2.2 Skull and Brain System

2.2.1 The Skull

The skull is a cortical grain structure which forms the head in vertebrates (Dempster 1967) and is comprised of two parts, the cranium and the mandible. The skull supports the structure of the face and provides a protective cavity for the brain tissue from injuries during externally applied mechanical forces, such as blast and impact. The skull bones are generally made up of the frontal bone, forming the forehead; two parietal bones, which are the biggest part of the skull distributed on either side; the occipital bone, the base of the skull; and the two temporal bones (Figure 2.1). Sutures are rigid joints between the bones of the skull and suture lines are the most distinguishing mark on the skull bones. These fibrous joints as synarthroses provide the

compliance and elasticity of the skull. The growth pattern of the skull is affected by the sutures, which gradually harden during early childhood.

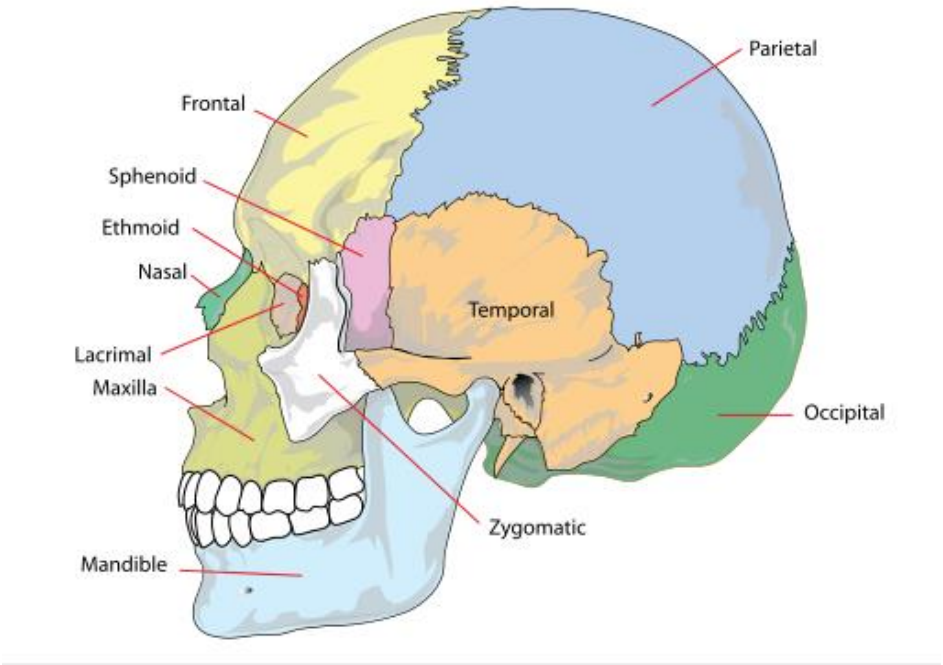

Figure 2.1– Skull structure scheme. Image by Edoarado - Own work based on: Human skull side simplified (bones), freely available in the public domain (LadyofHats 2007).

2.2.2 Anatomy of Cranial Bone

Cranial bones have various structural properties that change with age. Fetal cranial bone is a thin cortical bone layer and highly sensitive to gestational age and cranial bone fibre orientation (McPherson and Kriewall 1980). Mature cranial bone differentiates into a composite structure made up of a three-layer sandwich sphere with compact cortical bones and inner cancellous bone (diploe) (Figure 2.2). The cranial bones are considered as transversely isotropic (McElhaney et al. 1970) and the mechanical response of the skull is strongly affected by the

structural arrangement of the diploe (Endo 1966). The morphological variation of cranial bones was found to be large (Law 1993) and this is considered as the most significant factor to cause discrepancies in the mechanical properties. Sutures are surrounded and reinforced by compact bone, and the area with thicker diploe is away from sutures. The outer compact bones have a dense structure with less than 30% porosity, while diploe is highly porous (Alexander et al. 2020).

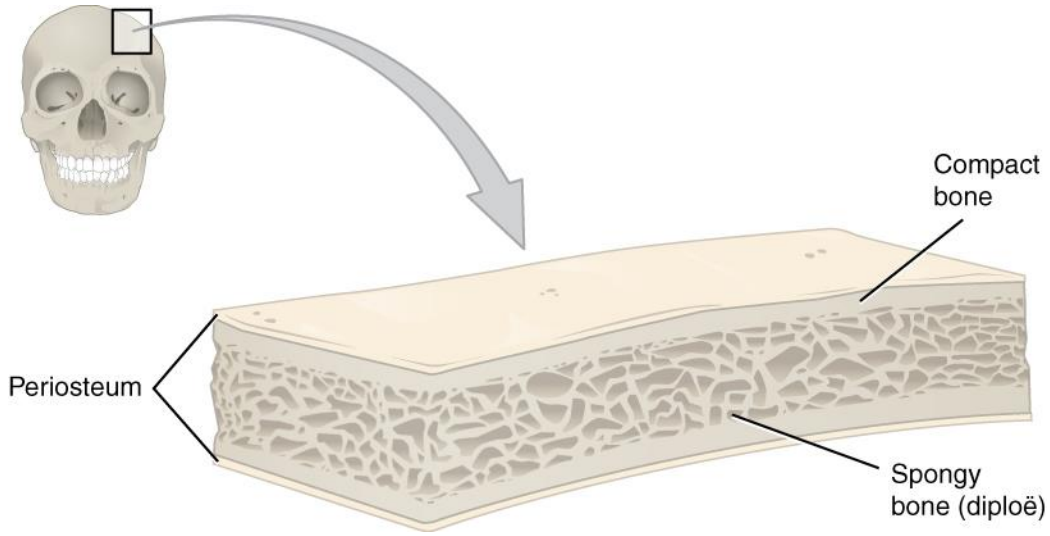

Figure 2.2 – Anatomy of human cranial bone from skull. Image by OpenStax College, available under Creative Commons Attribution 3.0. (Anatomy & Physiology 2013).

2.2.3 Brain Tissue

The brain is considered as one of the most vulnerable organs in the body; it is immersed in cerebrospinal fluid (CSF) and surrounded by the skull. The brain consists of the cerebrum, the brainstem and the cerebellum. The cerebrum, the biggest part of brain tissue, has two hemispheres (left and right connected by corpus callosum white matter tissue) and each hemisphere is conventionally subdivided into four main lobes including frontal, temporal, parietal and occipital lobes (Figure 2.3). Brain tissue can be divided into grey and white matter. The grey matter consisting of cortex and the basal ganglia is made of neurons with the function of data processing, and the white matter consisting of corona radiate and corpus callosum is made of myelinated nerve axons (Prange et al. 2000). The brain is wrapped by three membranes of the dura mater, arachnoid mater and the pia mater, which protect the nervous system (Figure 2.4). CSF circulates around the space between the arachnoid mater and the pia mater.

The effect of microstructural heterogeneity of brain tissue has recently received attention (Budday et al. 2015; Pervin and Chen 2009) and it is necessary to investigate the connection between the macroscopic mechanical behaviour and the regional microstructure for accurate prediction of injury across the brain structure. Brain tissue can be divided into grey and white matter and is covered with the thin layer of pia and arachnoid membranes. The grey matter is made of neurons with the function of data processing distributed around the surface of the cortex, and the white matter consists of myelinated nerve axons which can be highly oriented

and connect various grey matter areas. Previous studies showed grey matter seems to be less stiff than white matter through indentation tests (Budday et al. 2015; Feng et al. 2013). Recently, a study showed there is regionally microstructural variation even within the grey and white matter tissue (Budday et al. 2017). Brain tissue was further differentiated into locations of corpus callosum, corona radiata, cortex and basal ganglia (Prange and Margulies 2002). Corona radiata and corpus callosum are considered as white matter, while the latter has more oriented nerve fibres connecting the two hemispheres. Cortex and basal ganglia are considered as grey matter. The investigation of regionally mechanical properties in brain tissue would be helpful for clinic analysis as the degree of injury may vary with regions. In addition to the regional heterogeneity, white matter structure has been found to be transversely isotropic because of the highly aligned axonal fibres, while grey matter is simply isotropic (Arbogast and Margulies 1999; Feng et al. 2017). Therefore, the mechanical response of white matter is potentially affected by the fibre direction (Ning et al. 2006).

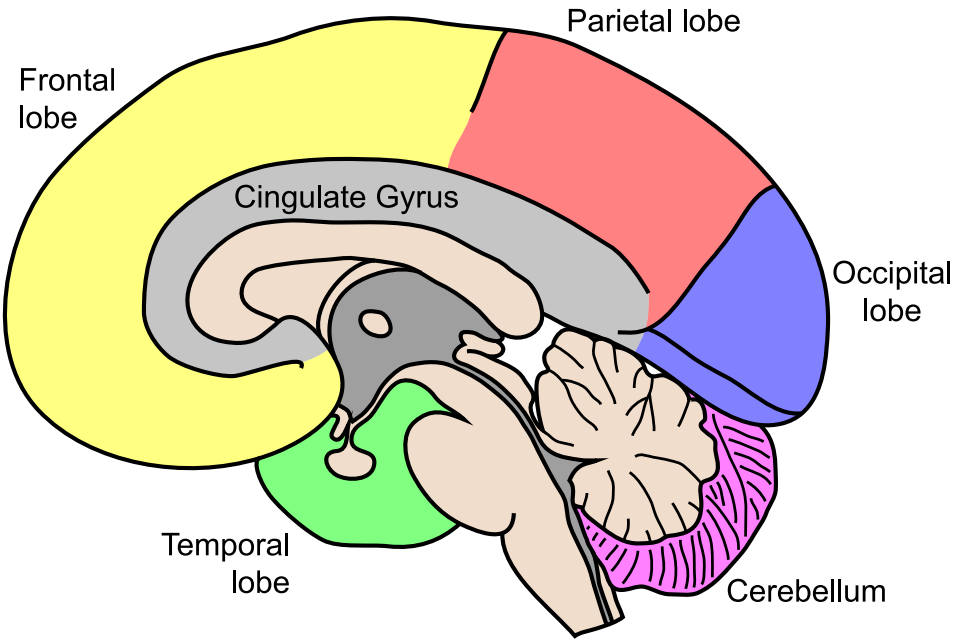

Figure 2.3 – Brain anatomy in sagittal plane. Image by Own work, available under Creative Commons Attribution 3.0. (NEUROtiker 2007).

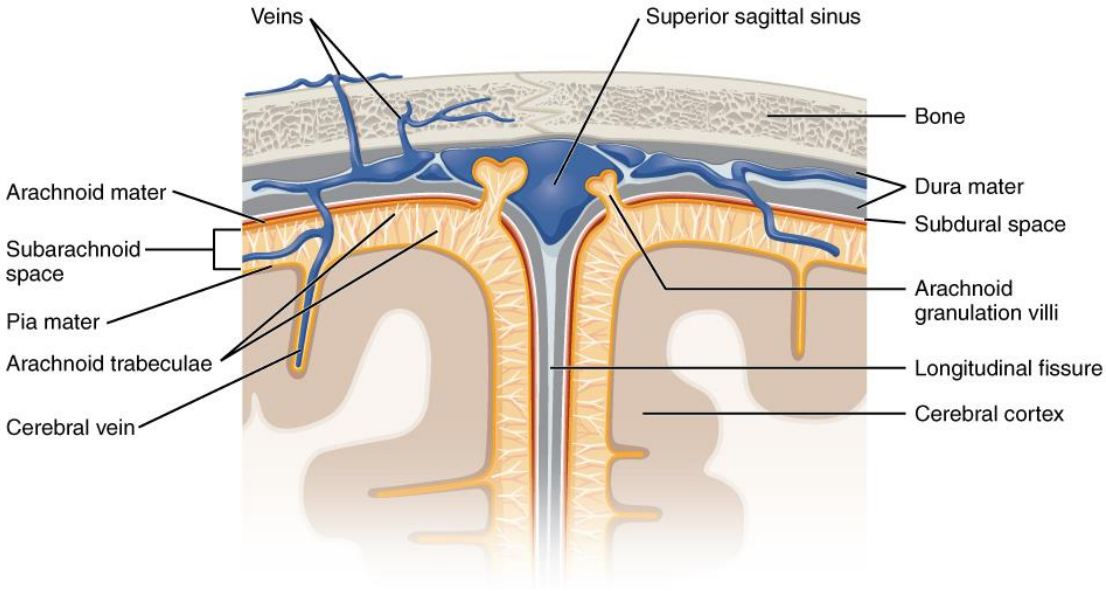

Figure 2.4 – Illustration of meninges and brain-skull interface. Image by OpenStax College, available under Creative Commons Attribution 4.0. (Anatomy & Physiology 2016).

2.2.4 Traumatic Brain Injury

Although the brain is well protected by the skull, brain tissue is still easily injured when experiencing various loading conditions. Traumatic brain injury (TBI) is a major cause of death and disability induced by external dynamic forces (Taylor et al. 2017) and is a critical public health problem worldwide (Hyder et al. 2007). The primary causes of brain injury include violence, sports, vehicle crashes and construction where brain trauma occurs as a consequence of a sudden acceleration or deceleration within the cranium (Kushner 1998). In the United States, approximately 1.5 million traumatic brain injuries occur per year (Bruns Jr and Hauser 2003) and traumatic brain injury is among the most severe type of injury in terms of long-term implications for survivors and case fatality (Rodriguez et al. 2006). The direction and type of forces may contribute to brain injuries including angular, shear and translational forces. In addition, the sudden acceleration or deceleration, blast waves and penetrating impact can cause brain injuries. Although TBI pathology and neuronal function have been the focus of many studies, many injury conditions are still unclear.

The severity of traumatic brain injury can be classified into mild, moderate and severe categories. Concussion known as mild traumatic brain injury (mTBI) is one of the most common types of TBI which occurs at least 10 times more frequently than moderate and severe conditions (Nguyen et al. 2016). Primary injuries of concussion can be caused either at the place of impact or on the side opposite the impact region, which is thought as the coup-contrecoup

phenomenon (Meaney and Smith 2011). The exact mechanism of the coup-contrecoup injury in concussion is controversial. Generally, it is thought that the impact of inertia is important in brain injuries where the brain keeps moving with the skull stopped by external loading (Shaw 2002). In addition, the increased intracranial pressure wave may play a role in the injury (Mckee and Daneshvar 2015). It also can be affected by many other factors including the skull, cerebrospinal fluid, and the membranes between the brain and skull.

When the brain rapidly moves within the skull inducing traumatic shearing force, white matter with partial grey matter appears to be damaged and deformed during the traumatic forces, leading to diffuse axonal injury (DAI) (Smith and Meaney 2000). DAI pathology reveals the mechanical damage of the axon which is slowly disconnected in white matter (Johnson et al. 2013). The severity of DAI covers from mild to severe and its dynamic impact on infants can cause shaken baby syndrome (SBS) as diffuse injury (Elinder et al. 2018). Lesions in DAI patients can be found through computed tomography (CT) or magnetic resonance imaging (MRI) scans (Figure 2.5).

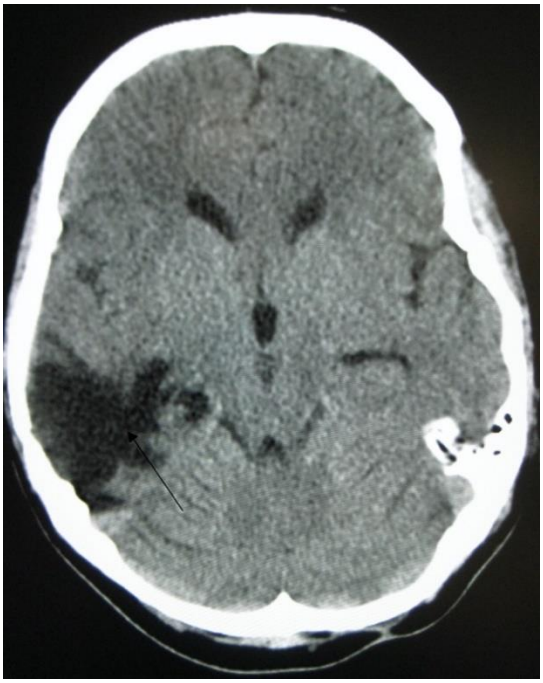

Figure 2.5 – A CT scan showing traumatic brain injury with a black arrow indicating the injurious location. Image by Own work, available under Creative Commons Attribution 3.0. (James Heilman 2010)

2.3 Mechanics of Materials

2.3.1 Introduction

Constitutive models are of importance for the FE modelling of brain tissue. The underlying mechanical relationships can provide essential information for understanding the tissue behaviour. The mechanical properties of brain tissue can be obtained from experimental tests, which also depends on the loading conditions. In the following section viscoelastic properties are described. The mechanical properties of brain tissue throughout this thesis are used to quantify tissues and combined with constitutive laws in numerical simulations.

2.3.2 Stress and Strain

When evaluating the mechanical properties of a material, a uniaxial mechanical test is common to be performed where a force versus displacement curve is measured. However, in order to be independent of sample size, the results are preferably shown as stress versus strain. In structural mechanics, there are various definitions of stress and strain which have different applications in FE analysis. The term stress (σ) is used to measure the force applied to a certain cross-sectional area of an object (Equation 2.1). Strain (ε) is the deformation or displacement change over the original length resulting from an applied stress (Equation 2.2). Stiffness (k) which measures the resistance of a structure in response to an applied force can be calculated from Equation 2.3 and is influenced by material geometry.

$$\sigma = \frac{F}{A_0} \qquad \text{Equation 2.1}$$

$$\varepsilon = \frac{L - L_0}{L_0} \qquad \text{Equation 2.2}$$

$$k = \frac{F}{L - L_0} \qquad \text{Equation 2.3}$$

where F is the applied force, A_0 is the original cross-sectional area, L is the length after load is applied and L_0 is the original length, which are shown in Figure 2.6.

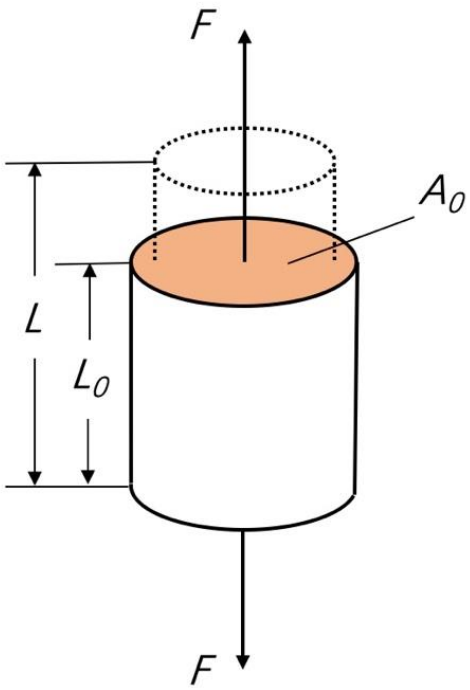

Figure 2.6 – Cylinder specimen subjected to a tensile force (F) with original cross sectional area (A_0), original length (L_0) and length after an applied force (L).

The discussion above focused on engineering stress and strain, which are commonly used because it is easier to generate experimental data and the mechanical properties obtained are adequate for most engineering calculations. For compression testing, the compressive force results in shortening instead of elongation with the different direction of stress and strain. The confined compression test was first chosen in chapter 3 because the general mechanical behaviour of brain tissue was investigated in macroscope where the brain is considered as the soft tissue constrained by the skull. The confined testing is thus the nature of the boundary conditions at skull/brain interface. For the subsequent chapters, the focus of the work was microstructural heterogeneity of brain tissue, and the unconfined compression testing was

applied to investigate regional and directional mechanical properties, which is consistent to previous studies (Budday et al. 2017; Li et al. 2019). Other fundamental measurements are true stress and strain, which are defined by studying the force acting on an infinitesimal area element in deformed body, accounting for changes in cross-sectional area. The correlation between engineering stress-strain curve and true stress-strain curve was investigated (Faridmehr et al. 2014) and at small deformations, the true stress and strain are basically indistinguishable from the engineering stress and strain. Figure 2.7 shows a typical stress-strain curve.

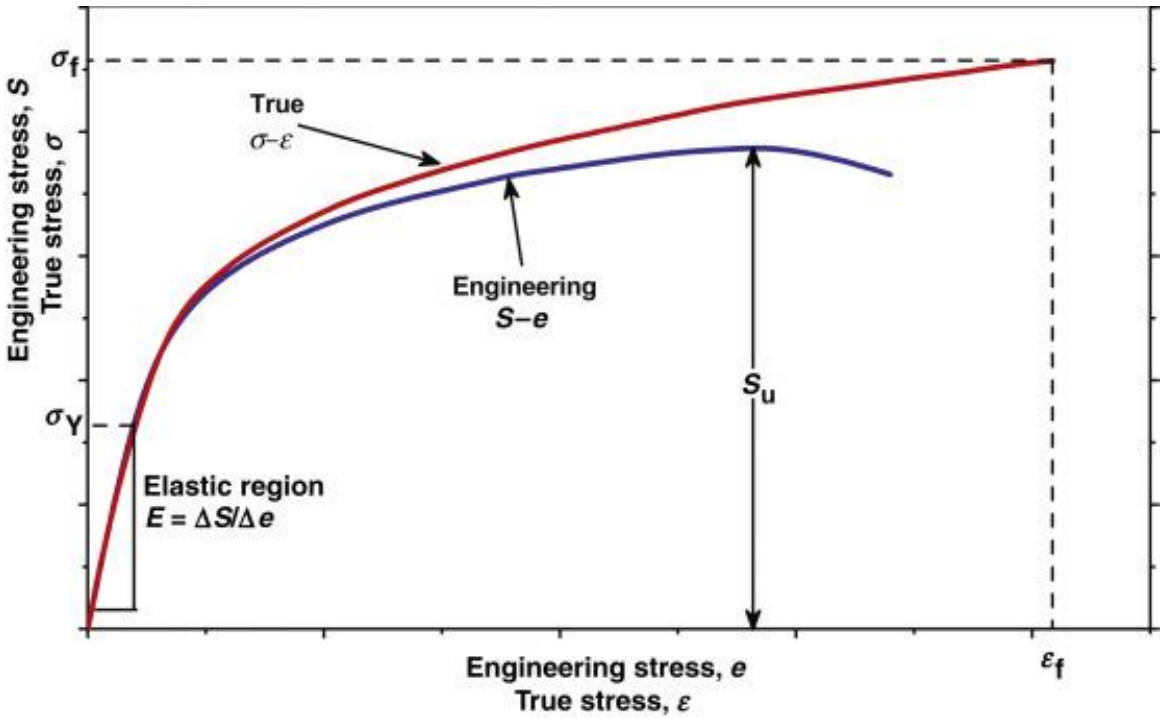

Figure 2.7 – Typical stress-strain curve (adapted from Laurence W. McKeen (McKeen 2016)). At the small deformation, the engineering and true stress-strain curves are overlapped showing linear elastic behaviour. Yield stress σ_Y is the end point of the linear elastic region. S_u is the ultimate tensile strength and σ_f, ε_f denote true fracture stress and strain, respectively.

2.3.3 Elasticity

In engineering, the elasticity of a material is quantified by elastic modulus such as Young' modulus measuring an object's resistance to being deformed elastically when subject to a stress. Hooke's law describes perfect elasticity where the force is directly proportional to the distance of deformation at any displacement. However, most materials are only purely elastic only up to small deformation, which is regarded as linear elasticity. From Figure 2.7, the slope of the straight line denoting the elastic region is the Young' modulus (E) which is a mechanical property measuring the stiffness of a material and can be determined using Equation 2.4.

$$E = \frac{\sigma}{\varepsilon} \qquad \text{Equation 2.4}$$

From Figure 2.6, the deformation of the cylindrical specimen has contracted in directions perpendicular to the loading direction. The negative ratio of transverse strain (ε_t) to axial strain (ε) is known as Poisson's ratio:

$$\nu = -\frac{\varepsilon_t}{\varepsilon} \qquad \text{Equation 2.5}$$

The allowable range of Poisson's ratio is between -1 and 0.5, where positive values indicate that the material shrinks in the transverse direction when the specimen is pulled. For soft materials, such as biological tissue, this value is near 0.5 and for many metals and alloys, this value is near 0.3 (Liu et al. 2006).

In the vast majority of simulations of linear elastic materials, an isotropic material model was selected which does not have directional sensitivity. To describe such a material, Young's modulus (E), shear modulus (G) and Poisson' ratio (ν) are the most commonly used parameters in tables of material data and the shear modulus can be calculated as:

$$G = \frac{E}{2(1+\nu)} \qquad \text{Equation 2.6}$$

2.3.4 Hyperelasticity

For materials such as rubber whose stress-strain curve is non-linear, hyperelastic material models have been widely used to describe this behaviour. There are constitutive models characterized by a strain-energy density function where a hypothesis is applied that the stress in a material can be obtained by taking the derivative of strain energy with respect to strain (Muhr 2005). Generally, hyperelastic material models are applied to represent the large deformation behaviour of materials in FE simulations and biological tissue is assumed to be incompressible. Compared with a linearly elastic model where materials are mainly described by two material constants such as Young's modulus and Poisson's ratio, the strain-energy density (W) is used to derive nonlinear constitutive models, which is a function of principle strain invariants (Ogden 1997). The strain invariants are shown as follows:

$$W = W(I_1, I_2, I_3)$$ Equation 2.7

$$I_1 = \lambda_1^2 + \lambda_2^2 + \lambda_3^2$$ Equation 2.8

$$I_2 = \lambda_1^2\lambda_2^2 + \lambda_2^2\lambda_3^2 + \lambda_3^2\lambda_1^2$$ Equation 2.9

$$I_3 = \lambda_1^2\lambda_2^2\lambda_3^2$$ Equation 2.10

where λ_1, λ_2, λ_3 are the principle stretches or principle extension ratios, linked by the relationship $\lambda_1\lambda_2\lambda_3 = 1$, due to incompressibility. During uniaxial mechanical testing, the specimens are assumed to be deformed homogenously. For this deformation state, the principle stretch ratios in the directions orthogonal to the loading axis will be identical. Thus, due to symmetry and incompressibility, the stretch ratios are now of the form:

$$\lambda_1 = \lambda, \qquad \lambda_2 = \lambda_3 = \lambda^{-1}$$ Equation 2.11

where $\lambda < 1$ is in compression. The first and second strain invariants then become:

$$I_1 = \lambda^2 + 2\lambda^{-1}, \qquad I_2 = \lambda^{-2} + 2\lambda$$ Equation 2.12

The strain-energy density (W) is a function of the stretch ratio only. In uniaxial compression, the stretch ($\lambda = \frac{L}{L_0} = 1 + \frac{L-L_0}{L_0} = 1 + \varepsilon$) can be calculated by the deformed length of the specimen (L) divided by the initial length (L_0). The stress component along the direction of loading S_{11} has been mentioned in section 2.4.2 as the ratio of the measured force and the cross-

sectional area in the undeformed state. The measured nominal stress is used to compare the predictions of the hyperelastic models (Ogden 1997).

$$S_{11} = \frac{d\widehat{w}}{d\lambda}, \qquad \widehat{w}(\lambda) = W(I_1, I_2) \qquad \text{Equation 2.13}$$

Different hyperelastic material models are constructed by specifying different elastic strain energy expressions. Below are some common models used to describe biological tissue.

The total strain energy density for a Neo-Hookean material model (W^{NH}) and the nominal stress (S_{11}^{NH}) are given by:

$$W^{NH} = \frac{\mu_0}{2}(I_1 - 3) \qquad \text{Equation 2.14}$$

$$S_{11}^{NH} = \mu_0(\lambda - \lambda^{-2}) \qquad \text{Equation 2.15}$$

where μ_0 is a material parameter which can be obtained by curve fitting.

The form of the strain-energy potential for the Gent model (W^{GNT}) depends on the first strain invariant only (Gent 1996). It yields the corresponding nominal stress (S_{11}^{GNT}) as follow:

$$W^{GNT} = -\frac{\mu_0}{2} J_m \ln\left(1 - \frac{I_1 - 3}{J_m}\right) \qquad \text{Equation 2.16}$$

$$S_{11}^{GNT} = \frac{\mu_0 J_m}{J_m - \lambda^2 - 2\lambda^{-1} + 3}(\lambda - \lambda^{-2}) \qquad \text{Equation 2.17}$$

where μ_0 and J_m are the material constants which can be optimized with experimental data.

The Ogden model has been widely used in literature to describe the nonlinear mechanical behaviour of brain tissue at large deformation (Budday et al. 2017; Forte et al. 2017). The Ogden strain energy density (W^{Ogd}) and corresponding nominal stress (S_{11}^{Ogd}) are defined as:

$$W^{Ogd} = \frac{2\mu_0}{\alpha^2}(\lambda_1^\alpha + \lambda_2^\alpha + \lambda_3^\alpha - 3) \qquad \text{Equation 2.18}$$

$$S_{11}^{Ogd} = \frac{2\mu_0}{\alpha}\left\{\lambda^{\alpha-1} - \lambda^{-\left(\frac{\alpha}{2}+1\right)}\right\} \qquad \text{Equation 2.19}$$

where μ_0 is the instantaneous shear modulus and α is the stiffening parameter accounting for the nonlinearity of the stress-strain response.

2.3.5 Viscoelasticity

Almost all biological tissues exhibit viscoelastic behaviour and the viscoelastic properties are essential in their constitutive function (Vicente 2012). Viscoelastic materials can be considered as having both elastic and viscous components. For a purely elastic material, the strain reacts instantly to the stress, and when the stress is removed it also reacts instantly (Figure 2.8 (b)). For a perfectly viscous material, there is no instantaneous strain and elastic recovery, but a permanent strain (Figure 2.8 (c)). In Figure 2.8 (d), a typical response of a viscoelastic material subject to a constant load and to the subsequent unload, is shown. This behaviour includes elastic and permanent viscous strain, and the time-dependent response is regarded as *creep*. At first, an instantaneous strain occurs with loading followed by an increasing strain with a decreasing strain rate.

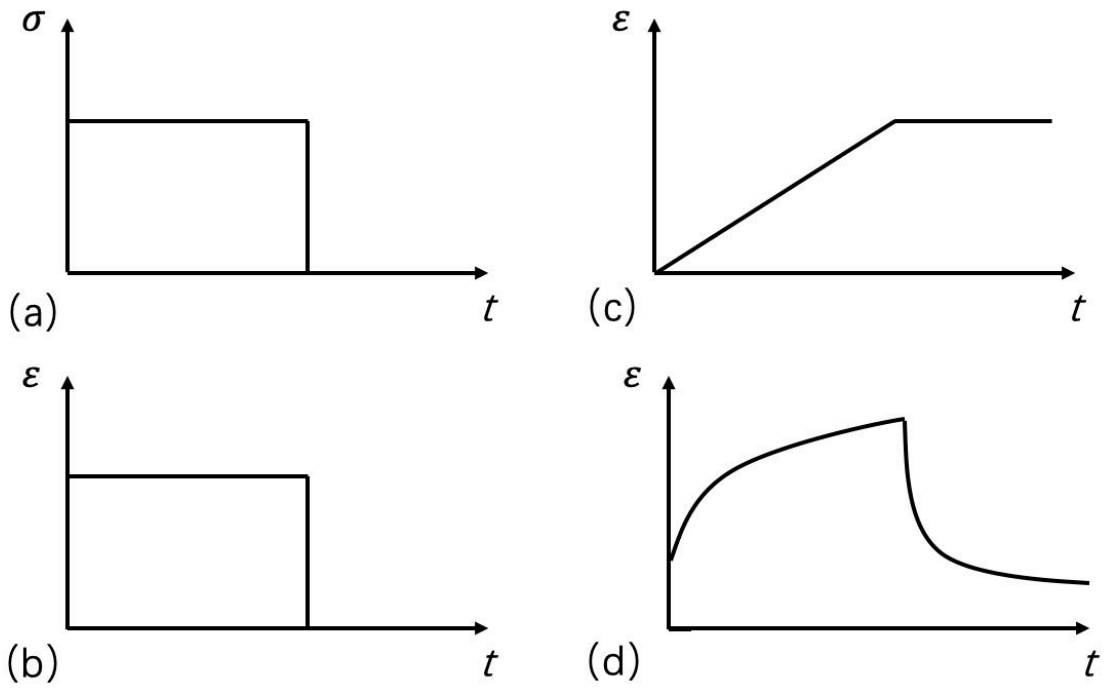

Figure 2.8 – With (a) a step stress excitation, (b) strain responses of idealistically elastic materials, (c) viscous materials and (d) viscoelastic materials.

Figure 2.9 shows the typical response of a viscoelastic material to a relaxation test subject to a constant strain. The process of stress relaxation shows how the stress induced in the material reduces following sudden deformation, from the corresponding stress-strain data and the viscoelastic response of the material can be evaluated.

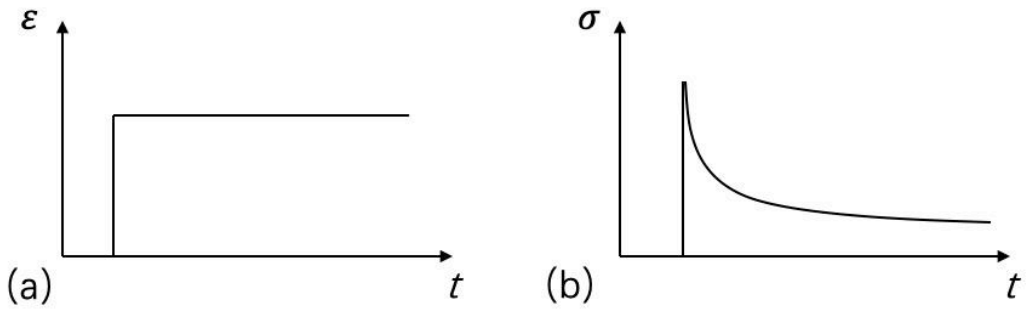

Figure 2.9 – With (a) a step strain excitation, (b) stress response of a viscoelastic material shows a relaxation process where the magnitude of stress decreases over time.

For a viscoelastic material, a lag exists between the unloading and loading portions of the curve (Figure 2.10). Hysteresis is a measure of observing the dissipated energy for the material (Menard and Menard 2020). Hysteresis can be calculated from the area in grey in Figure 2.10 and a larger hysteresis area means the greater amount of energy dissipated.

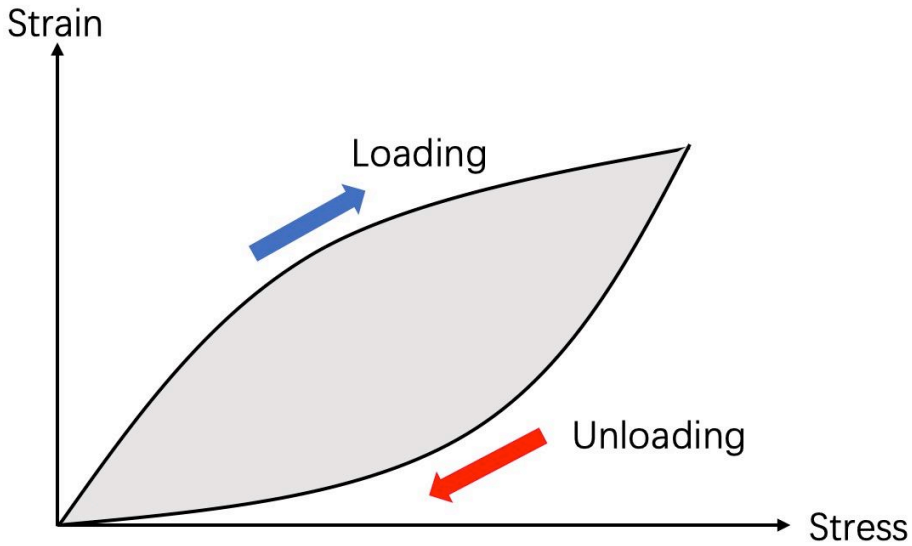

Figure 2.10 – Stress-strain hysteresis loops. The grey area inside the curve represents the energy lost.

2.3.5.1 Linear Viscoelasticity

Linear viscoelasticity is a special type of viscoelastic theory describing materials for which the relationship between stress and strain is linear. Linear viscoelasticity is commonly applied in computational models for polymers and biological tissues to capture their viscoelastic behaviour (Gidde and Pawar 2017; Qian et al. 2018). The mechanical behaviour of brain tissue under external forces shows viscoelastic properties and it includes elastic and viscous deformation which can be described by linear viscoelastic theory with the spring and dashpot elements (Qian et al. 2018). A linear viscoelastic model is built up by considering simple linear elements such as the linear elastic spring and the linear viscous dash pot, where the stress is in linear relation with strain and strain rate. The constitutive equations for a spring and a dashpot component are simply expressed by Equation 2.20 and Equation 2.21, respectively.

$$\sigma = \frac{1}{J}\varepsilon \qquad \text{Equation 2.20}$$

$$\sigma = \eta\frac{d\varepsilon}{dt} \qquad \text{Equation 2.21}$$

where σ is the stress, ε is the strain, J and η are known as compliance (the inverse of the stiffness) and viscosity of fluid, respectively (Figure 2.11).

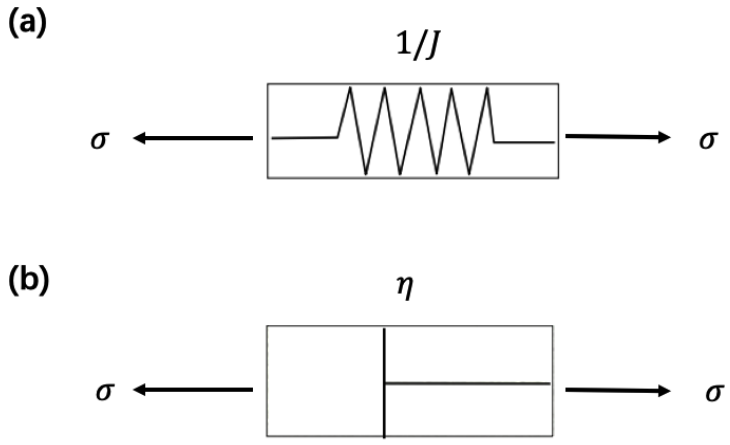

Figure 2.11 – (a) Spring and (b) dash-pot elements in linear viscoelastic models.

Through different combinations of the linear elements, there are various physical models generated to describe the time-dependent behaviour, including the Maxwell model consisting of a spring and a dash pot in series and Kelvin model consisting of a spring and a dash pot in parallel (Figure 2.12). The corresponding constitutive equation for a Maxwell model is:

$$\sigma + \eta J \frac{d\sigma}{dt} = \eta \frac{d\varepsilon}{dt} \qquad \text{Equation 2.22}$$

and for a Kelvin model is:

$$\sigma = \frac{\varepsilon}{J} + \eta \frac{d\varepsilon}{dt} \qquad \text{Equation 2.23}$$

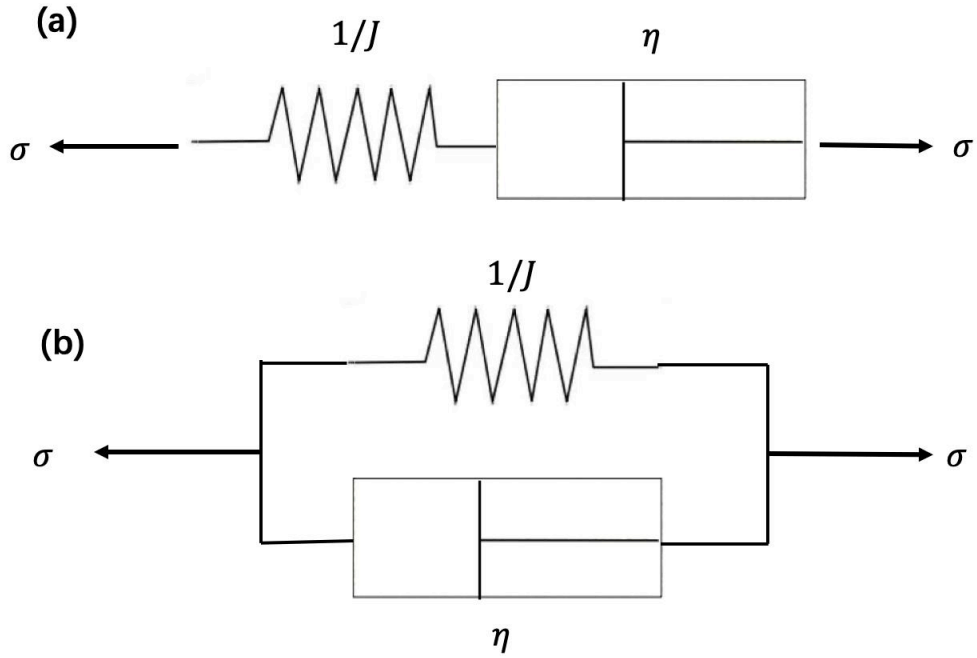

Figure 2.12 – (a) Maxwell material model consisting of a spring and a dash pot in series and (b) Kelvin material model consisting of a spring and a dash pot in parallel.

These simple models can only exhibit a part of viscoelastic characterization. Complicated models can be constructed by combining more elements. The generalized Maxwell model is the most widely used method for a linear model of viscoelasticity consisting of *N* spring-dashpot pair branches and a main elastic branch with different parameter values (Figure 2.13). The isolated spring ensures the solid behaviour (an instantaneous impact response) and the model presumes the relaxation does not occur at a single time but at various times with spring-dashpot branches.

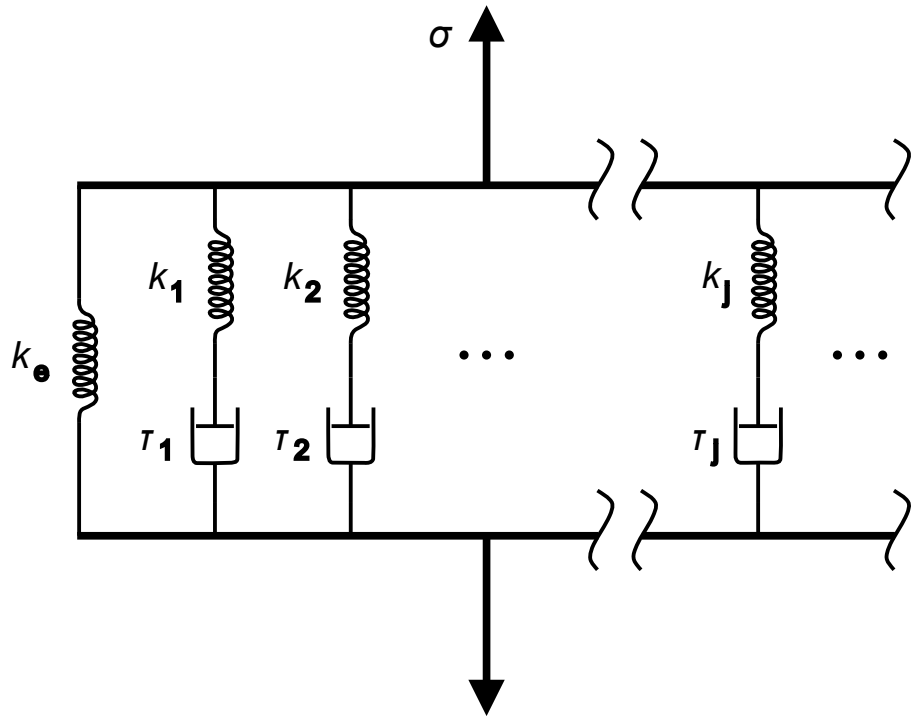

Figure 2.13 – A schematic interpretation of the generalized Maxwell model. Image freely available in the public domain (Pekaje 2007).

2.3.5.2 Prony Series

For viscoelastic materials, the stress depends on the strain history. The stress in a viscoelastic model is obtained by the following constitutive formulation based on the Boltzmann's superposition integral (Boltzmann 1878).

$$\sigma(t) = \int_{-\infty}^{t} u(t-\tau)\frac{d\delta}{d\tau}d\tau \qquad \text{Equation 2.24}$$

where σ is the deviatoric stress tensor, δ is the deviatoric strain tensor and $u(t)$ is the linear relaxation modulus.

During the relaxation step, the stress relaxes over time due to the viscous part of the material.

The relaxation function is widely approximated by a Prony series:

$$u(t) = u_e + \sum_{i=1}^{N} g_i \exp\left(-\frac{t}{\tau_i}\right) \qquad \text{Equation 2.25}$$

where the *N* relaxation modes are determined by the corresponding Prony constants g_i and retardation times constants τ_i. u_e is the equilibrium modulus. This method is commonly used to fit experimental data with a minimization algorithm to collect the parameters which are able to be applied in FE simulations. The initial elastic modulus is related to the equilibrium:

$$u_0 = u_e + \sum_{i=1}^{N} g_i \qquad \text{Equation 2.26}$$

Then, the Prony series can also be represented in an alternative form:

$$u(t) = u_0 - \sum_{i=1}^{N} g_i \left[1 - \exp\left(-\frac{t}{\tau_i}\right)\right] \qquad \text{Equation 2.27}$$

2.3.5.3 Quasi-linear viscoelasticity

For linear viscoelasticity, the relaxation function is a function of time and limited to the linear viscoelastic region (LVR). Quasi-linear viscoelasticity (QLV) has been applied to fit with large strain experimental data and this model assumes the effects of strain and time are separable. The QLV model has been widely used to predict the pattern of injury in large strain conditions in computational modelling (Jannesar et al. 2018; Mendizabal et al. 2015). It decomposes the mechanical behaviour of a material into two effects including a time-independent elastic response and a linear viscoelastic stress relaxation response. These models can be derived from separate experiments. For the large strain behaviour, the QLV model can be represented with a hyperelastic model using elastic effect identified in section 0.

2.3.5.4 Dynamic Mechanical Analysis

Viscoelasticity can also be studied using dynamic mechanical analysis (DMA). DMA is a method which can be used to characterize a material's viscoelastic properties over specific frequencies covering physiological and injury loading conditions (Bartlett et al. 2020). Unlike conventional stress-strain tests, an oscillatory deformation is applied to materials with a phase delay from the force. It is useful because it provides details of the short-term effects of loading on viscoelastic properties. The schematic overview of the sinusoidal load and displacement data is shown in Figure 2.14.

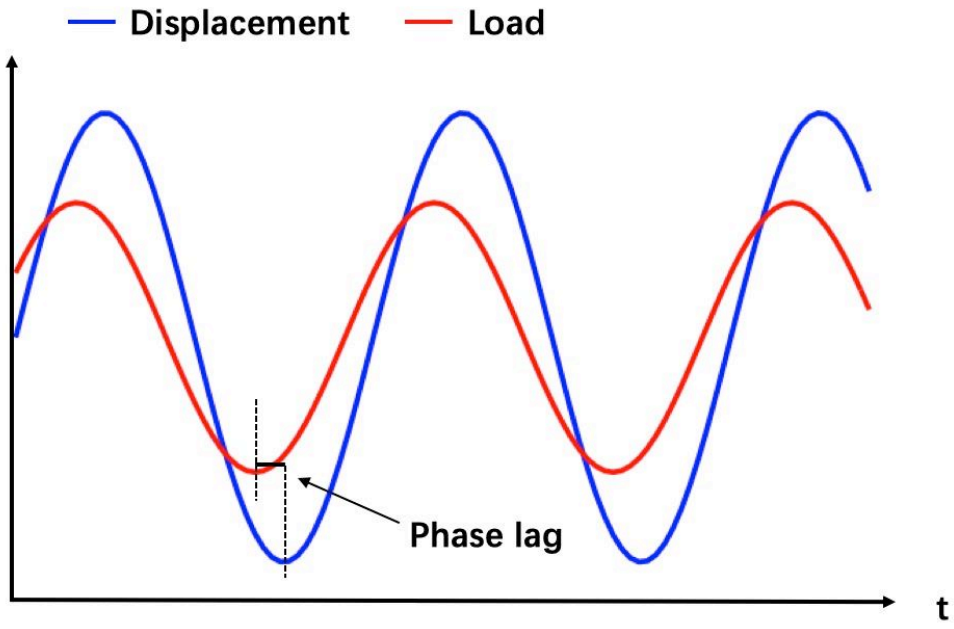

Figure 2.14 – A schematic representation of sinusoidal load and displacement waves of a viscoelastic material.

Fast Fourier transform (FFT) is applied to analyse the force and displacement waves (Figure 2.14). The dynamic stiffness (k*) and the phase angle (δ) are characterized subsequently. The data-set length for force (F^*) and displacement (d^*) at the fundamental frequency are quantified and used to calculate the dynamic stiffness:

$$k^* = \frac{F^*}{d^*} \qquad \text{Equation 2.28}$$

Viscoelastic properties of a structure can be characterized by a storage and loss stiffness (Aspden 1991). The storage stiffness characterizes the ability of the tissue to store energy in the elastic phase. The loss stiffness characterizes the ability of the tissue to dissipate energy in the viscous phase, mostly lost as heat. The storage (k') and loss (k'') stiffness regarded as the real

and imaginary portion of dynamic stiffness are calculated:

$$k' = k^* \cos \delta \qquad \text{Equation 2.29}$$

$$k'' = k^* \sin \delta \qquad \text{Equation 2.30}$$

The phase angle δ is the phase lag between the applied compressive force and displacement. For a perfectly elastic material, there is no phase lag between resulting stress and strain. For a purely viscous material, there is a 90-degree phase lag of stress with respect to strain. The ratio of loss to storage stiffness is tan delta ($\tan(\delta)$) which is a measure of energy dissipating in a system. A material with greater ratio displays the greater proportion of viscous behaviour in the system. The relationship between storage stiffness, loss stiffness and phase angle is shown in Figure 2.15.

$$\tan(\delta) = \frac{k''}{k'} \qquad \text{Equation 2.31}$$

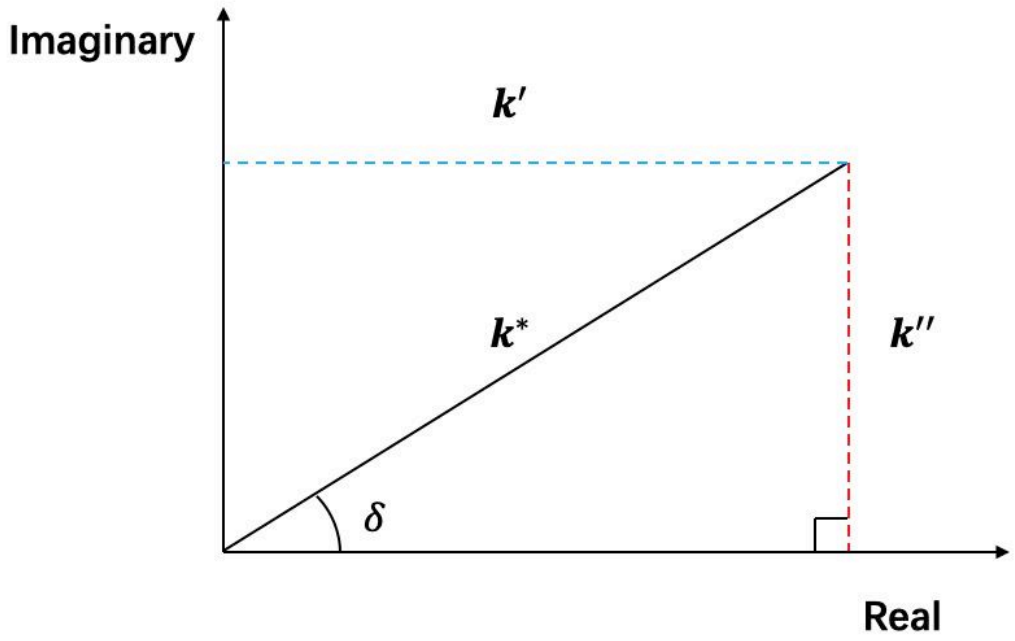

Figure 2.15 – Vectorial relationship between the dynamic (k*), storage (k') and loss (k") stiffness with phase lag (δ).

The viscoelastic properties of a material can be quantified through a shape factor (S), where the dynamic modulus (E^*) can be calculated from the dynamic stiffness which describes viscoelastic properties of a structure. Correspondingly, storage (E') and loss moduli (E") can be calculated by converting from the relevant stiffness using a shape factor:

$$E' = \frac{k^* cos\delta}{S} \qquad \text{Equation 2.32}$$

$$E'' = \frac{k^* sin\delta}{S} \qquad \text{Equation 2.33}$$

$$S = \frac{\pi d^2}{4h} \qquad \text{Equation 2.34}$$

where h and d are the thickness and diameter of a cylindrical specimen, respectively.

Using DMA can characterize bulk mechanical properties of a material in the frequency domain. This flexible and automated technique compared to creep and stress relaxation tests has an advantage of determining viscoelastic properties more quickly and can obtain accurate data without very high-resolution data acquisition. DMA is widely used to map mechanical properties of soft viscoelastic materials, including biomaterials (Bartlett et al. 2020), bladder (Barnes et al. 2015) and articular cartilage (Lawless et al. 2017).

2.4 Modelling and Mechanical Testing of Brain Tissue

2.4.1 Finite Element Analysis and Constitutive Models

Computational simulations of brain tissue have emerged with progress in brain mechanical investigations over the past decades. This type of modelling is promising as it can be applied to predict brain mechanics (Goriely et al. 2015) and develop a methodology to assess head injury (Sahoo et al. 2016). For the mild traumatic brain injury, the physiology of brain can be affected for hours to years and the symptoms of brain injuries may occur immediately or a few weeks later. Due to the existence of these uncertain cases, the predictive abilities of brain injuries become important and have been studied intensively leading to head simulation models (Sahoo et al. 2014). In addition, finite element (FE) simulations have been studied to analyze the smart protection systems such as impacts of a construction helmet (Wu et al. 2017) and predict brain disease progression and development (Weickenmeier et al. 2017). An FE model of the human head is shown in Figure 2.16. However, the accuracy and variety of these computational models

on brain tissue requires quantitative data from experiments and the development of constitutive models to capture the viscoelastic behaviour of this tissue.

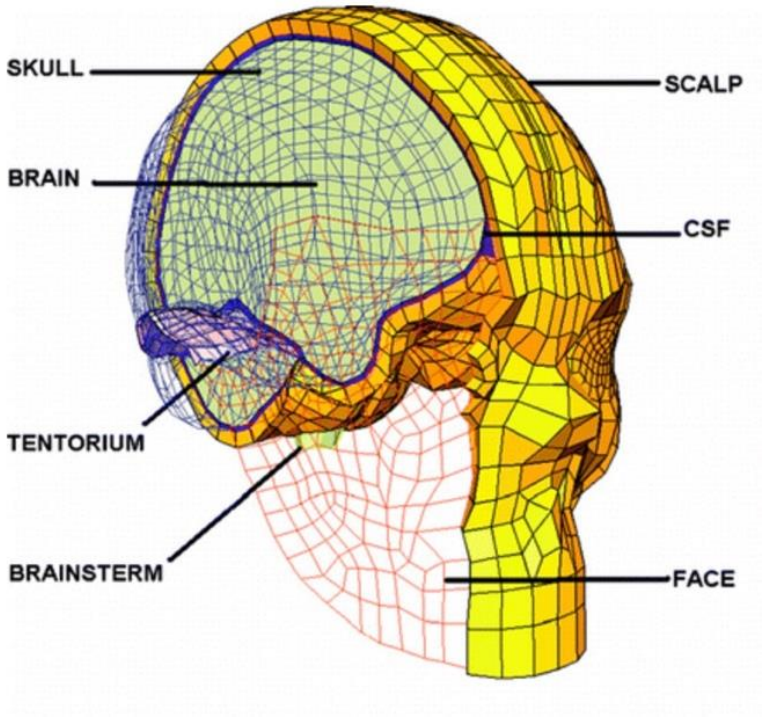

Figure 2.16 – Finite element model of human head illustrating the main anatomical features with a cross section (reproduced with permission from Taylor & Francis (Deck, & Willinger 2014)).

To develop finite element models of brain tissue, the appropriate constitutive laws are essential. Most previous studies characterized viscoelastic behaviour in the time domain and have used a Prony series in the single viscous solid phase (Budday et al. 2017). Some studies applied a biphasic theory to describe the time-dependent response of brain tissue (Cheng and Bilston 2007; Forte et al. 2017), which was first established for the study of articular cartilage (Mow et al. 1980) and then extended to integrate the strain-dependent permeability and elasticity of solid matrix with finite deformation (Holmes 1986).

For most biological materials under large strains, the theory of nonlinear elastic models is often adopted to describe the mechanical behaviour (e.g. hyperelastic models). Hyperelastic models are commonly used to simulate brain tissue (Budday et al. 2017; Li et al. 2019) or other general soft tissues (Lapeer et al. 2010) which shows an nonlinear stress-strain relationship at experimental tests under large deformation. Further, the specific component of hyperelastic models has been determined following comparison of different constitutive models (e.g. neo-Hookean, Mooney-Rivlin, Gent or Ogden) (Rashid et al. 2013). Among these models, Ogden models have been used for various biological tissues (Jannesar et al. 2018; Li et al. 2019), and tend to better map the non-linear stress-strain curve.

Regarding head injuries, except "quasi-static" and time-dependent loading conditions, the brain could also experience dynamic impact in the frequency domain where the strong shaking force occurs within the skull (Elinder et al. 2018). Therefore, the frequency-dependent properties of brain tissue are vital in head computational simulations when the dynamic mechanical response is analysed. However, the application of constitutive laws describing the frequency-dependent viscoelastic behaviour of brain tissue in compression is limited.

2.4.2 Mechanical Testing of Brain Tissue

The mechanical characterization of brain tissue has been the focus of several studies. However, the obtained results are not always consistent across different studies due to the complexity of the soft tissue. Further, a wide range of loading conditions and protocols have been performed on brain tissue and there is lack of a standard testing method. Most protocols analyse brain tissue within the time domain and with "quasi-static" test conditions. The effect of strain rate on mechanical properties of porcine brain tissue has been analysed by indentation tests (Qian et al. 2018). Unconfined compression experiments have been performed to investigate the porous properties of the bovine white matter using a poro-viscoelastic model (Cheng and Bilston 2007). The influence of heterogeneity on porcine brain tissue was studied through tensile tests (Velardi et al. 2006). Recently, the mechanical behaviour and regional properties of brain tissue have been investigated through the combination of compression, shear and tensile tests under multiple loading conditions (Budday et al. 2017). In addition, the mechanical properties of brain tissue have been previously investigated in the frequency domain. Dynamic frequency sweep tests have been performed to characterize material properties of human brain (Fallenstein et al. 1969) and nonlinear constitutive models for bovine brain (Darvish and Crandall 2001), mostly conducted in shear. These studies have quantitatively measured mechanical properties of brain tissue (Table 2-1). In addition, the compressive loading plays an important role in head trauma as many deformations of initial impact is compressive (Bar-Kochba et al. 2016; Young et al. 2015). The brain could also experience the compressive waves

during the course of head impact (Morse et al. 2014). However, the effect of dynamic viscoelastic characterization of the brain tissue through dynamic mechanical analysis (DMA) under compression has not been quantified and only one dynamic oscillatory strain study of compression load can be found, described in a review paper where fifty years of brain tissue mechanical testing were investigated (Chatelin et al. 2010). DMA is a versatile, flexible and automated technique to map the bulk mechanical properties of soft viscoelastic materials. It can determine both the elastic and viscous components of a material through compressive movement to collect comprehensive mechanical characterization of brain tissue.

Table 2-1 – Mechanical testing of brain tissue from literature.

Testing Method	Model	Main Findings	Limitations	Study
Indention test	Porcine	Shear modulus from 0.3 kPa to 0.7 kPa, with the strain rate fluctuating from 0.002 s^{-1} to 0.017 s^{-1}	Limited to interregional variation of brain tissue	(Qian et al. 2018)
Combination of shear, compression and tension tests	Human	One-term Ogden model can represent the hyperelastic behaviour with a shear modulus of 0.4 to 1.4 kPa	No viscoelastic models to describe relaxation response	(Budday et al. 2017)
Shear test	Porcine	The maximum shear stress at strain rates of 30, 60, 90 and 120/s was 1.15 ± 0.25, 1.34 ± 0.19, 2.19 ± 0.225 and 2.52 ± 0.27 kPa (mean ± SD)	Estimation of material properties was based on mixture of white and grey matter	(Rashid et al. 2013)
Compression test	Bovine	The stress–strain behaviour at high strain rates reveals a significant rate dependency of the grey matter and white matter	No relaxation tests were conducted to derive viscoelasticity	(Pervin and Chen 2009)
Tensile test	Porcine	The tensile engineering stress at 30% strain was 3.1 ± 0.49, 4.3 ± 0.86, 6.5 ± 0.76 kPa (mean ± SD) at strain rates of 30, 60 and 90/s	Limited to homogenous deformation due to the bonding of brain tissue	(Rashid et al. 2014)

Dynamic shear test	Human	The storage modulus lies between 0.6 to 1.1 kPa and loss modulus lies between 0.35 to 0.6 kPa	Only white matter of brain tissue was tested	(Fallenst.Gt et al. 1969)
Oscillatory shear test	Human / Porcine	The storage modulus increased from 2.1 to 16.8 kPa and the loss modulus increased from 0.4 to 18.7 kPa between 0.1 and 6300 Hz. No significant difference between the viscoelastic behaviour of porcine and human brain white matter	The presented results were based on limited amount of brain samples	(Nicolle et al. 2004)

Many previous studies have selected animal brains to conduct in vitro tests as a substitute for human brains because the former is more readily available. The human brain samples were found to be 29% stiffer than the porcine brain samples through shear stress relaxation (Prange and Margulies 2002). Human brain samples were shown to be 40% stiffer than bovine samples using the same testing method (Takhounts et al. 2003). These experiments were performed in the time domain with stress-strain methods while the results in the frequency domain were different. Galford and McElhaney (Galford and Mcelhaney 1970) found, from vibration experiments, the dynamic storage and loss moduli of monkey brain tissue to be 1.4 and 2 times higher than that of human brain tissue, respectively. However, through oscillatory shear tests the moduli of human and porcine brain tissue were found to be similar (Nicolle et al. 2004). Therefore, there are similarities reported in previous studies on the mechanical response of brain tissue between human and porcine, implying that porcine brains may be used as models for human brains (Rashid et al. 2012).

2.4.3 Effect of Testing Condition

Testing conditions and protocols in the research of material properties have a significant influence on experimental results. The complex shear modulus of porcine brain tissue at 5% applied strain was found to be lower than at 2.5% strain (Arbogast et al. 1997). A similar trend was identified that the variations of shear modulus on bovine brain tissue are relevant to strain (Darvish and Crandall 2001). The contact stiffness of bovine samples was observed to have a linear relationship with the indenter size (Budday et al. 2015). In addition, the variations are also affected by the factors of sample species, tissue heterogeneity and even environmental temperature (Rashid et al. 2012).

2.4.4 Comparison of Time and Frequency Domain Characterization

The mechanical characterization of brain tissue has been generally analysed in the frequency or time domains. Frequency-dependent dynamic modulus is defined as the ratio of force amplitude to displacement amplitude over a range of frequencies and provides information for both elastic and viscous components of biological tissues. Time-dependent relaxation modulus describes the phenomenon of viscous effect of a material where stress decreases under constant strain. Brain injuries may be induced by angular, shear and translational force. Oscillations of the head leading to brain shaking within the skull can also produce brain trauma (Laksari et al. 2015). Some studies investigated brain tissue in the time domain (Velardi et al. 2006) while dynamic sweep tests on brain tissue in the frequency domain have also been performed (Darvish

and Crandall 2001). Although a range of dynamic mechanical data are available for various materials in the literature, it has rarely been applied in modelling to analyse and design structures, mainly because models are often solved under steady state conditions providing limited information about the stiffness of tissues.

Viscoelastic characterization can be implemented either in the time or the frequency domain and these models are capable of describing the mechanical properties of a material from both testing domains. Based on the equivalent mathematical equations including integral and differential theory with shared linear viscoelastic material parameters described in detail in section 2.3.5, it should be possible to link between time dependent and frequency dependent viscoelastic properties (Tschoegl 2012). Even though frequency dependent properties and corresponding viscoelastic models of brain tissue have been recently studied (Li et al. 2020), it remains unclear whether such data can be used in computational models to predict mechanical behaviour under various loading conditions such as under time-dependent loading. It is crucial to understand the relationship between different testing methods on material properties of brain tissue because it enables the viscoelastic properties of the brain to be measured under realistic, dynamic conditions and makes this information available to existing models which predict trauma.

2.5 Chapter Summary

This background chapter summarizes modelling of brain tissue and its related injuries. Different types of traumatic brain injury, which are a major cause of death, are presented and can be caused by external dynamic forces. Finite Element simulations have been widely performed to predict and analyse brain injuries, so quantitative results from experiments are required to improve these models. Dynamic mechanical analysis is a dynamic method which can be used to measure the viscoelastic properties of a material over a range of frequencies under various testing conditions. The mechanical characterization of brain tissue has been generally analysed in the frequency and time domain. Understanding the relationship between the time and frequency dependent properties can make the most of existing data and convert the mechanics of the brain under dynamic conditions to enable mathematical modelling in a time domain.

In the next chapter, the frequency-dependent mechanical properties of brain tissue have been studied extensively by compressive DMA under various testing conditions. Indenters with varying diameters were used to study the effect on viscoelastic properties under a sinusoidally varying displacement with varying mean displacements.

3 Frequency Dependent Viscoelastic Properties of Porcine Brain Tissue

3.1 Introduction

Brain tissue, as discussed in the Background chapter, is considered as one of the most vulnerable organs in the human body. Although the brain is well protected by the skull, damage experienced by brain tissue has been linked to the mechanism of loading (Taylor et al. 2017), such as the effect of strain rate (Qian et al. 2018), loading deformation conditions (MacManus et al. 2017) and shear oscillation of load (Darvish and Crandall 2001). Additionally, regarding head injuries, the brain could experience dynamic loading conditions such as shaken baby syndrome (SBS) where the violent shaking occurs with the head moving backwards and forwards (Elinder et al. 2018). Its material properties have been widely investigated in shear, but there are potential differences which exist in loading protocols between shear and compression tests. The compressive force is also important in the analysis of brain injuries, yet detailed dynamic measurements relevant to compressive strains are lacking (Chatelin et al. 2010).

Different testing conditions can have significant influences on experimental results. While viscoelastic properties of brain tissue have been characterized, the effect of indenter size and mean indentation depth on dynamic properties such as storage and loss moduli has not been assessed by compressive DMA. The severity of brain injuries is also relevant to the strain rate

and the magnitude of the displacement of brain away from an initial centre line (Maas et al. 2008; Pfister et al. 2003). Therefore, the understanding of frequency-dependent properties per external loading condition, such as indenter size or strain is important.

The aim of the work presented in this chapter was to characterize the macroscopic frequency dependent viscoelastic properties of porcine brain tissue using DMA under compression. The variation of dynamic stiffness properties was assessed by comparing different indenter sizes and indentation depths. The storage and loss moduli were also analysed over a range of loading frequencies.

3.2 Materials and Methods

3.2.1 Specimen Preparation

Four half porcine brains under 8 months old were obtained from a supplier (Dissect Supplies, Kings Heath, Birmingham, UK). Following arrival in the laboratory the samples were wrapped in tissue paper soaked in Ringer's solution (Oxoid Ltd, Basingstoke, UK) and then stored at -40 ◦C in a freezer in double heat-sealed plastic bags (Li et al. 2020; Mahmood et al. 2018). From previous studies, such freezing treatment does not change the mechanical properties of biological tissues (Szarko et al. 2010). Before each mechanical test, a half brain was taken out from the freezer and placed in a fridge, thawed in Ringer's solution overnight at around 4 ◦C ahead of dissection and preparation for mechanical testing.

Ten test specimens which comprised both white and grey matter were obtained from the four half porcine brains. Each specimen was tested for different scenarios described in section 3.2.4 to collect adequate data for statistical analysis, which is consistent to a previous study where the same brain specimen was tested under multiple loading modes (Budday et al. 2017). In order to be able to understand the effect of frequency on viscoelastic properties, it is necessary for the frequency test to be performed on the same samples, which is consistent to previous studies (Barnes et al. 2016; Budday et al. 2017).After the cerebellum, spinal cord and medulla oblongata were removed, the cerebral hemi- spheres were mainly composed of the frontal, parietal and occipital lobes and cut in the coronal plane using a surgical scalpel (Swann-Morton Limited, Sheffield, UK). Specimens were dissected into cylindrical shaped samples (Figure 3.1) through the anterior-posterior direction. The brain samples were 7 ± 1 mm (mean ± deviation) in thickness and 28 ± 1 mm in diameter measured using a Vernier calliper (Draper Tools Ltd, Hampshire, UK) shown in Figure 3.2.

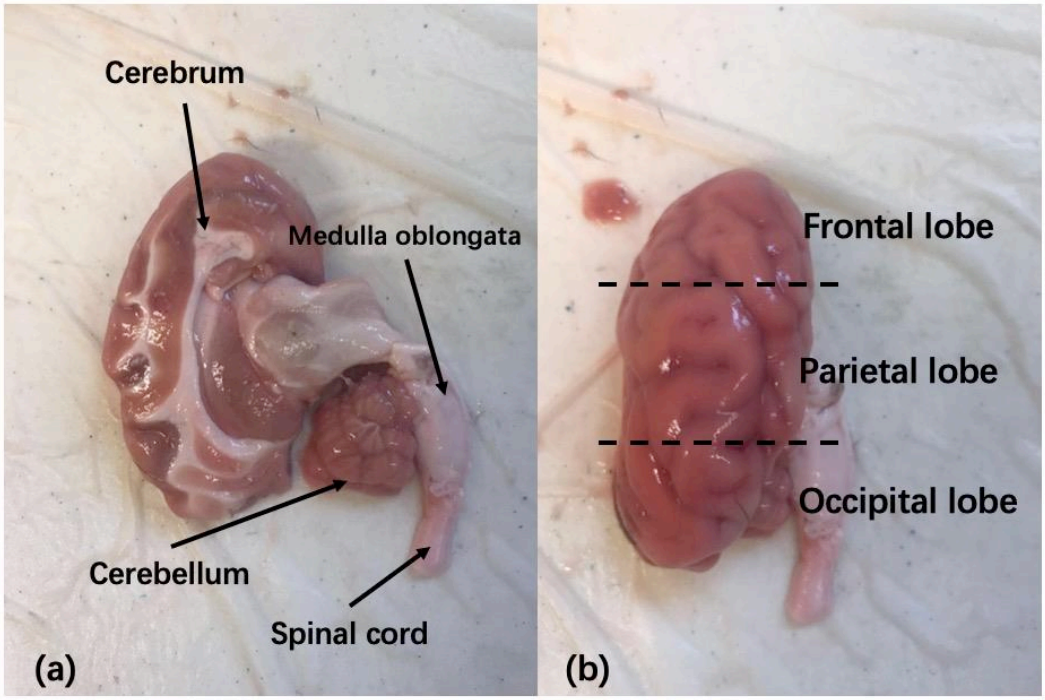

Figure 3.1 – A half porcine brain before dissection. (a) an anatomy of brain in coronal plane showing the cerebrum, cerebellum, medulla oblongata and spinal cord. (b) From the view of top, the cerebral sample was mainly made of the frontal, parietal and occipital lobes.

Figure 3.2 – A representative image of a test brain specimen. The dimension of each specimen was measured before mechanical testing.

3.2.2 Experimental Device

In this study, the macroscopic mechanical response of brain tissue was the main focus and the brain tissue is considered as the soft tissue constrained by the skull. The confined container was designed and manufactured, with the same diameter of 28 mm to the tested brain samples (Figure 3.3). The selection of confined testing is based on the nature of the boundary conditions at the skull/brain interface.

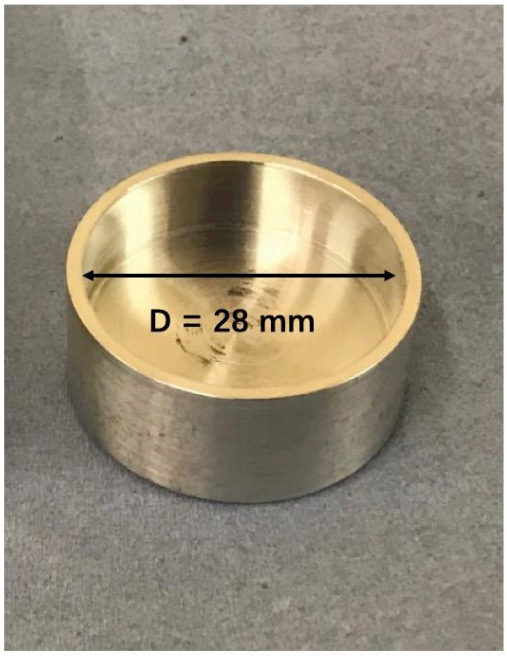

Figure 3.3 – A custom-designed container with diameter of 28 mm for compression testing.

To investigate the impact of indenter size on the mechanical properties of brain tissue, three circular flat indenters with diameters of 8, 12 and 16 mm were manufactured to compress brain samples in dynamic mechanical testing (Figure 3.4). The indenter sizes used were large enough to ensure the homogenous behaviour of tissue during the process of testing.

Figure 3.4 – Three circular flat indenters with diameters of 16 mm, 12 mm and 8 mm.

3.2.3 Preliminary Testing

The brain tissue is considered extremely soft and due to the high stress relaxation nature, displacement control in DMA testing was preferred. A sinusoidally varying displacement was applied to the samples to perform preliminary tests.

The cylinder brain specimens were tested from 0.1 to 35 Hz and 35 to 0.1 Hz with a pre-cycling at 5 Hz to investigate whether the order of the testing alter the measured mechanical properties of brain tissue and whether the preconditioning cycle is necessary. Three samples were tested with three different mean displacements of 20% specimen height (Figure 3.5), 15% specimen height (Figure 3.6) and 10% specimen height (Figure 3.7), respectively.

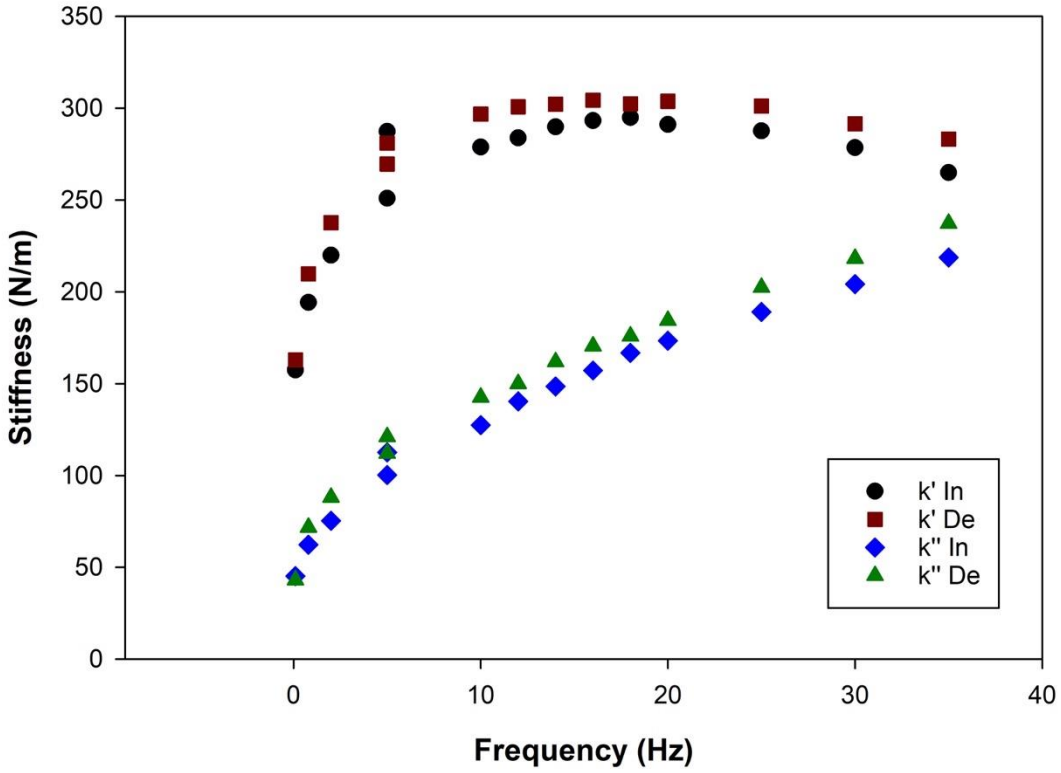

Figure 3.5 – Storage (*k'*) and loss (*k''*) stiffness against frequency under a 20% specimen height mean displacement. The range of tested frequency was between 0.1 and 35 Hz. The *In* refers to an increasing tested frequency and *De* refers to decreasing tested frequency.

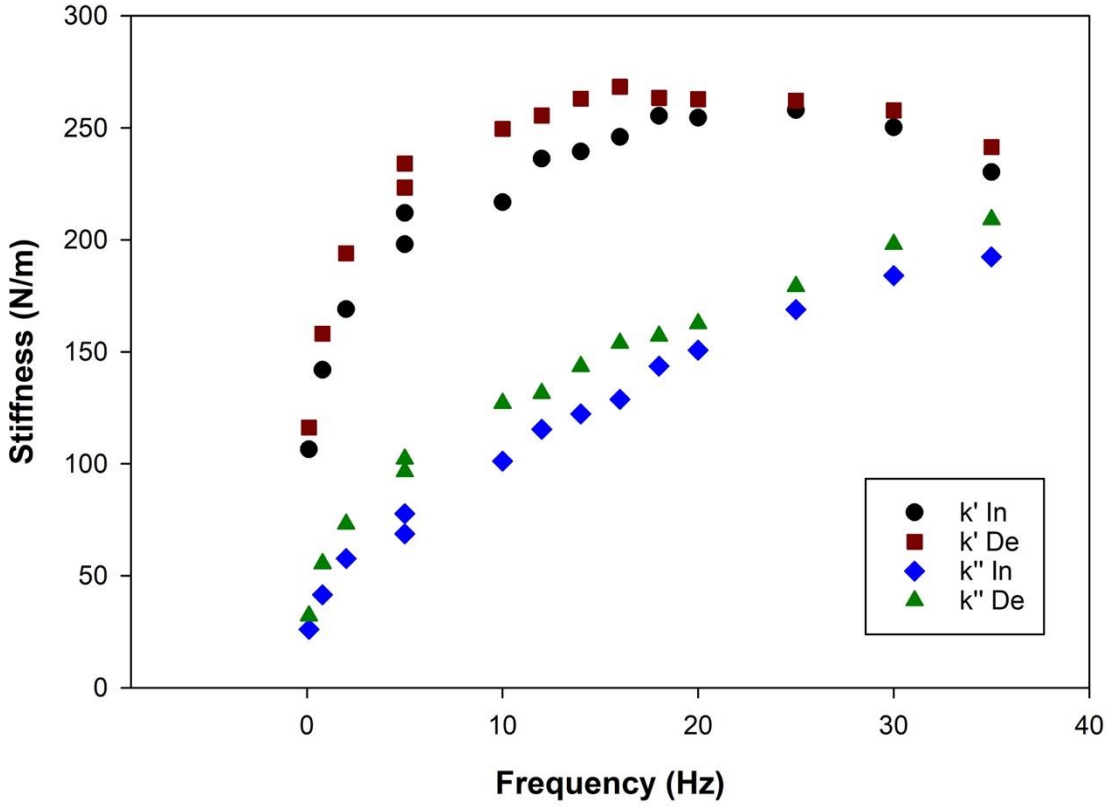

Figure 3.6 – Storage (*k'*) and loss (*k''*) stiffness against frequency under a 15% specimen height mean displacement. The range of tested frequency was between 0.1 and 35 Hz. The *In* refers to an increasing tested frequency and *De* refers to decreasing tested frequency.

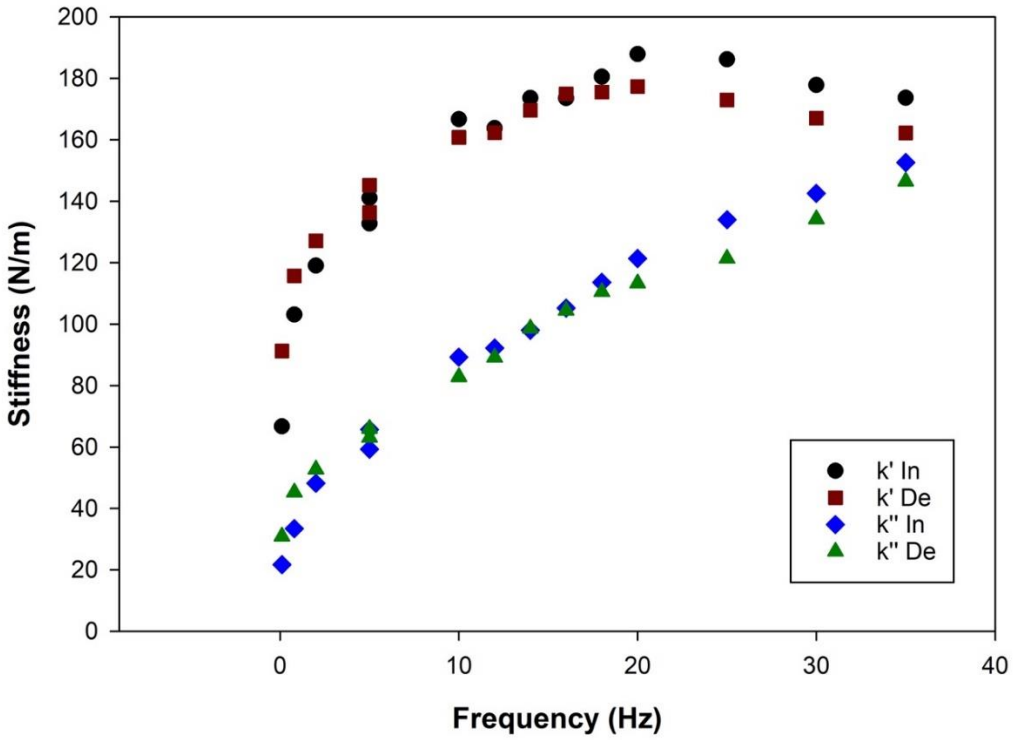

Figure 3.7 – Storage (*k'*) and loss (*k''*) stiffness against frequency under a 10% specimen height mean displacement. The range of tested frequency was between 0.1 and 35 Hz. The *In* refers to an increasing tested frequency and *De* refers to decreasing tested frequency.

From the preliminary tests, the preconditioning cycle of 5 Hz was recorded, and it was seen that pre-cycling had effects on the mechanical properties of brain tissue as the relevant results for storage and loss stiffness differed from the general trend. Preliminary tests also showed that the results were similar whether the specimen was tested from 0.1 to 35 Hz or 35 to 0.1 Hz. Therefore, in subsequent tests, an order of increasing frequency was used. The brain samples were tested under a dehydrated condition in the preliminary testing. However, there was adhesive contact between the brain sample and indenter leading to different mechanical properties. Thus, the brain samples were kept hydrated during the following mechanical testing.

3.2.4 Porcine Brain Dynamic Experiment

Ten brain specimens were placed in a 28 mm diameter custom-designed container and compressed using a circular flat indenter. Three different indenter diameters of 8, 12 and 16 mm were used during the dynamic testing (Figure 3.8). To minimize the friction between the brain specimens and the compression indenter, samples were hydrated with Ringer's solution before each mechanical test. All samples were tested by applying a sinusoidally varying displacement with a mean displacement (MD) of 1.4 mm (20% of the specimen height) and an amplitude of 0.14 mm, i.e. between 1.26 and 1.54 mm, over the frequency range from 0.1 to 35 Hz in 14 steps. The acquisition frequency at 35 Hz is 5 kHz. An example of the force against displacement data is shown in Figure 3.9. The frequency range of 0.1 to 35 Hz covers most of the loading frequencies to which the brain might be exposed during physiological and traumatic loading (Laksari et al. 2015). For mild traumatic brain injuries (mTBI), oscillatory force with approximate 20 Hz could be possible cause and the highest frequency of 35 Hz applied in testing is relevant to diffuse axonal injury (DAI) (Rashid et al. 2013). For the 16 mm diameter indenter two further mean displacements of 1.05 mm (15% of the specimen height, with an amplitude of 0.105 mm) and 0.7 mm (10% of the specimen height, with an amplitude of 0.07 mm) were investigated (Table 3-1). The mean displacement range covered mechanical levels of brain tissue from spontaneous recovery to irreversible injury (Thibault et al. 1990; Zou and Schmiedeler 2008). Between each test, the brain specimens were irrigated with Ringer's solution to keep hydrated. Before the data collection procedure, a preconditioning cycle of 5

Hz was applied (Barnes et al. 2016; Wilcox et al. 2014) following the same displacement parameters detailed above. Preconditioning is a well-established process for the mechanical testing of biological tissue. A previous study has performed similar preconditioning cycles on human brain to ensure a repeatable mechanical response (Budday et al. 2017). By analogy, quasi-static tests use preloading on bovine brain to ensure a consistent and comparable starting point for test (Cheng and Bilston 2007). Preconditioning cycles are needed to counter the artefacts which occur in mechanical behaviour from the fact that ex vivo tissue has been excised. The thawed tissue is loaded initially and following a few preconditioning cycles, the tissue then behaves consistently.

Table 3-1 – Testing protocol for sequential mechanical testing. Ten brain specimens were tested under multiple loading modes.

	Indenter Diameter (mm)	Mean Displacement (% of h)	Amplitude (mm)
1	8	20%h	0.14
2	12	20%h	0.14
3	16	20%h	0.14
4	16	15%h	0.105
5	16	10%h	0.07

h, specimen height

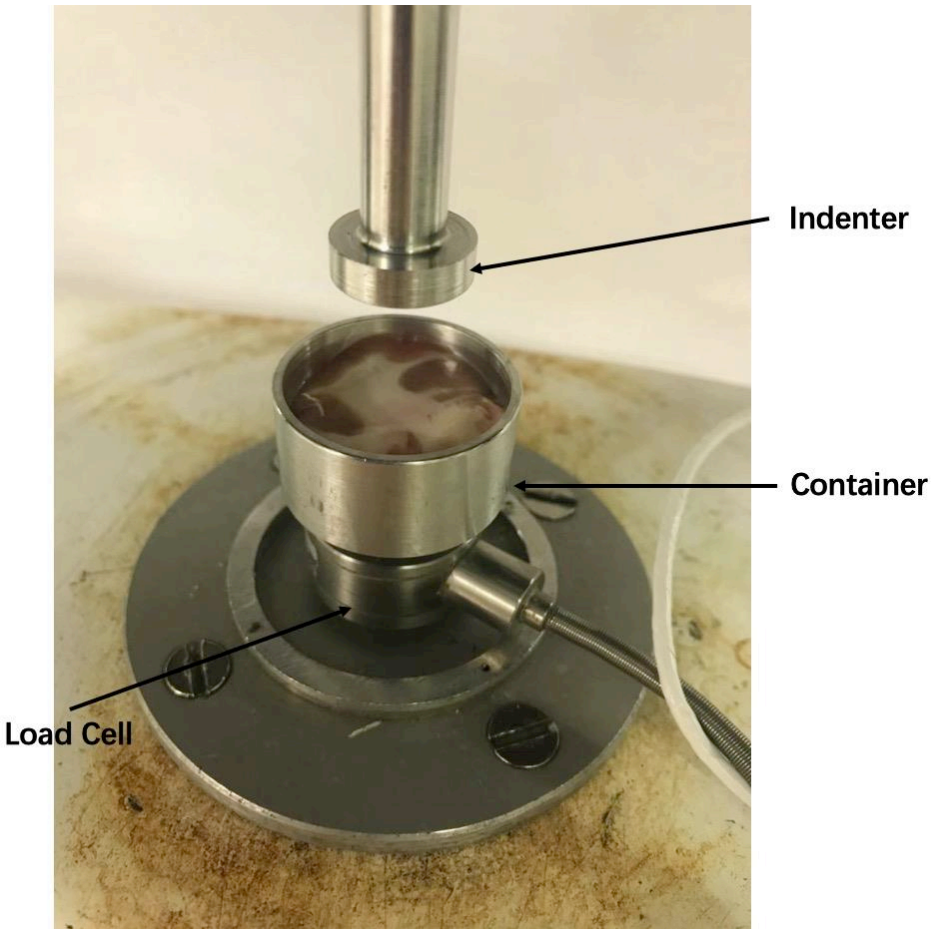

Figure 3.8 – Compressive testing setup for the porcine brain specimens including the customized container and indenter.

The frequency-dependent data of each brain sample were collected and for different scenarios described in Table 3-1, the corresponding average dynamic response was calculated with mean value and standard deviation. The mean mechanical responses of brain tissue were further used to curve fit with equations described in section 3.3. This would lead to less understanding of coefficient sensitivity compared to fit equations to each sample.

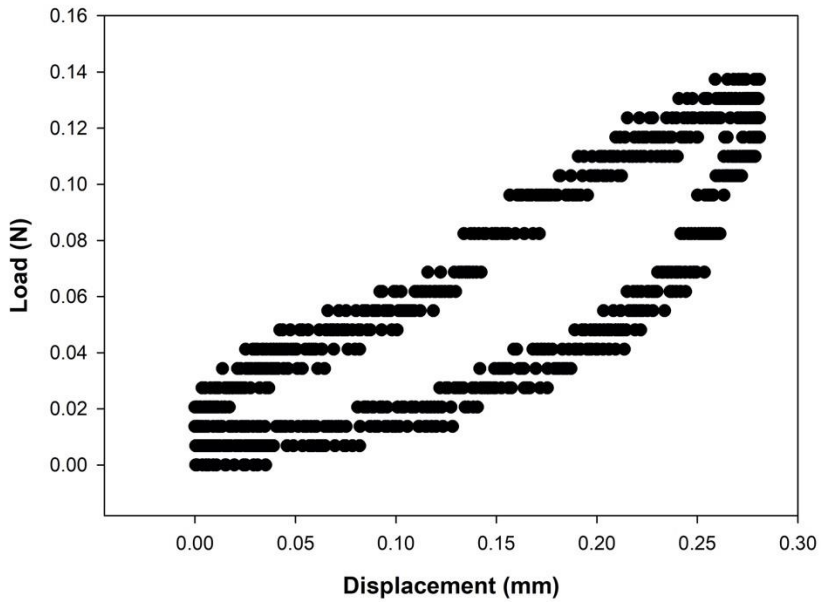

Figure 3.9 – Representative load displacement experimental data, from multiple cycles, for a given sample at 22 Hz.

A Bose ElectroForce 3200 (Bose Corporation, ElectroForce Systems Group, Minnesota, USA) testing machine operated using WinTest Dynamic Mechanical Analysis software (Bose Corporation, ElectroForce Systems Group, Minnesota, USA) was used to determine the viscoelastic properties of the brain tissue samples; the set-up configuration is displayed in Figure 3.10. This approach has been previously used to test biological and synthetic materials (Baxter et al. 2017; Lawless et al. 2017). A 225 N load cell was used which measures force with a resolution of 0.002 N over a wide range of frequencies. The Wintest DMA Analysis software uses a fast Fourier transform (FFT) to analyse the force and displacement waves. The dynamic stiffness (k^*) and the phase angle (δ) were characterized subsequently. Dynamic stiffness was determined as the ratio of force amplitude to displacement amplitude. The phase angle was

calculated as the phase difference between the force and displacement. The ratio of loss to storage stiffness (*k''/k'*) as the *tanδ* is a measure of energy dissipating in a system. A material with greater *k''/k'* ratio displays the greater proportion of viscous behaviour in the system. The method the software used is described in detail in section 2.3.5. The storage (*k'*) and loss stiffness (*k''*) were calculated using Equation 3.1 and Equation 3.2.

$$k' = k^* \cos \delta \qquad \text{Equation 3.1}$$

$$k'' = k^* \sin \delta \qquad \text{Equation 3.2}$$

Considering the effect of the indenter size, storage (*E'*) and loss moduli (*E''*) were calculated by converting from the relevant stiffness using a shape factor (*S*) calculated using Equation 3.4 and Equation 3.5 (Fulcher et al. 2009). The shape factor for cylindrical samples can be calculated from Equation 3.3.

$$S = \left(\frac{\pi}{h}\right)\left(\frac{d}{2}\right)^2 \qquad \text{Equation 3.3}$$

$$E' = \frac{k'}{S} \qquad \text{Equation 3.4}$$

$$E'' = \frac{k''}{S} \qquad \text{Equation 3.5}$$

where *h* is the sample thickness, *d* is the diameter of a specimen. In this instance, the diameter *d* was considered to be equivalent to the diameter of the indenter.

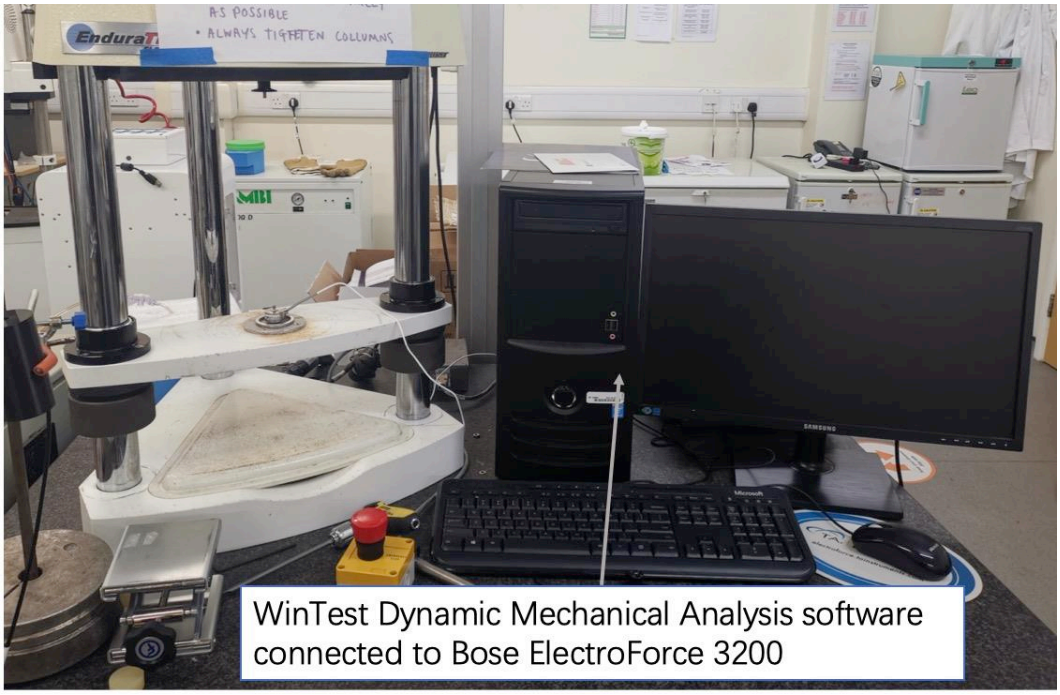

Figure 3.10 – The experimental set-up of a full testing system shows the application of the Bose ElectroForce 3200 connected to WinTest DMA software.

3.2.5 Data Analysis

Sigmaplot Version 13.0 (Systat Software Inc., London, UK) was used to perform regression analysis for the curve fit of stiffness and modulus against frequency. The relationship between brain specimens in terms of one variable (i.e. indenter size or mean displacement) were analysed by a one-way analysis of variance method (ANOVA). It would provide statistical results at various tested frequencies for three indenter sizes or mean displacements. A Kruskal-Wallis ANOVA on ranks was used if the normality test (Shapiro-Wilk) failed ($p < 0.05$). If ANOVA showed a statistically significant difference ($p < 0.05$), a Student-Newman-Keuls Method (SNK) was used for all pairwise comparisons of testing groups which would be significant when $p < 0.05$.

3.3 Results

Figure 3.11 (a) shows storage stiffness properties for three individual brain samples. The storage stiffness for all tested samples increased with frequency initially, then decreased at higher frequencies. The trend of storage stiffness can be characterized by a logarithmic curve fit (Equation 3.6) from 0.1 to 18 Hz and a second order polynomial fit (Equation 3.7) up to the end frequency sweep.

$$k' = A \ln f + B \quad for\ 0.1 < f < 18 \qquad \text{Equation 3.6}$$

$$k' = Cf^2 + D(f) + F \quad for\ 18 \leq f \leq 35 \qquad \text{Equation 3.7}$$

where, k' is the storage stiffness, f is frequency and A, B, C, D and F are empirically derived storage constants by the least-squares fit method, which are summarized in Table 3-2.

Figure 3.11 (b) shows loss stiffness properties for three individual brain samples. The loss stiffness increased with increasing frequency and was lower than storage stiffness for most frequencies tested while for the end testing frequency, the storage and loss stiffness was found to be similar. The trend of loss stiffness can be characterized by a second order polynomial fit across all frequencies tested (Equation 3.8) which has the same equation to the second part of storage with different constants. All constants were found to be statistically significant ($p < 0.05$) indicating there is a non-zero correlation between the independent variable and the dependent variable.

$$k'' = H(f^2) + I(f) + J \quad for\ 0.1 \leq f \leq 35$$ Equation 3.8

here, k'' is the loss stiffness, f is frequency and H, I and J are empirically derived loss constants by the least-squares fit method summarized in Table 3-2.

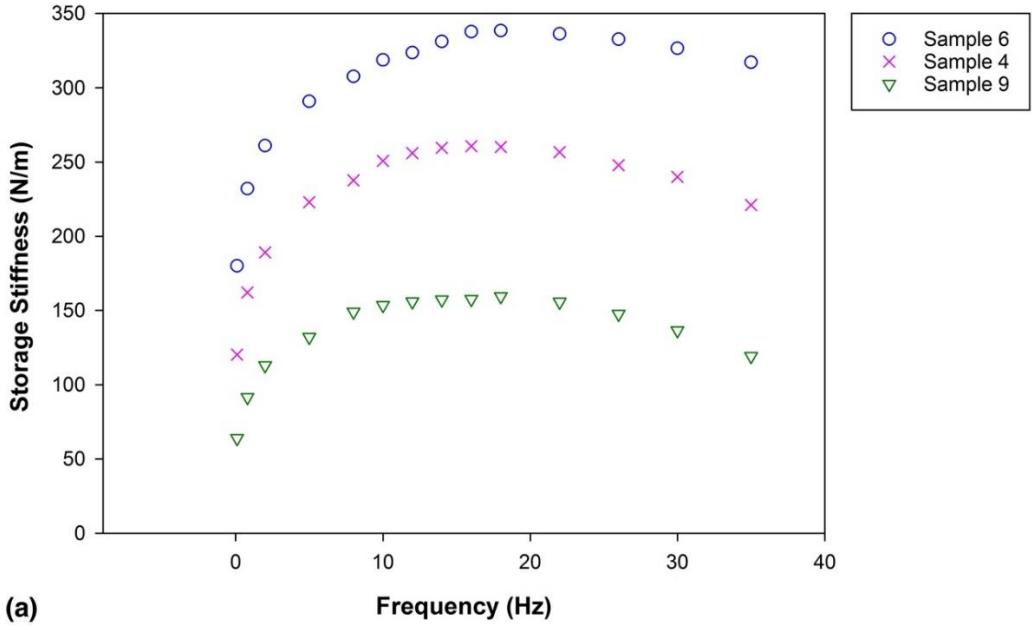

(a)

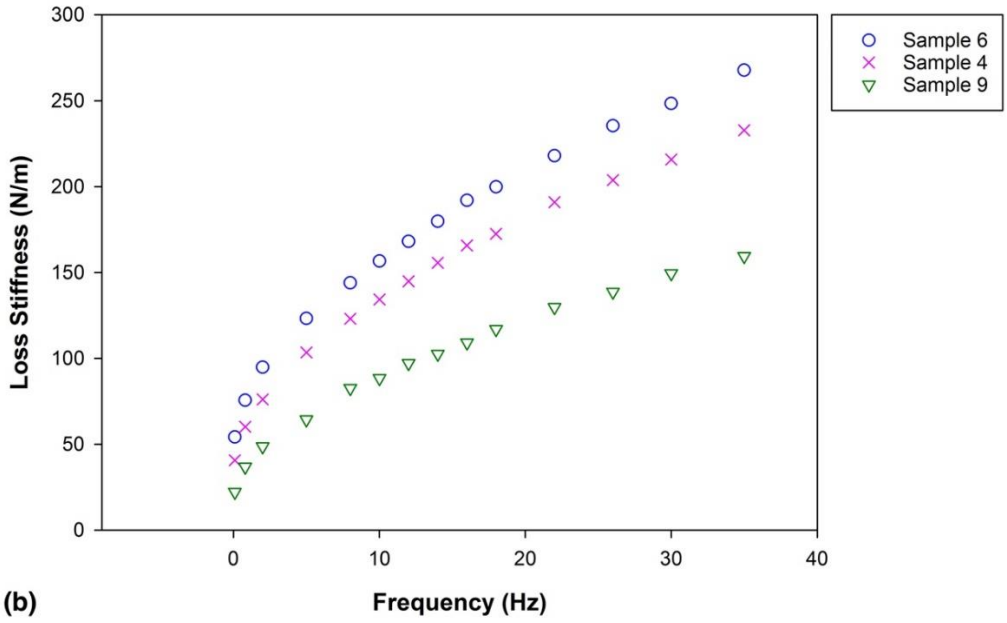

Figure 3.11 – Variation of stiffness with frequency for three individual samples from a single hemisphere tested using a 16 mm-diameter indenter and under a 20% specimen height mean displacement. (a) storage stiffness and (b) loss stiffness.

For specimens tested under various mean displacements, there was a statistically significant increase in storage stiffness ($p < 0.05$) of 1.6 (35 Hz) to 2.4 (0.1 Hz) times as the mean displacement increased from 10%h to 20%h (Figure 3.12). The loss stiffness with 20%h MD was significantly higher than with 10%h MD ($p < 0.05$) while there was no significant difference ($p > 0.05$) for other two pairs (i.e. 10%h and 15%h MD; 15% and 20% MD). For the average storage and loss stiffness, the mean displacement of 20%h (229.7 N/m and 140.3 N/m) was greatest, followed by the mean displacement of 15%h (171.2 N/m and 111.0 N/ m) and the mean displacement of 10%h (133.6 N/m and 87.4 N/m) had the lowest value. For the generation of standard deviation, it is one measurement on each of the ten brain samples to give ten measurements.

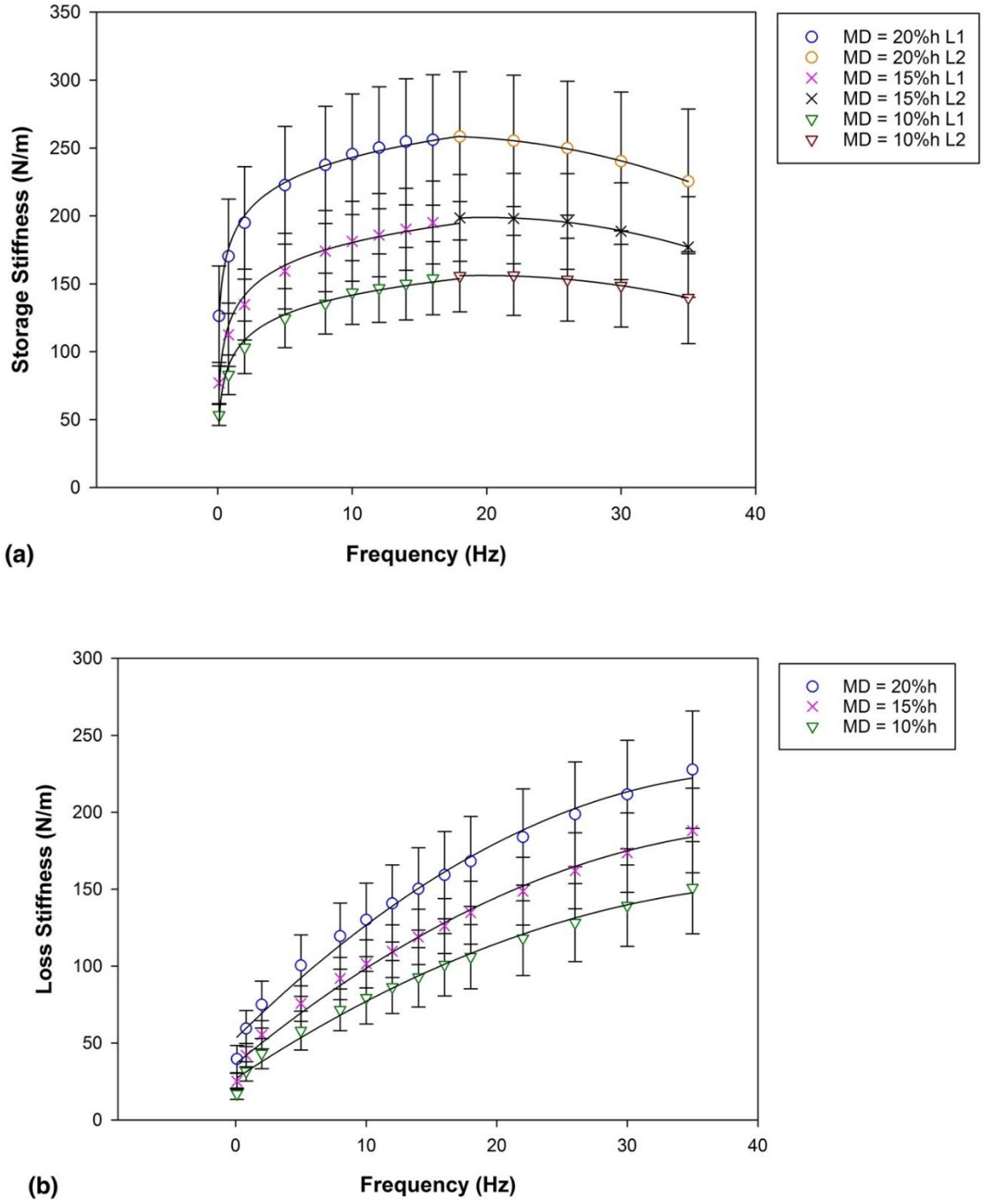

Figure 3.12 – Variation of stiffness with frequency for brain tissue tested under three different mean displacements of 10%, 15% and 20% of the specimen height with the 16 mm diameter indenter. (a) mean storage and (b) mean loss stiffness (N/m). In (a), L1 represents a logarithmic curve fit (Equation 3.6) from 0.1 to 18 Hz and L2 represents a second order polynomial fit (Equation 3.7) up to the end frequency sweep. In (b), a logarithmic curve (Equation 3.8) was fitted across all frequencies tested. Error bars represent standard deviation.

For specimens tested using varying indenter sizes, the average stiffness (Figure 3.13) against frequency follows the same trend of individual samples. The dynamic storage and loss stiffness response of brain tissue was dependent on the indenter size, increasing with indenter diameter ($p < 0.05$). The storage stiffness increased up to 258.4 N/m at a diameter of 16 mm, 144.2 N/m at a diameter of 12 mm and 67.9 N/m at a diameter of 8 mm and then experienced a decreasing trend at higher frequencies. The loss stiffness had an increasing trend across all tested frequencies from 39.6 N/m to 227.7 N/m at a diameter of 16 mm, 21.5 N/m to 123.0 N/m at a diameter of 12 mm and 10.2 N/m to 58.7 N/m at diameter of 8 mm. Increasing the indenter diameter led to an increase of stiffness (k' and k'') by 1.83 ± 0.05 (mean ± deviation) from D = 12 mm to D = 16 mm, 2.12 ± 0.04 from D = 8 mm to D = 12 mm and 3.88 ± 0.12 from D = 8 to D = 16 mm.

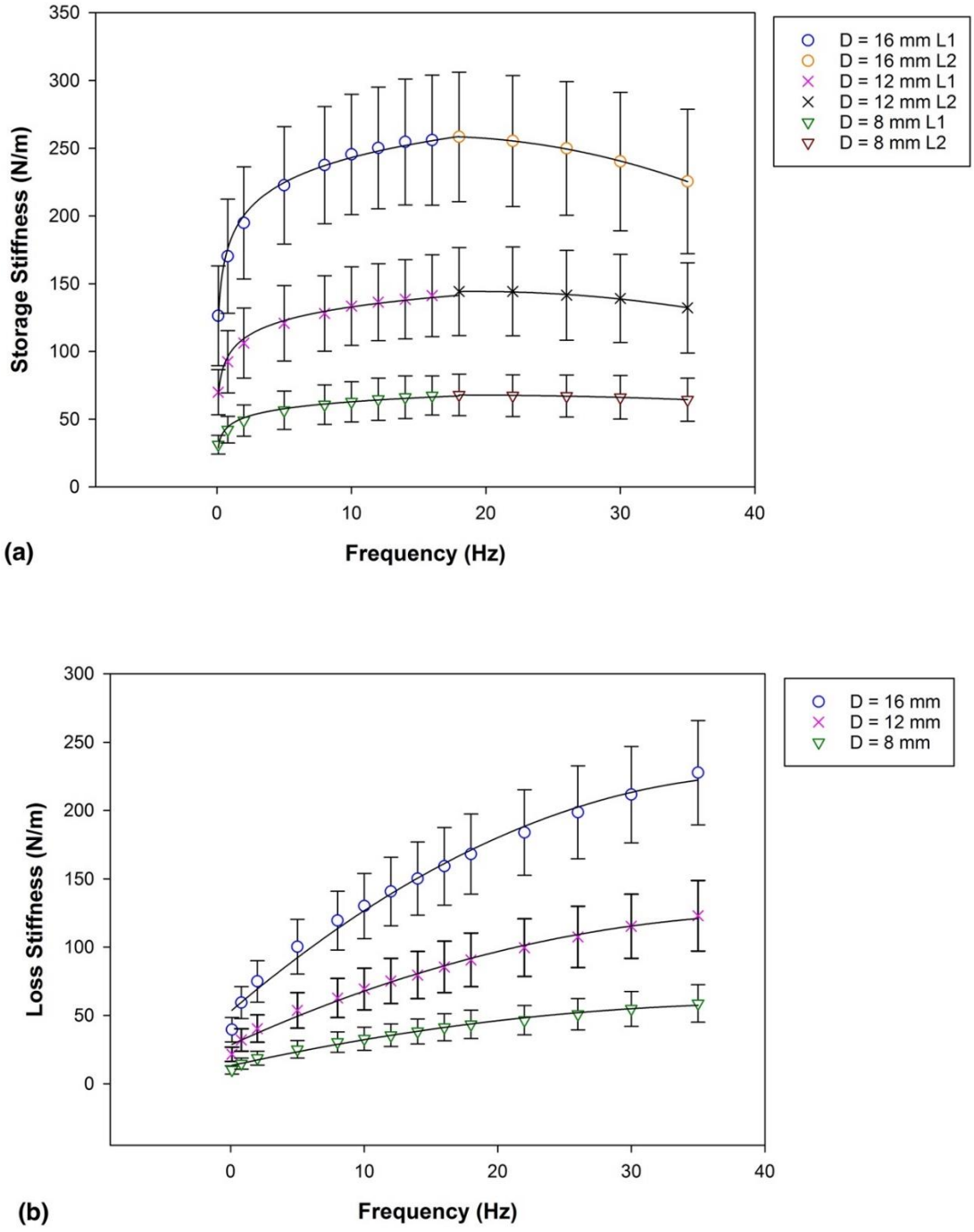

Figure 3.13 – Variation of stiffness with frequency of brain tissue tested under three indenter diameters of 16 mm, 12 mm and 8 mm with the mean displacement of 1.4 mm (20% of the specimen height). (a) mean storage and (b) mean loss stiffness (N/m). In (a), L1 represents a logarithmic curve fit (Equation 3.6) from 0.1 to 18 Hz and L2 represents a second order polynomial fit (Equation 3.7) up to the end frequency sweep. In (b), a logarithmic curve (Equation 3.8) was fitted across all frequencies tested. Error bars represent standard deviation.

Figure 3.14 shows the mean storage and loss moduli against frequency for all tested samples. The storage modulus increased up to 9.14 kPa with an average value of 8.09 kPa and loss modulus ranged between 1.38 kPa and 7.91 kPa with an average value of 4.85 kPa. The converted results of the average stiffness from brain specimens tested under three indenter diameters of 16 mm, 12 mm and 8 mm were not significantly different ($p > 0.05$).

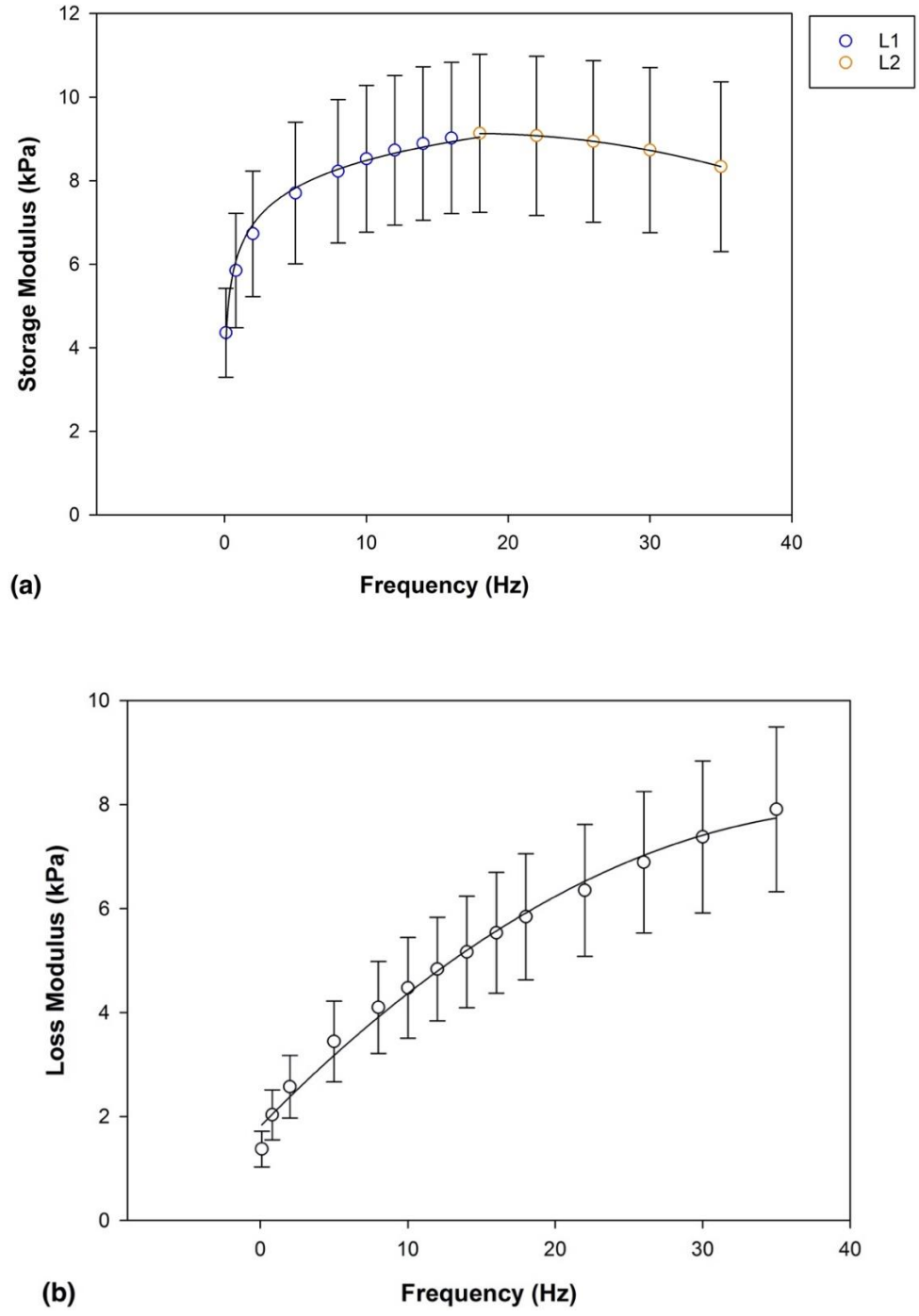

Figure 3.14 – Variation of modulus with frequency. (a) mean storage and (b) mean loss modulus (kPa) of brain tissue obtained from three indenter sizes with the mean displacement of 1.4 mm (20% of the specimen height). In (a), L1 represents a logarithmic curve fit (Equation 3.6) from 0.1 to 18 Hz and L2 represents a second order polynomial fit (Equation 3.7) up to the end frequency sweep. In (b), a logarithmic curve (Equation 3.8) was fitted across all frequencies tested. Error bars represent standard deviation.

From the samples tested, the mean $tan\delta$ (i.e. ratio of k''/k') of brain tissue showed an increasing trend with frequencies, ranging from 0.32 to 0.98 (Figure 3.15). No significant differences in $tan\delta$ were found for different diameters and mean indentations ($p > 0.05$).

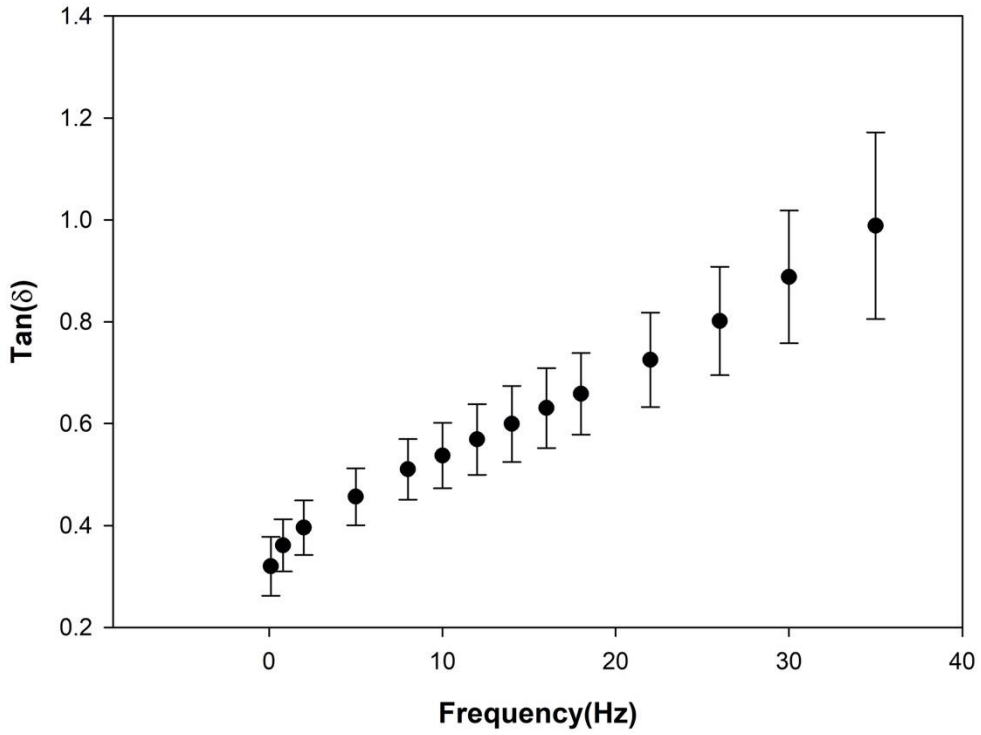

Figure 3.15 – Variation of *tan (δ)* with frequency for all the brain samples tested. Error bars represent standard deviation.

Table 3-2 – Curve fit results derived from mean stiffness against frequency plots of Figure 3.12 for three mean displacements and Figure 3.13 for three indenter diameters. Curve fit results also derived from mean storage and loss modulus against frequency plots of Figure 3.14 ($p \leq 0.05$ for all trends). Coefficients are in N/m for stiffness while they are in kPa for modulus.

Constant			Stiffness constants (N/m)						Modulus Constants
			Mean displacement (% of h)			Indenter diameter (mm)			
			10%h	15%h	20%h	8	12	16	(kPa)
A	Storage		20.61	24.15	26.57	7.37	14.57	26.57	0.95
B	Storage		94.23	124.79	181.91	45.91	99.36	181.91	6.29
		R^2	0.98	0.98	0.99	0.99	0.99	0.99	0.99
C	Storage		-0.069	-0.096	-0.092	-0.011	-0.048	-0.092	-0.003
D	Storage		2.73	3.82	2.91	0.38	1.83	2.91	0.089
F	Storage		129.39	160.79	235.76	64.61	126.85	235.76	8.36
		R^2	0.99	0.99	0.99	0.99	0.99	0.99	0.99
H	Loss		-0.063	-0.08	-0.102	-0.026	-0.052	-0.102	-0.003
I	Loss		5.66	7.02	8.39	2.16	4.46	8.40	0.30
J	Loss		26.83	36.38	52.96	13.23	28.39	52.96	1.82
		R^2	0.99	0.99	0.99	0.99	0.99	0.99	0.99

h, specimen height

3.4 Discussion

This chapter has presented work that used dynamic mechanical analysis under compression to demonstrate that brain tissue is viscoelastic with both storage and loss stiffness, and moduli, being frequency dependent. Further, the viscoelastic storage and loss stiffness are dependent on the indentation mean displacement and the indenter size, increasing with higher mean displacement and larger indenter diameters. The viscoelastic storage and loss moduli are independent on the indenter size. For all samples tested under different testing protocols, the trends for storage and loss stiffness were similar. Many other studies used the similar curve fit method to define viscoelastic material properties including heart chordae (Wilcox et al. 2014) and mitral valve (Baxter et al. 2017). In this study, the storage stiffness, and moduli of porcine brain showed an increasing trend at initial frequencies and then a decreasing trend at higher frequencies. This finding is consistent with previous results for porcine bladder (Barnes et al. 2015), mitral valve leaflet (Baxter et al. 2017), and human/porcine brain (Weickenmeier et al. 2018), for the latter magnetic resonance elastography (MRE) was performed to describe the material properties. Loss stiffness of porcine brain exhibited an increasing trend with frequency; a similar tendency has been found in brain tissue by dynamic testing in shear (Hrapko et al. 2006) and MRE methods (Guertler et al. 2018). In spite of differences in testing devices and experimental conditions, the general trends were consistent with previous studies. The dynamic stiffness properties (Figure 3.11) varied with frequencies for the three samples, dissected from the same cerebral hemisphere which implies sample variability.

The storage and loss stiffness of porcine brain tissue decreased with lower mean displacement of the indenter. The size of indenter significantly altered the storage and loss stiffness of brain tissue, both of which decreased with decreasing indenter diameter which can be found in bovine brain under indentation testing (Budday et al. 2015). Furthermore, the change of stiffness throughout the tested frequencies was significant. For brain samples tested under the three indenter diameters, the average minimum values of storage and loss stiffness were approximately 48% and 17% of the corresponding maximum values, which were consistent to three indenter diameters. For brain samples tested under three mean displacements, however, the change of stiffness varied from 48% to 34% and 17%–11% with lower mean displacement for storage and loss stiffness, respectively. This indicates that the mean displacement has a greater effect on the frequency-dependent trend of stiffness as compared to the indenter size.

The storage and loss modulus were derived from the relevant stiffness. Compared to stiffer biomaterials such as articular cartilage (Espino et al. 2014) in compression, adhesion in soft biological materials plays a significant role in contact mechanics affecting the impacting area and inducing mechanical errors (Carrillo et al. 2005; Kohn and Ebenstein 2013). To avoid this issue, a circular flat indenter was selected (Barnes et al. 2016; Budday et al. 2015) rather than a hemispherical indenter (Shepherd et al. 1999). When the custom-designed flat indenter was performed on brain tissue, the impacting area remains constant over the whole sinusoidal displacement range (Blum and Ovaert 2012; Cheng et al. 2000). As the thickness of each sample was controlled, the modulus of the specimen is considered to be inversely proportional to the

square of the indenter diameter and proportional to the specimen stiffness. Some previous studies (Budday et al. 2015; Liu et al. 2009a) have indicated that modulus is independent of the indentation depth where the contact stiffness assumed as the ratio of the linear stress-strain curve is constant. In DMA testing the strain-rate is continuously changing during oscillation at a frequency so the dynamic stiffness might vary with different indentation depth. A range of shape factors are available in literature for indentation studies (Delaine-Smith et al. 2016). Although different shape factors will alter the predicted values across studies, it is worth noting that as it is a constant any predicted trends are not affected within a study; instead, predictions between studies may be offset.

Many studies have measured mechanical properties for porcine brain tissue. Rashid found the elastic secant modulus to be 19–65.2 kPa (Rashid et al. 2012), Budday found the modulus of white matter tissue to be 1.604 kPa (Budday et al. 2015), while Miller found the instantaneous Young's modulus was 3.24 kPa (Miller et al. 2000). The average dynamic modulus through the frequency tested for the cylindrical samples in this study was 9.4 kPa that is comparable to the range studied by Tamura *et al.* where the initial elastic modulus was found to be between 5.7 and 23.8 kPa (Tamura et al. 2007). However, all of these studies were performed in the time domain (i.e. static stress-strain experiments) which are difficult to compare the results of this investigation because dynamic modulus obtained in the frequency domain is different to Young's modulus.

Many soft biological tissues have been tested under oscillatory shear methods to analyze the viscoelastic properties (Arbogast and Margulies 1997). In comparison to a study (Fallenst.Gt et al. 1969), where human brain tissue was tested in vitro at 9–10 Hz with shear storage modulus ranging between 0.6 and 1.1 kPa and loss modulus ranging between 0.35 and 0.6 kPa, the axial compressive moduli reported in this chapter were higher at comparable frequencies. However, any comparison is limited by the potential differences in loading protocols between shear and compression tests.

This study was based on the viscoelastic properties of brain which combined white and grey matter. There is future opportunity to investigate the regional variation of brain tissue under dynamic mechanical analysis. Indeed, some studies have found variation between the white and grey matter (Nicolle et al. 2004; Prange and Margulies 2002) and the interregional heterogeneities of brain tissue (Elkin et al. 2011). These are described in detail in section 2.2.3. However, the results presented in this chapter provide a useful measure of the mechanical behaviour of brain tissue. Average material properties of brain tissue have often been studied, e.g. by Rashid and Qian through compression (Rashid et al. 2012) and indentation tests (Qian et al. 2018), respectively. Generally, white matter with aligned fibre tracts is considered more anisotropic than grey matter.

Realistic viscoelastic properties of brain are important for the computational modelling of the brain. Finite element (FE) models of brain provide a non-invasive way to analyse the brain

response to head impacts (Koncan et al. 2019). The viscoelastic parameters as material constants in simulations were mostly taken from indentation (MacManus et al. 2017), stress-strain and stress relaxation tests (Cheng and Bilston 2007; Forte et al. 2017) where an N-term Prony series was used to fit the experimental data. The frequency-dependent properties of brain tissue are also important in FE simulations to analyse the mechanical response under dynamic loading. A comparison between time and frequency dependent properties of brain tissue in the previous literature is limited due to different experimental protocols (Chatelin et al. 2010), however, a recent study found that it is possible to predict the frequency-dependent properties based on experiments in the time domain (Zupančič 2018). A linear viscoelastic model was adopted to model biological tissues under cyclic loading, characterized by the storage and loss moduli. Further, methods to convert data from the frequency domain to time-domain are reported in literature (Bartolini et al. 2018); the maximum strain rate in this study ranges approximately between 7 and 14/s. Based on this approach, the frequency dependent values presented in this chapter could be used to fit viscoelastic constitutive models such as through Prony series representations following adaptation of the storage and loss moduli obtained to represent the mechanical behaviour of brain tissue.

A limitation of this study is that a small amount of geometric variability occurred when preparing samples. The extremely soft nature of brain tissue also leads to some deformation of specimens under their own weight during the preparation (Budday et al. 2017). However, the diameter of samples was measured using callipers prior to testing, this ensured that the resultant

moduli accounted for any variability in specimen shape during preparation. Further, the indenter sizes in this study are large enough to ensure the homogenous behaviour of tissue (Samadi-Dooki et al. 2018).

In this study, a freeze-thaw protocol has been used to store specimens. Although there are some limitations when comparing frozen to fresh soft biological tissue, the data from the results showed extensive overlap between the frozen and fresh samples (Clark 1973). Previous studies reporting tests on porcine liver (Wex et al. 2014), ligaments (Woo et al. 1986) and aortic specimens (O'Leary et al. 2014) revealed limited changes in mechanical properties of biological materials. Further, the method of freezing preservation including freezing temperature may be more critical to mechanical properties (Aidulis et al. 2002; Goh et al. 2010). In this study, the storage protocol of tissue at - 40 ◦C, consistent with established procedures to maintain initial stress-strain response of soft tissues (Baxter et al. 2017; Chow and Zhang 2011).

3.5 Chapter Summary

It can be concluded that porcine brain tissue shows frequency dependent-viscoelastic properties over the range of frequencies tested, 0.1–35 Hz. The experiments focus on the macrostructural mechanical response of brain tissue. Variation of viscoelastic properties with anatomical location, and white/grey matter was not the focus of this chapter. The storage stiffness exhibited a combination of a logarithmically increasing trend and a quadratic decreasing trend against frequency while the loss stiffness exhibited a quadratic increasing trend against frequency. The curve-fitted equations with parameters showed good correlation ($p < 0.05$ and $R^2 > 0.9$) to the experimental trends. The dynamic stiffness properties were affected by different indenter sizes and indentation depths. The storage and loss stiffness decreased with lower mean displacement of the indenter. The indenter with a larger diameter led to higher storage and loss stiffness while the storage and loss moduli were constant with a mean value of 8.09 kPa and 4.85 kPa, respectively. These findings could be used in diagnosis of traumatic brain injury and head simulations in frequency domain.

In the next chapter, the mechanical behaviour of brain tissue has been studied to characterize the regional and directional response of the tissue. In addition, the material parameters were obtained using a linear viscoelastic model, using a Prony series in the frequency domain and a numerical model to simulate the compressive mechanical behaviour of bovine brain tissue across a range of frequencies.

4 Dynamic mechanical characterization and viscoelastic modeling of bovine brain tissue

4.1 Introduction

Computational models can provide a non-invasive method by which to analyse brain injuries and predict the mechanical response of the tissue. The brain injuries are expected to be induced by dynamic loading, mostly in compression and measurement of dynamic viscoelastic properties are essential to improve the accuracy and variety of finite element simulations on brain tissue. The accuracy and variety of these computational models requires quantitative data from experiments and are also dependent on the constitutive models used within simulations.

Previous studies on brain tissue have investigated elastic modulus (Rashid et al. 2014) and the microstructural heterogeneity including white and grey matter (Budday et al. 2015) through stress-strain tests. It is important to understand the connection between the macroscopic mechanical behaviour and the regional microstructure for accurate prediction of injury across the brain structure. In addition, fibre orientation of white matter has been considered transversely isotropic because of the highly aligned axonal fibres (Feng et al. 2017). While mechanical properties of brain tissue have been characterized, the regional and directional effects on frequency-dependent viscoelastic properties have not been assessed by compressive DMA.

In this chapter, the frequency-dependent viscoelastic properties of bovine brain tissue were characterized using Dynamic Mechanical Analysis. The white matter (corona radiata and corpus callosum) and grey matter (cortex and basal ganglia) were investigated under compression over a range of loading frequencies to characterize the regional and directional properties. The storage and loss moduli were analysed, and a frequency-dependent constitutive model was calibrated using experimental data, to characterize the mechanical behaviour of brains.

4.2 Materials and Methods

4.2.1 Specimen Preparation

Eight bovine brains under 12 months of age, were obtained from a supplier (Samples for Schools https://www.samples-for-schools.co.uk/, UK). After delivery to the laboratory, the brain samples were wrapped in tissue paper and soaked in Ringer's solution (Oxoid Ltd, Basingstoke, UK). Samples were then stored at −40 °C in a freezer in double heat-sealed plastic bags (Lawless et al. 2017; Li et al. 2020). When the brains were required for testing, samples were taken out from the freezer and left in Ringer's solution for 12 hours ahead of dissection. From previous studies, freeze-thaw treatment does not change the mechanical properties of biological tissue (Chan and Titze 2003; Wex et al. 2014).

After the cerebellum and brainstem were removed, the cerebrum was cut in the coronal plane

using a surgical scalpel (Swann-Morton Limited, Sheffield, UK). To investigate the regional properties of brain tissue, the specimens were collected from the four locations of cerebrum including corona radiata and corpus callosum, cortex and basal ganglia (Figure 4.1). This categorization is consistent with previous studies (Budday et al. 2015; Budday et al. 2017). A circular trephine with the diameter of 8 mm was used through the anterior-posterior direction to extract homogeneous specimens into cylindrically shaped samples (Figure 4.2). Samples from the region of corpus callosum were extracted in the two orientations (i.e. (D1) orthogonal to nerve fibre bundles in the sagittal plane and (D2) aligned with the nerve fibre tracts in the coronal plane) to investigate the directional properties (Figure 4.3). The cerebral cortex is usually folded, and this circumvolution leads to a greater surface area for grey matter. The soft nature of brain tissue resulted in some deformation of specimens under their own weight during the preparation, which may have increased the variability of the dimension measured. Brain samples were 5 ± 0.5 mm (mean ± deviation) in thickness and 8 ± 0.1 mm in diameter, measured prior to testing using a Vernier calliper (Draper Tools Ltd, Hampshire, UK).

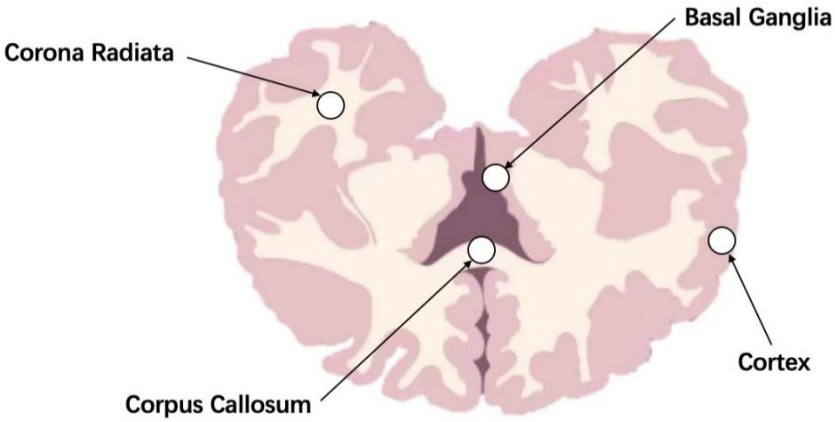

Figure 4.1 – Locations of specimen extraction from four brain regions, including corona radiata and corpus callosum, cortex and basal ganglia.

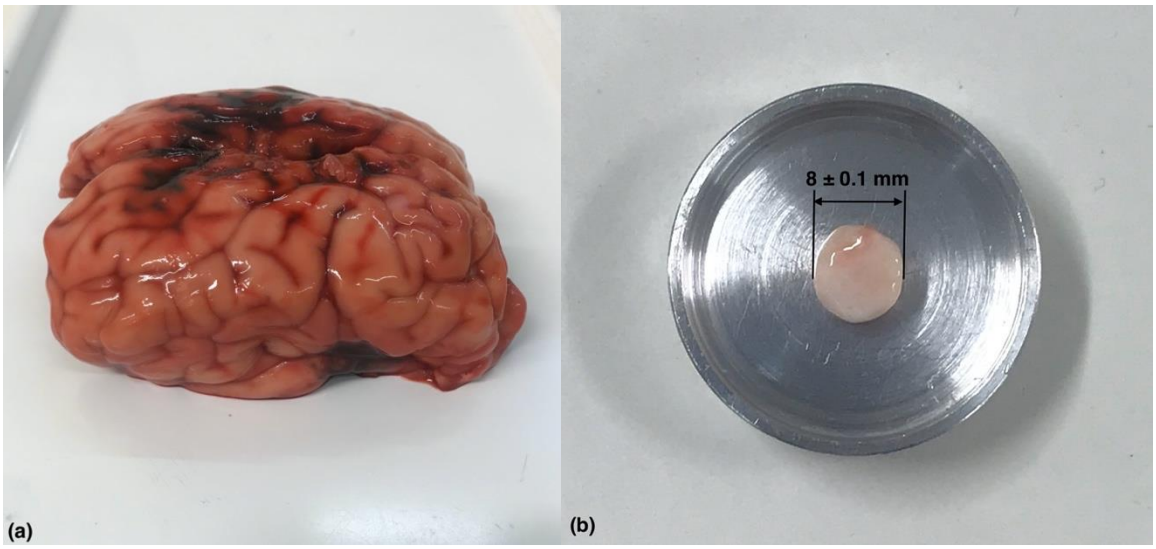

Figure 4.2 – (a) A bovine brain obtained for mechanical testing. (b) Representative brain specimen in cylindrical shape of 8 ± 0.1 mm diameter.

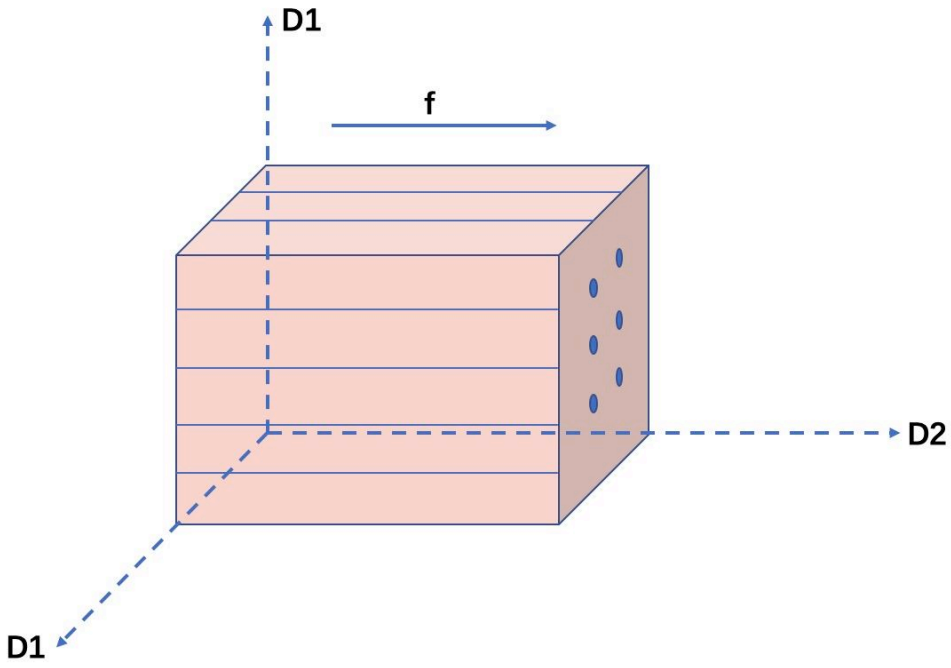

Figure 4.3 – Schematic graphic of loading direction. Samples from the region of corpus callosum were tested orthogonal to nerve fibre direction D1 and aligned with the nerve fibre tracts D2. Vector f represents the nerve fibre direction.

4.2.2 Preliminary Testing

In chapter 3, the porcine brains were tested to determine the general mechanical behaviour in macroscope where the brain samples were mixture of white and grey matter. As the experiments in this chapter were designed to investigate the mechanical behaviour of brain tissue regarding regional and directional properties, the type of specimens, locations and orientation were delicately considered. The bovine brains were larger than porcine brains and the mass of bovine brains was approximately 400 g being almost twice that of porcine brains generating a greater area which could be seen clearly during the dissection. It was then selected as the material to extensively determine the brain mechanical properties. A circular trephine with a diameter of 8

mm was used to extract specimens. Previous studies performed similar cutting protocols to obtain the specific brain samples on porcine (Li et al. 2019) and human brain (Budday et al. 2017) with comparable diameters.

Using DMA, a sinusoidal deformation was applied on the samples and in order to accurately characterize dynamic mechanical properties, the material samples were required to be deformed at an amplitude which is within the linear viscoelastic region. Before a sequence of dynamic mechanical tests on brain samples was undertaken, amplitude sweep tests were performed to determine the linear region. In the sweep test, the frequency of the test was fixed at 1 Hz and the amplitude is incrementally increased from 10 μm to 90 μm in steps of 10 μm. To analyze the linear viscoelastic region, the storage modulus was plotted against the amplitude (Figure 4.4) and the end of the linear region was found when the initial storage modulus changes by 5 %. The same method has been used in various other studies (Jiang and Lu 2009; Kaboorani and Blanchet 2014) to determine the LVR of viscoelastic materials.

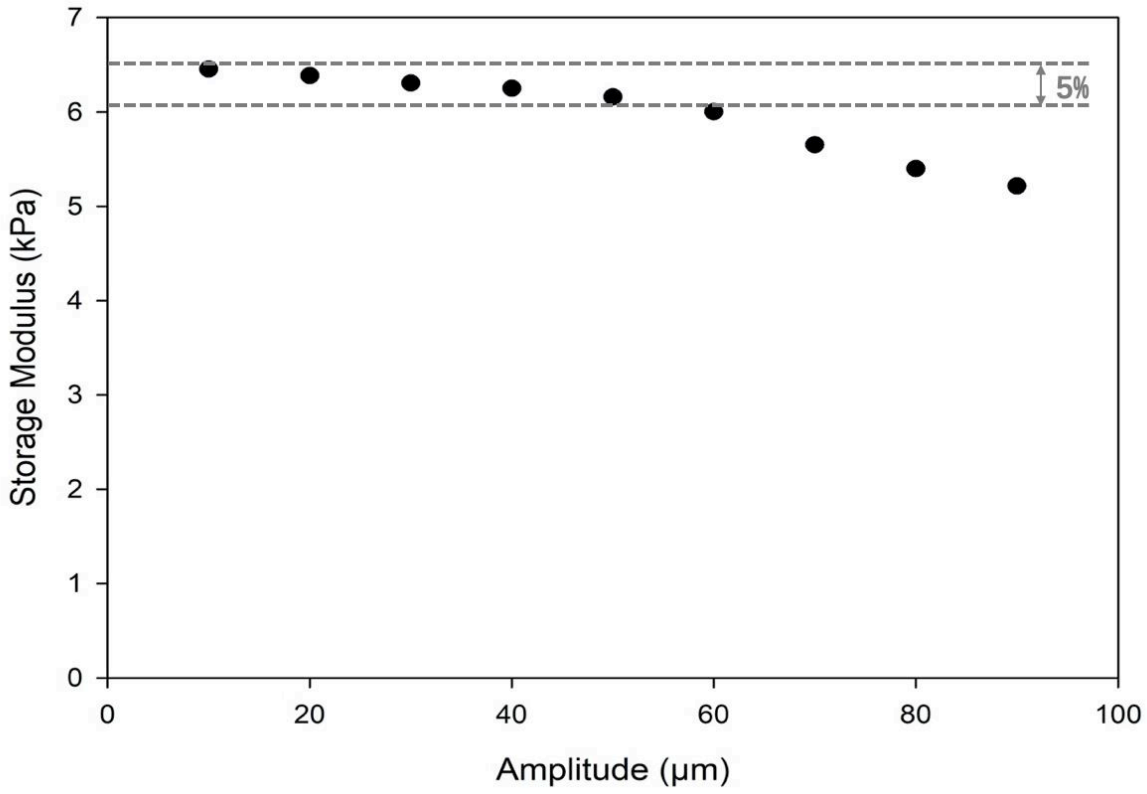

Figure 4.4 – Representative storage modulus of brain tissue tested against amplitude which is as the control variable.

Figure 4.4 shows the typical result of storage modulus versus amplitude for brain tissue. When the amplitude increased to 60 μm, the corresponding storage modulus was below the 5% line from the initial value. So, in the following mechanical tests on brain samples, the amplitude was chosen as 50 μm. Within the linear viscoelastic region, the response of the material was considered to be independent of the magnitude of the deformation and the structure of a material was assumed to be undamaged.

4.2.3 Dynamic Mechanical Analysis Frequency Sweep

The Bose testing machine was equipped with a 225 N load cell with a resolution of 0.002 N and a high accuracy displacement sensor with a resolution of 0.001 mm. A Fast Fourier Transform (FFT) was used to analyse the displacement sine wave input and load sine wave output. The phase angle (δ) was determined as the phase relationship between the force and displacement and the software calculates the dynamic stiffness (k^*). The WinTest DMA software calculated storage (E') and loss (E'') modulus by converting the relevant stiffness and phase data through a shape factor (S) as shown in Equation 4.1 and Equation 4.2. The shape factor for cylindrical specimens was calculated from Equation 4.3. The method the software used is described in detail in section 2.3.5. To measure how energy dissipates in the tissue structure, the tan delta ($tan\delta$) as the ratio of loss to storage modulus (E''/E') was calculated for every frequency at different brain regions. The viscous response of a material increases with greater E''/E' ratio in a system.

$$E' = \frac{k^* \cos \delta}{S} \qquad \text{Equation 4.1}$$

$$E'' = \frac{k^* \sin \delta}{S} \qquad \text{Equation 4.2}$$

$$S = \frac{\pi d^2}{4h} \qquad \text{Equation 4.3}$$

where d is the diameter and h is the thickness of a specimen.

4.2.4 Experimental Setup

The specimens were placed in the sample holder after dissection and preparation (Figure 4.5). Amplitude sweep tests were performed at 1 Hz for about 680 cycles to determine the amplitude range within the linear viscoelastic region of the material, followed by the subsequent mechanical tests. All samples were compressed with a mean displacement of 1 mm (20% of a specimen height) using a circular flat indenter, followed by a sinusoidally varying displacement with an amplitude of 0.05 mm (i.e. between 0.95 and 1.05 mm), across a frequency sweep between 0.5 and 35 Hz in 12 steps for approximate 5000 cycles. The range of frequencies is relevant to the strain rates comparable with previous studies on bovine (Cheng and Bilston 2007), porcine (Prange and Margulies 2002) and human brains (Forte et al. 2017). Prior to the data collection procedure, a preload of 10 mN was initially applied to specimens to ensure a zero configuration and a preconditioning cycle of 1 Hz with 0.05 mm amplitude was then performed to stabilize the samples (Ohman et al. 2009). All tests were performed at room temperature with the sampling rate of acquisition at 5 kHz for the highest frequency tested. A total of 96 brain samples were tested from four locations containing 23 corona radiata samples, 32 corpus callosum samples, 20 basal ganglia samples and 21 cortex samples (Table 4-1). The specimens were hydrated with Ringer's solution before each test to minimize the friction between the compressed platen and the brain samples. During preliminary investigations the order of the tested frequencies did not alter the measured mechanical properties.

Figure 4.5 – Experimental setup for the compressive DMA of bovine brain tissue specimens.

Table 4-1 – Test matrix for the dynamic compression of the brain specimens.

	Location	Direction	Number of tissue specimens tested
White matter	Corona radiata	D1	23
	Corpus callosum	D1	22
		D2	10
Grey matter	Basal ganglia	D1	20
	Cortex	D1	21

4.2.5 Data Analysis

To determine the effect of the regionally and directionally frequency-dependent behaviour of brain tissue, Sigmaplot Version 14.0 (Systat Software Inc., London, UK) was used to perform the statistical comparisons. For the generation of error bars, it is one measurement on each sample. For each measurement, a frequency sweep was performed in 12 steps for approximate 5000 cycles providing the values of storage and loss modulus at each tested frequency. Storage and loss modulus and phase angle were compared at each frequency. A one-way analysis of variance (ANOVA) was performed to investigate significant differences. When ANOVA showed a statistically significant difference ($p < 0.05$), a Tukey HSD post-hoc analysis was used for all pairwise comparisons between various brain regions and directions in compressive DMA testing. The results for all analysis were considered statistically significant with a probability value of less than 0.05.

4.2.6 Constitutive Modeling

For viscoelastic materials, the deviatoric stress is not linearly related to the deviatoric strain. To characterize the viscoelastic behaviour of brain tissue, linear viscoelastic (LV) theory was applied to model the strain rates of brain injury (Qian et al. 2018) or combined with other constitutive laws (Forte et al. 2018; Wang and Sarntinoranont 2019). The linear viscoelastic model can be effectively conducted in commercial Finite Element software with the experimental parameters. In a range of small deformations, the stress in this model was obtained

by the following constitutive formulation based on the Boltzmann's superposition integral (Boltzmann 1878).

$$\sigma(t) = \int_{-\infty}^{t} u(t-\tau)\frac{d\varepsilon}{d\tau}d\tau \qquad \text{Equation 4.4}$$

where σ is the deviatoric stress tensor, ε is the deviatoric strain tensor and *u(t)* is the linear relaxation modulus. In this equation, the strain *ε(t)* is considered to be zero for t $\leqslant$ 0, and it could be transferred in the Laplace form by assuming the imaginary variable *s* to *jω* as:

$$u^*(j\omega) = s\hat{u}(s) = \frac{\hat{\sigma}(s)}{\hat{\delta}(s)} = \frac{\hat{\sigma}(j\omega)}{\hat{\delta}(j\omega)} \qquad \text{Equation 4.5}$$

where $\hat{u}, \hat{\sigma}$ and $\hat{\delta}$ are relaxation modulus, stress and strain tensor in the Laplace domain, respectively. ω is a single angular frequency, the real part relevant to the actual force and $j = \sqrt{-1}$ standing for the imaginary number. $u^*(j\omega)$ is the complex modulus which can be given by the dynamic storage u' and loss u'' modulus as:

$$u^* = u' + ju'' \qquad \text{Equation 4.6}$$

In the physical models, a discrete relaxation function is considered with the expression as a discrete set of exponential decays defined in Equation 4.7. Using this discrete function with Equation 4.4 to Equation 4.6, the complex modulus can be defined from Equation 4.8. Further, the dynamic storage and loss modulus of the generalized Maxwell model can be obtained as given by Equation 4.9 and Equation 4.10 in the Prony series form.

$$u(t) = u_e + \sum_{i=1}^{N} g_i \exp\left(-t/\tau_i\right) \quad \text{Equation 4.7}$$

$$u^*(j\omega) = u_e + \sum_{i=1}^{N} g_i \frac{\tau_i j\omega}{1 + \tau_i j\omega} \quad \text{Equation 4.8}$$

$$u'(\omega) = u_e + \sum_{i=1}^{N} g_i \frac{(\omega\tau_i)^2}{1 + (\omega\tau_i)^2} \quad \text{Equation 4.9}$$

$$u''(\omega) = \sum_{i=1}^{N} g_i \frac{\omega\tau_i}{1 + (\omega\tau_i)^2} \quad \text{Equation 4.10}$$

where the *N* relaxation modes are determined by the corresponding Prony constants g_i and retardation times constants τ_i. u_e is the equilibrium modulus.

The nonlinear least square method is an optimization technique that can be used to build regression models with nonlinear features, and it has been previously carried out when analysing brain mechanical behaviour (Budday et al. 2017; Cheng and Bilston 2007). Compared to linear least squares method, nonlinear regression is much more flexible in the shapes of the curves fitted. To estimate the parameters of a frequency dependent discrete relaxation function showing nonlinear features, a non-linear least squares algorithm was conducted, and the optimization constraint were iteratively updated until the coefficients of the Prony coefficients g_i and retardation times τ_i converged with optimality tolerance of three decimal accuracy. The average experimental results for various regions or directions were used to calibrate the constitutive models based on the average square of deviation between the

predicted dynamic modulus and the measured dynamic modulus from experiment through Equation 4.11. The long-term modulus was obtained from the preliminary studies with low frequency testing conditions. The Prony coefficients g_i and retardation times τ_i were initially assumed, based on the exponentially ascending order of the control variables. A minimum of three pairs of Prony constants were required to represent the viscoelastic behavior of the brain tissue (Cheng and Bilston 2007) and from the preliminary studies, a four term Prony series was needed for these frequency-dependent linear viscoelastic models (Miller 1999):

$$\min(g,\tau) = \sum_{k=1}^{M}\left\{\left(\frac{u'(\omega_k)}{\tilde{u}'_k} - 1\right)^2 + \left(\frac{u''(\omega_k)}{\tilde{u}''_k} - 1\right)^2\right\} \qquad \text{Equation 4.11}$$

where $u'(\omega_k)$, $u''(\omega_k)$ are the calculated values from Equation 4.9 and Equation 4.10, and $\tilde{u}'_k$, $\tilde{u}''_k$ are the measured data at M frequencies ω_k. The goodness of fit of data to the given model was assessed using the coefficient of determination R^2.

The mean frequency-dependent behaviour of brain tissue for different regions and orientations was each simulated in COMSOL Multiphysics 5.5 (COMSOL, Stockholm, Sweden). The FE axisymmetric models were created using a cylindrical geometry with the average diameter and height of tested samples (8 mm in diameter, 5 mm in height), as shown in Figure 4.6. A mesh convergence analysis was conducted to validate the mesh density with the final mesh size of 0.2 mm. The top and bottom platens were modelled as rigid surfaces. The contact analysis between the platens and brain tissue specimens was performed in the simulation and the

relevant friction coefficient of 0.1 in the lateral direction was adopted, which is within the range estimated for the soft tissue (Rashid et al. 2012). A Poisson's ratio of 0.49 for an incompressible material was selected to avoid any singularity conditions during the FE implementation (Maikos et al. 2008). The brain specimens were compressed by the top platen, subsequently followed by a harmonic perturbation of 0.05 mm over a range of frequencies, 0.5–35 Hz, while the bottom platen was set as a fixed constraint.

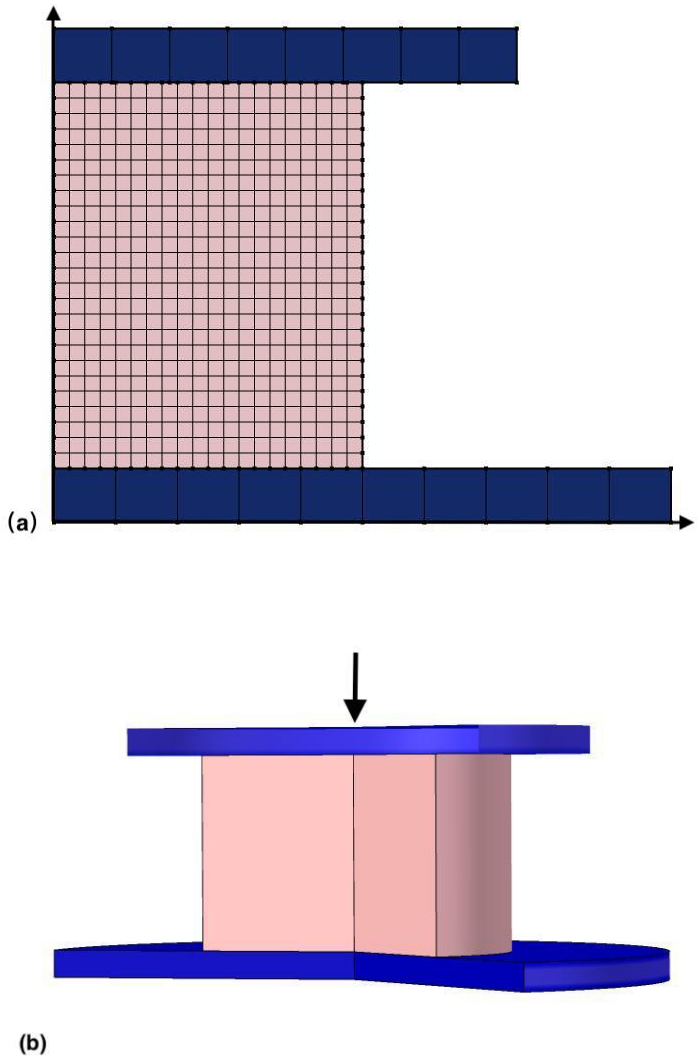

Figure 4.6 – Numerical simulation of the brain specimens under dynamic compressive testing in (a) FE axisymmetric and (b) partial revolution 2D configurations to easily identify the cross-section.

4.3 Results

4.3.1 Regional Dependency of Viscoelasticity

The mean storage and loss modulus of brain specimens showed an increasing trend with increasing frequency (Figure 4.7 (a) and (b)) for the different regions; the average loss modulus was lower than storage modulus for each tested frequency. To determine the regional properties of brain tissue, the data lines for corpus callosum region were derived from both D1 and D2 orientations while for other regions, the data lines were derived from D1 orientation. The tested specimens from the corpus callosum showed the greatest mean storage and loss modulus (18.19 kPa and 7.82 kPa, respectively) over frequencies, followed by the specimens from the corona radiata (12.28 kPa and 6.08 kPa, respectively). The specimens tested from the cortex had marginally higher mean storage and loss modulus (8.86 kPa and 3.85 kPa, respectively) than from the basal ganglia with a lowest value of 7.05 kPa and 3.02 kPa, respectively.

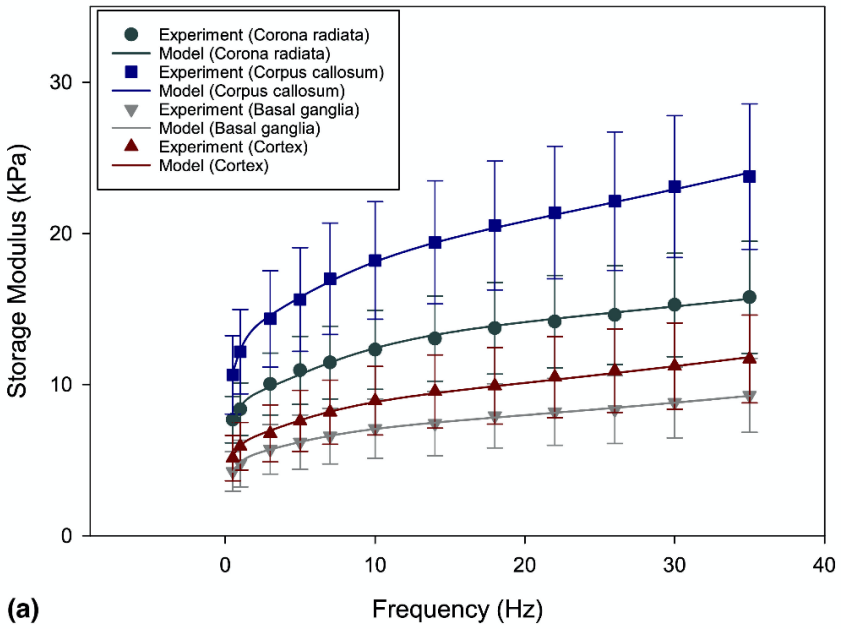
Experiment (Corona radiata)
Model (Corona radiata)
Experiment (Corpus callosum)
Model (Corpus callosum)
Experiment (Basal ganglia)
Model (Basal ganglia)
Experiment (Cortex)
Model (Cortex)
Storage Modulus (kPa)
0
10
20
30
0
10
20
30
40
Frequency (Hz)

(a)

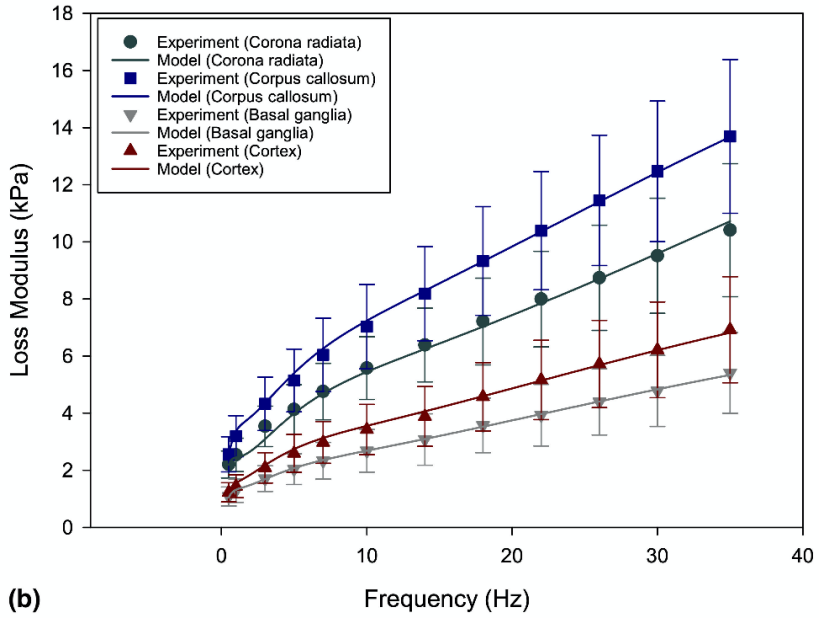
Experiment (Corona radiata)
Model (Corona radiata)
Experiment (Corpus callosum)
Model (Corpus callosum)
Experiment (Basal ganglia)
Model (Basal ganglia)
Experiment (Cortex)
Model (Cortex)
Loss Modulus (kPa)
0
2
4
6
8
10
12
14
16
18
0
10
20
30
40
Frequency (Hz)

(b)

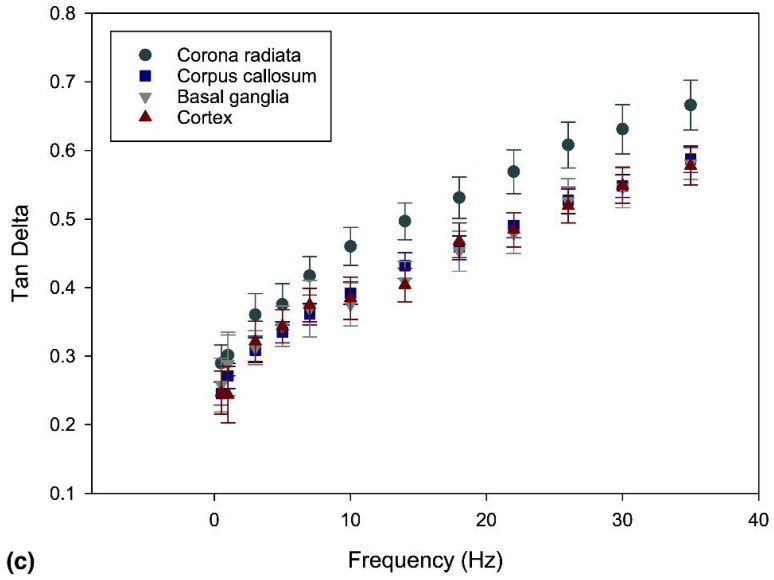

Figure 4.7 – Frequency-dependent viscoelastic properties for brain tissue tested from the different regions of corona radiata, corpus callosum, basal ganglia and cortex. Mean (a) storage and (b) loss modulus, against frequency from experiments with relevant linear viscoelastic model predictions and the trendlines are data predicted following simulations which were solved at loading frequencies from 0.5 Hz up to 35 Hz in incremental steps of 0.1 Hz; (c) mean tan delta against frequency. Error bars represent 95% confidence intervals.

The storage and loss modulus in the corpus callosum were significantly greater ($p < 0.05$) than in the basal ganglia and the cortex across all frequencies tested; the moduli in the basal ganglia and the cortex were not significantly different from each other. There was also no significant difference between the storage and loss modulus in the corona radiata and the corpus callosum ($p > 0.05$); however, from the frequency of 7 Hz a significant difference of storage modulus was considered between them (Figure 4.8 (a) and (b)). For all increments of frequencies, the storage modulus in the corona radiata, the cortex and the basal ganglia was not significantly different, while the loss modulus in the corona radiata was significantly larger than in the basal ganglia.

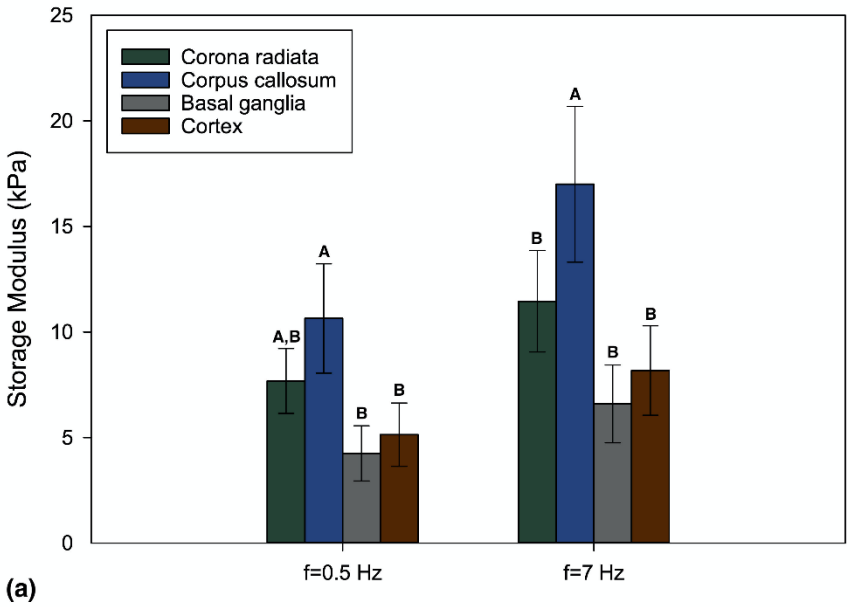
Storage Modulus (kPa)
25
20
15
10
5
0
Corona radiata
Corpus callosum
Basal ganglia
Cortex
A,B
A
B
B
B
A
B
B
f=0.5 Hz
f=7 Hz

(a)

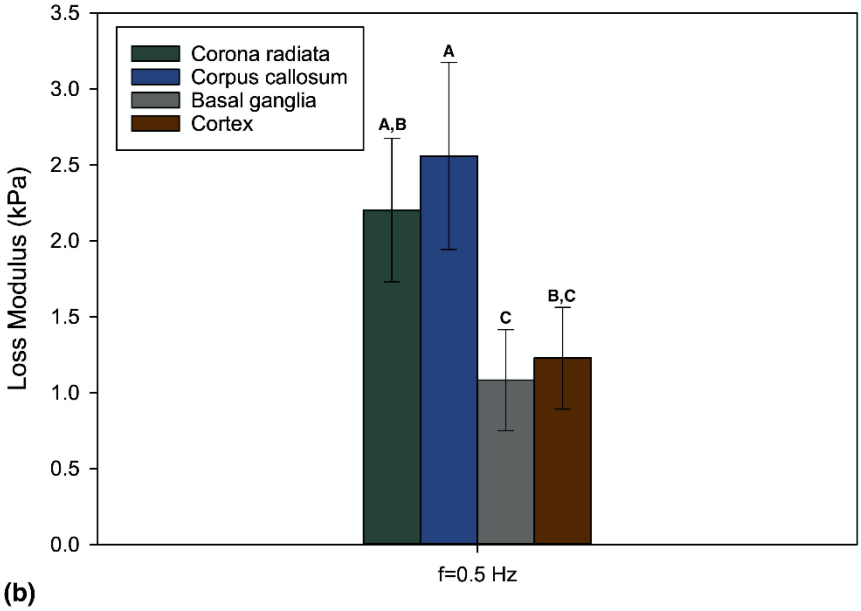
Loss Modulus (kPa)
3.5
3.0
2.5
2.0
1.5
1.0
0.5
0.0
Corona radiata
Corpus callosum
Basal ganglia
Cortex
A,B
A
C
B,C
f=0.5 Hz

(b)

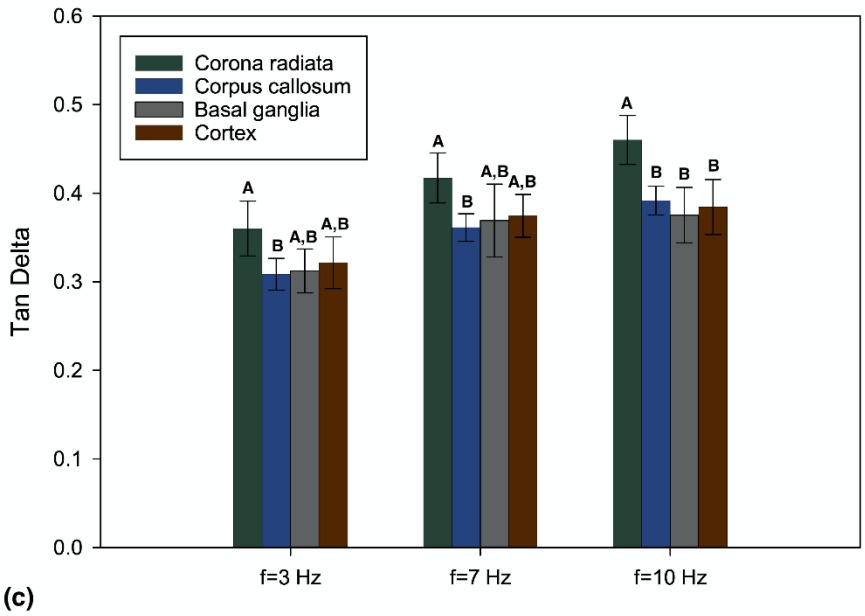

Figure 4.8 – Grouped vertical bars of frequency-dependent viscoelastic properties (mean ± 95% confidence intervals) for brain tissue tested from the different regions of corona radiata, corpus callosum, basal ganglia and cortex. The statistical results (a) the storage modulus showed the two types of significant differences i.e. from 0.5 to 7 Hz and up to the end frequency sweep, (b) the loss modulus showed the same significant differences of regions over all frequencies tested; (c) the tan delta indicated significant differences were only found at 3 and 7 Hz; however, at the other frequency increments from 10 Hz there were the same significant differences of regions. In each regional group, viscoelastic properties not sharing a letter are considered to be significantly different (Tukey HSD).

From the specimens tested, the average tan delta (i.e. ratio of E''/E') of brain tissue for each region showed an increasing trend with increasing frequency (Figure 4.7 (c)). The corona radiata exhibited the greater viscous behaviour with the $tan\delta$ ranging from 0.29 ± 0.03 (mean ± 95 % confidence intervals) to 0.67 ± 0.04; other regions showed a similar ability to dissipate energy with a mean value of around 0.41 across all frequencies. For the brain specimens tested below 10 Hz, the significant differences were only found between the tan delta in the corona radiata and the corpus callosum ($p < 0.05$) at 3 and 7 Hz, respectively. From the frequency of

10 Hz, the tan delta in the corona radiata was significantly greater than in other regions (Figure 4.8 (c)).

4.3.2 Directional Dependency of Viscoelasticity

The effect of the nerve fibre direction on frequency-dependent viscoelastic properties was investigated. The viscoelastic storage and loss moduli exhibited an increasing trend with frequencies for different directions. The brain specimens from corpus callosum tested orthogonal to the fibres (D1) showed a slightly lower mean storage and loss modulus (Figure 4.9 (a) and (b)). For the dynamic viscoelastic behaviour of brain specimens, no significant directional dependency on the storage modulus was revealed over all frequencies tested while the loss modulus was found significantly larger at 1.8 to 1.6 times (Figure 4.10 (a) and (b)) for specimens tested aligned to the fibre tracts (D2) below the frequency of 7 Hz ($p < 0.05$). The trend of tan delta was consistent with the specimens tested in different nerve fibre orientations (Figure 4.9 (c)) and no significant differences ($p > 0.05$) were found over the frequency range tested (Figure 4.10 (c)).

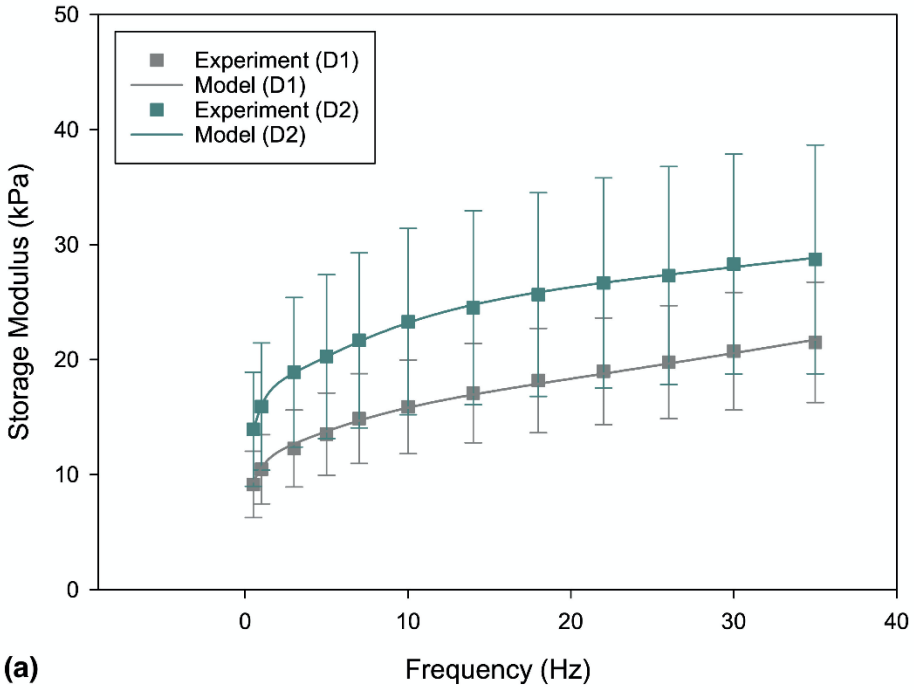
Experiment (D1)
Model (D1)
Experiment (D2)
Model (D2)
Storage Modulus (kPa)
0
10
20
30
40
50
0
10
20
30
40
Frequency (Hz)

(a)

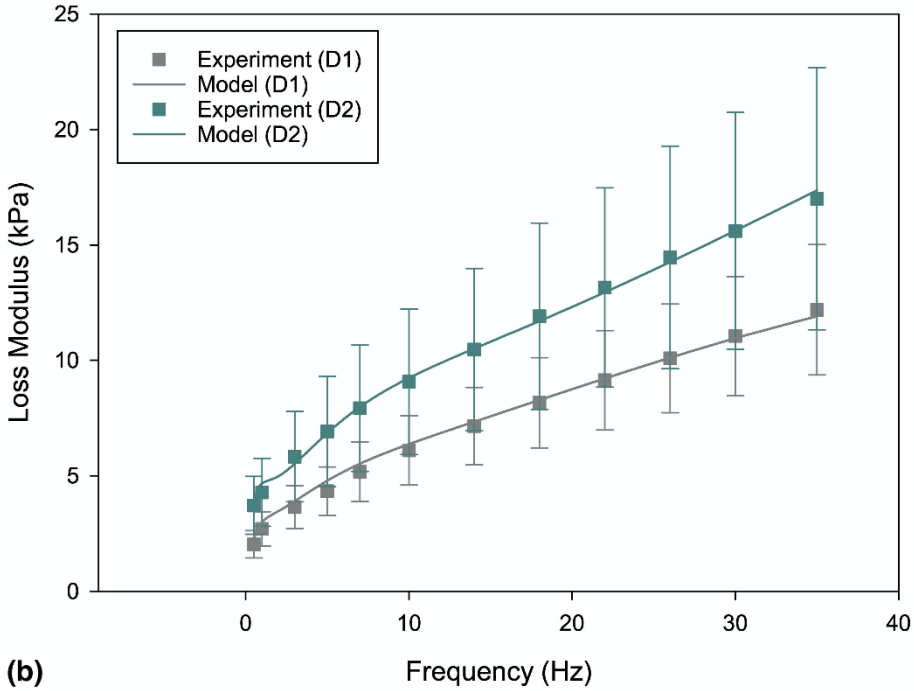
Experiment (D1)
Model (D1)
Experiment (D2)
Model (D2)
Loss Modulus (kPa)
0
5
10
15
20
25
0
10
20
30
40
Frequency (Hz)

(b)

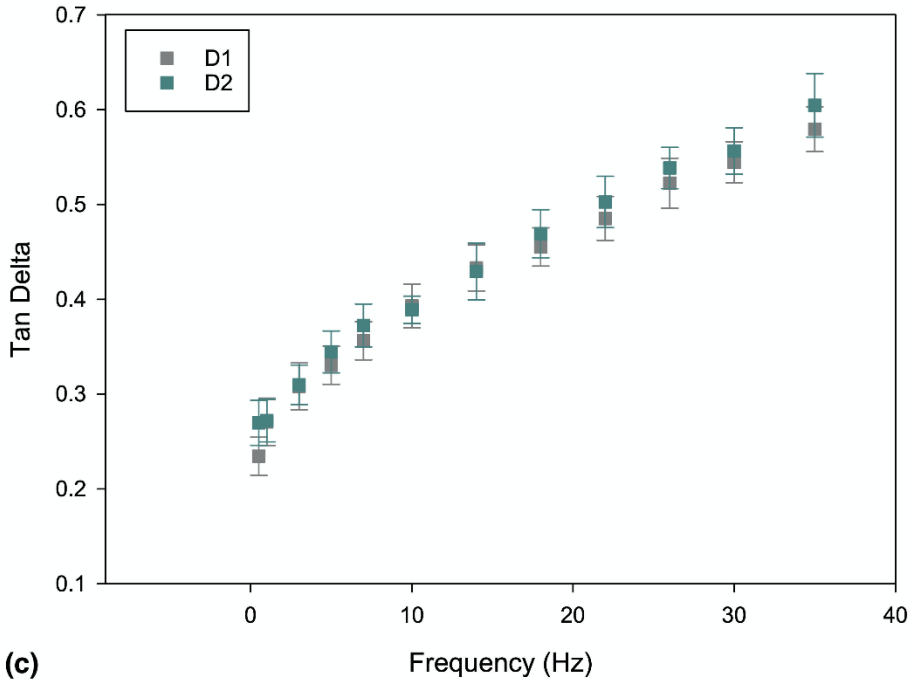

Figure 4.9 – Frequency-dependent viscoelastic properties for brain tissue tested from the different directions: orthogonal to nerve fibre bundles (D1) and aligned with the nerve fibre tracts (D2). Mean (a) storage and (b) loss modulus, against frequency from experiments with relevant linear viscoelastic model predictions and the trendlines are data predicted following simulations which were solved at loading frequencies from 0.5 Hz up to 35 Hz in incremental steps of 0.1 Hz; (c) mean tan delta against frequency. Error bars represent 95% confidence intervals.

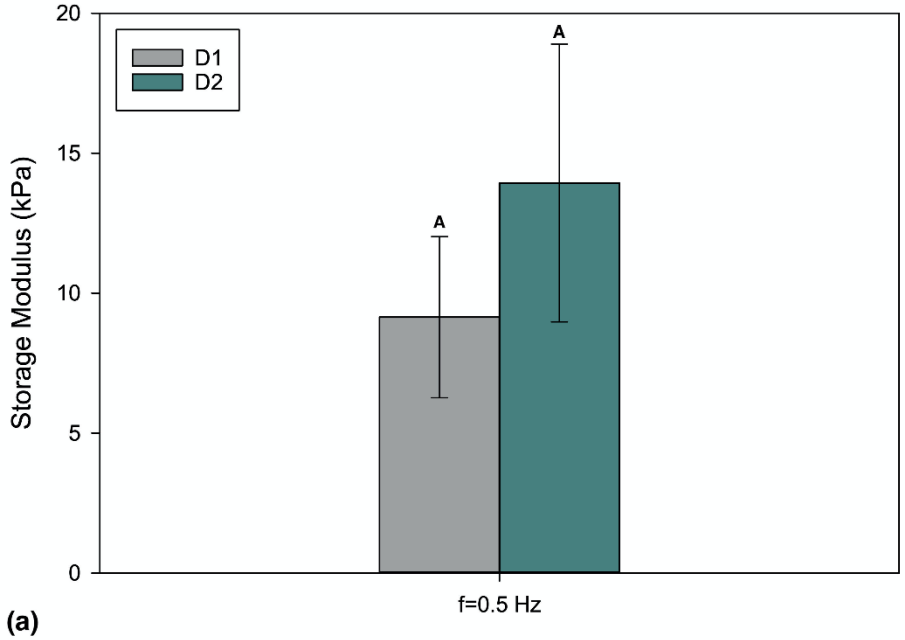
20
15
10
5
0
Storage Modulus (kPa)
D1
D2
A
A
f=0.5 Hz

(a)

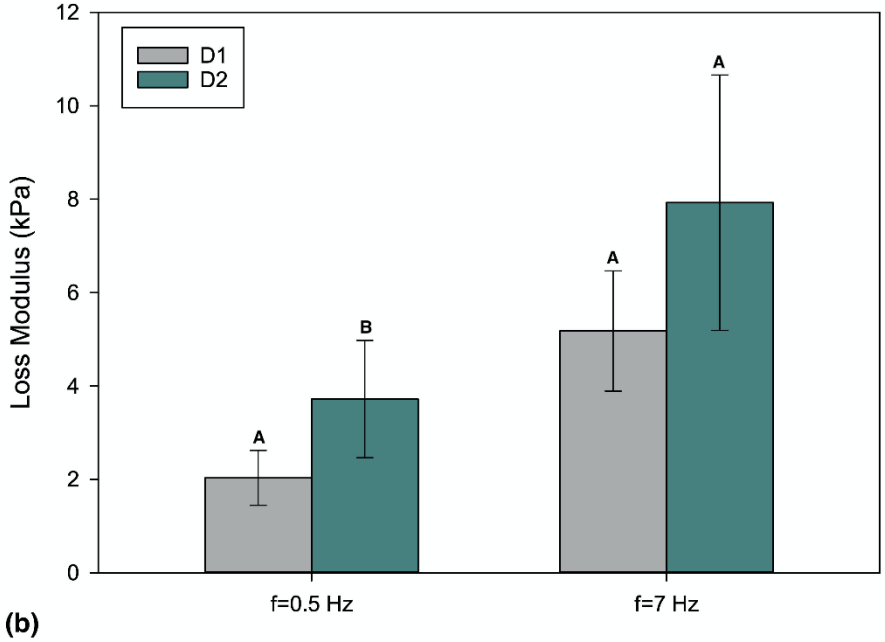
12
10
8
6
4
2
0
Loss Modulus (kPa)
D1
D2
A
B
A
A
f=0.5 Hz
f=7 Hz

(b)

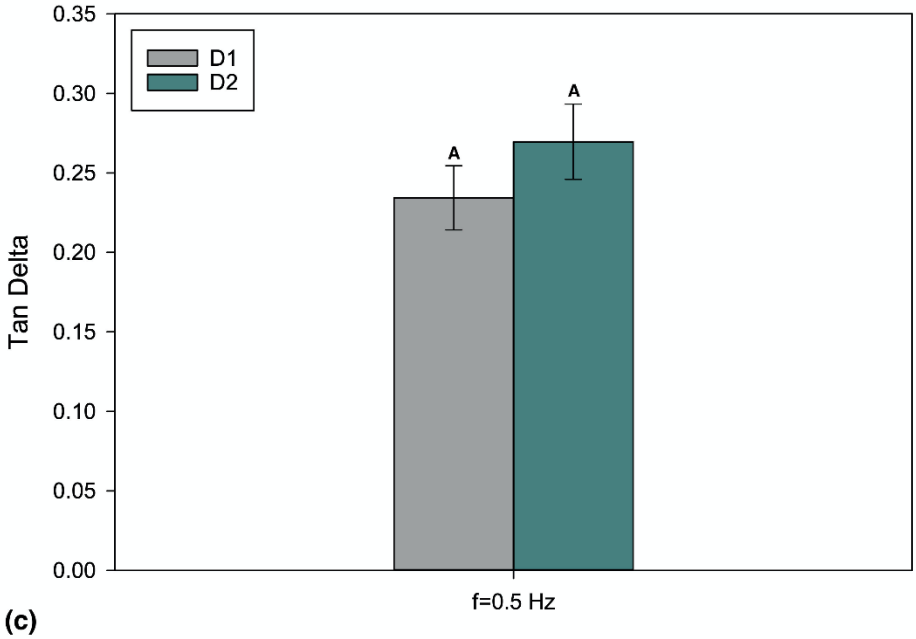

Figure 4.10 – Grouped vertical bars of frequency-dependent viscoelastic properties (mean ± 95% confidence intervals) for brain tissue tested from the different directions: orthogonal to nerve fibre bundles (D1) and aligned with the nerve fibre tracts (D2). The statistical results (a) the storage modulus showed no significant differences of directions over all frequencies tested; (b) the loss modulus showed a significant difference only from 0.5 to 7 Hz; (c) the tan delta showed no significant differences were found across frequencies. In each directional group, viscoelastic properties not sharing a letter are considered to be significantly different (Tukey HSD).

4.3.3 Frequency-Dependent Characterization

The mean dynamic viscoelastic properties of brain tissue against frequency are shown in Figure 4.11 for all 96 tested samples. The storage modulus increased from 7.39 kPa to 16.19 kPa with a mean value of 12.41 kPa and the loss modulus ranged between 1.87 kPa and 9.70 kPa with a mean value of 5.54 kPa. The average tan delta of brain tissue exhibited an increasing trend with frequencies ranging from 0.26 to 0.60, with an average value of 0.43.

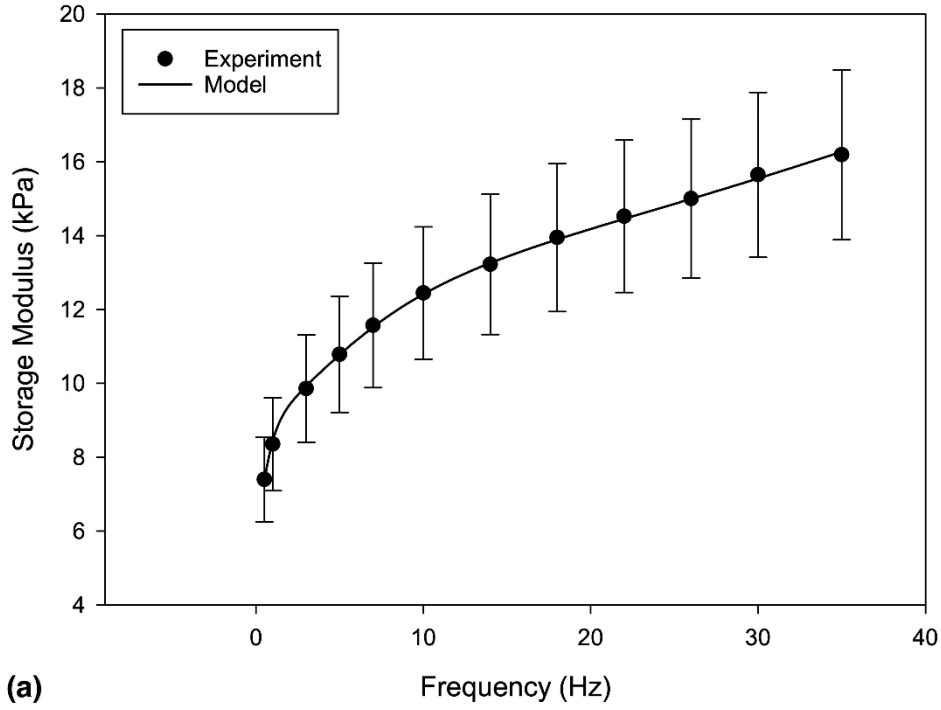

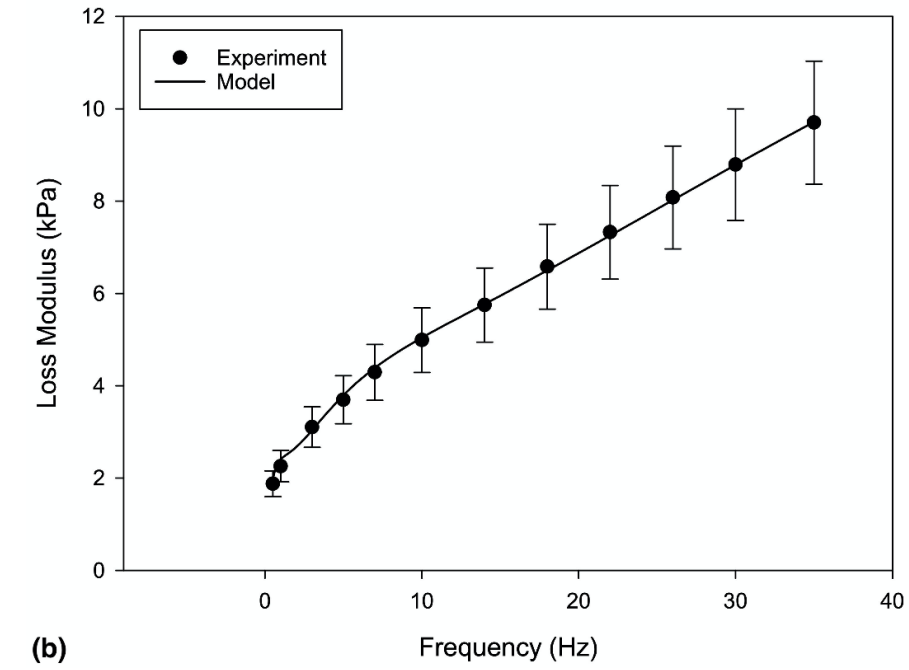

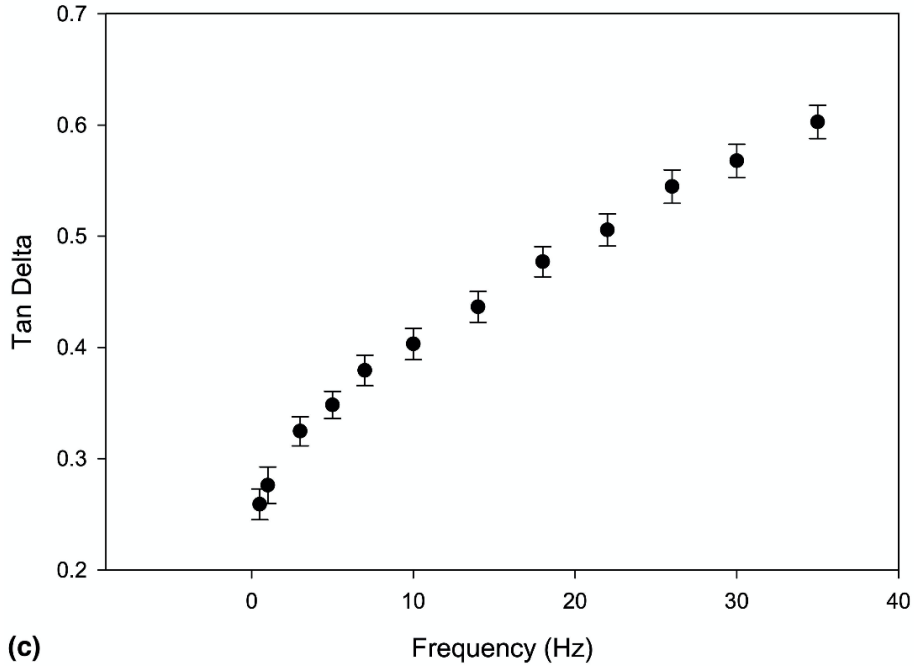

Figure 4.11 – Frequency-dependent viscoelastic properties for brain tissue for all specimens tested. Mean (a) storage and (b) loss modulus, against frequency from experiments with relevant linear viscoelastic model predictions and the trendlines are data predicted following simulations which were solved at loading frequencies from 0.5 Hz up to 35 Hz in incremental steps of 0.1 Hz; (c) mean tan delta against frequency. Error bars represent 95% confidence intervals.

4.3.4 Viscoelastic Model Fitting

The mean results of the experimental storage and loss moduli of the brain tissue tested from various regions, directions and all brain specimens were used to obtain the optimized parameters of a four term Prony series in the frequency-dependent linear viscoelastic model (Table 4-2) with the corresponding coefficients of determination. The long-term modulus u_e was found to be 83.9 Pa. The number of four pairs of Prony constants were adequate to keep the simulation accuracy in the models. For the linear viscoelastic model in the frequency domain, the FE simulations were able to represent the mechanical behaviour of brain tissue adequately from the mean storage and loss modulus (the trendlines from Figure 4.7, Figure 4.9 and Figure 4.11).

Table 4-2 – Constitutive parameters of frequency-dependent linear viscoelastic model derived from the mean dynamic viscoelastic properties over all frequencies for various regions, directions and general material characterization.

	Linear viscoelastic model parameter								
	Prony constant (kPa)				Relaxation time constant (s)				
	g_1	g_2	g_3	g_4	τ_1	τ_2	τ_3	τ_4	R^2
Corona radiata	5.80	3.54	4.93	58.75	6.59×10^{1}	2.57×10^{-1}	1.87×10^{-2}	7.58×10^{-4}	0.994
Corpus callosum	9.60	4.56	6.08	40.70	2.34×10^{1}	1.74×10^{-1}	1.89×10^{-2}	1.51×10^{-3}	0.998
Basal ganglia	3.59	1.76	2.14	15.44	5.00×10^{4}	2.09×10^{-1}	2.38×10^{-2}	1.63×10^{-3}	0.998
Cortex	4.57	1.88	3.05	18.85	5.00×10^{4}	2.15×10^{-1}	2.36×10^{-2}	1.71×10^{-3}	0.996
D1	8.53	3.77	4.91	29.36	1.12×10^{1}	1.60×10^{-1}	2.02×10^{-2}	1.98×10^{-3}	0.994
D2	11.94	6.42	8.60	97.49	1.12×10^{1}	1.95×10^{-1}	1.71×10^{-2}	7.21×10^{-4}	0.997
General	6.38	3.11	4.29	31.57	1.17×10^{1}	2.00×10^{-1}	2.01×10^{-2}	1.37×10^{-3}	0.998

4.4 Discussion

The research presented in this chapter has demonstrated the effect of regions and directions on the frequency-dependent viscoelastic properties of brain tissue using Dynamic Mechanical Analysis. As the compressive loading plays a significant role in head trauma (Bar-Kochba et al. 2016; Young et al. 2015) and the brain could be exposed to compressive waves during the course of head impact (Morse et al. 2014), it is essential to determine the compressive behaviour of the brain tissue over a range of frequencies. The dynamic storage modulus and tan delta from four regions showed different types of significant differences to various frequency ranges while the corresponding dynamic loss modulus exhibited the same significant difference of regions over all frequencies tested. No significant mechanical directional dependency was found in frequency-dependent viscoelastic properties except in loss modulus. For all specimens tested under the frequency sweep, the trends of dynamic properties were similar, with properties increasing with frequency. Preconditioning tests were performed in this study which is a well-established process for the mechanical testing of biological tissue. Similar preconditioning behaviour was conducted on human brain (Budday et al. 2017) and bovine brain (Cheng and Bilston 2007) to ensure a repeatable mechanical response. The experimental results were used to establish viscoelastic constitutive models following the adaptation of storage and loss modulus against frequency to capture the compressive mechanical response of brain tissue.

The dynamic mechanical properties of bovine brain tissue showed regional dependency.

Specimens tested from the corpus callosum exhibited a consistently significant difference with larger storage and loss modulus and tan delta than specimens tested from the basal ganglia, over all frequencies. In general, the dynamic storage and loss moduli of white matter (15.72 kPa and 7.09 kPa) in this study were greater than that of grey matter (7.97 kPa and 3.45 kPa). A similar trend for white and grey matter was found by some studies on human (Finan et al. 2017) and bovine brains (Budday et al. 2015) using indentation tests, but other studies reported the opposite trend on rat (Christ et al. 2010) and porcine brain tissue (Prange and Margulies 2002); all of these experiments were performed in the time domain with stress-strain testing. These discrepancies may be induced by the potential differences in loading protocols and the extremely sensitive properties of brain tissue. Further, recent investigations on magnetic resonance elastography (MRE) (Bayly et al. 2012; Clayton et al. 2012) in the frequency domain showed the modulus of white matter was approximately 2 times greater than that of grey matter, which is comparable to the results presented in this chapter. Although MRE has been used to characterize brain tissue *in vivo* (Weickenmeier et al. 2018), current applications are limited to accurately quantify regional dependent properties within the small structure of the tissue specimens.

Significant directional dependency of the dynamic viscoelastic properties was only observed for the loss modulus from 0.5 to 7 Hz in the corpus callosum, considered as a highly anisotropic brain region, with larger values aligned to the nerve fibre tracts. Some studies reported a similar trend on lamb brain white matter through dynamic shear tests (Feng et al. 2013) and porcine

brain tissue through tensile tests (Velardi et al. 2006). However, for the storage modulus and $tan\delta$, no significant differences were found over all tested frequencies and the bovine brain tissue is more likely to be isotropic, which is consistent to the previous studies on mouse brain tissue through indentation tests (MacManus et al. 2017) and bovine brain through compression (Pervin and Chen 2009).

The mean dynamic viscoelastic properties of bovine brain tissue are frequency-dependency and the storage modulus was constantly higher than the loss modulus for every frequency. In comparison to the work presented in chapter 3 on the general viscoelastic properties of porcine brain tissue where the mean storage and loss moduli were 8.09 kPa and 4.85 kPa, respectively, the bovine brain results in this chapter had higher dynamic moduli at comparable frequencies. However, the average tan delta of porcine brain showed higher range (0.34 to 0.98) than that of bovine brain presented in this chapter, which indicated a greater proportion of viscous behaviour in porcine brain tissue. In addition, animal brain tissues were tested using dynamic shear (Boudjema et al. 2017) and tensile methods (Barnes et al. 2015) to analyse the oscillatory characterization. Despite comparisons being limited by the potential discrepancies in the types of loading and tested specimen species, the general trends of the dynamic storage and loss moduli against frequency were found to be similar.

Due to the ethical restrictions and difficulties in obtaining human brain specimens, animal brains are often adopted for many mechanical experiments (Brands et al. 1999; Miller et al.

2000; Pan et al. 2018). The discrepancies for the mechanical properties between human and animal brain tissue has been controversial. Human brain tissue was previously reported with stiffer mechanical properties than porcine brain tissue (Prange et al. 2000), while the similar dynamic moduli of human and porcine brain tissue were found through dynamic shear tests (Nicolle et al. 2004) and the dynamic mechanical behaviour in different animal brain tissues were measured to be close (Pervin and Chen 2011). From the literature, the fresh human tissue exhibited relatively softer mechanical properties than samples obtained following human autopsy (Hohmann et al. 2019) which implied the animal brain tissue may generate more presentative data. Further, the anatomical structure between animal and human brains is analogous. Based on this similarity, the dynamic mechanical properties of bovine brains tested in this study may be used in the mechanical analysis and computational models of human brains.

To develop the brain FE models, dynamic viscoelastic properties of brain tissue are essential. Regarding head injuries, the brain could experience dynamic loading conditions such as shaken baby syndrome (SBS) where the violent shaking occurs with the head moving backwards and forwards (Elinder et al. 2018). However, due to the lack of experimental data for compressive frequency-dependent properties of brain tissue, most simulations were applied with the viscoelastic models to capture brain mechanical behaviour in the time domain (i.e. stress-strain curves) (Li et al. 2019; Samadi-Dooki et al. 2018). The stress versus time behaviour was studied previously from shear, compression and tensile tests (Rashid et al. 2012; Rashid et al. 2013, 2014) where the time dependent Prony parameters were estimated from the corresponding

relaxation functions. The DMA tests in this study provide critical information on the frequency-dependent viscoelastic behaviours of brain tissue for different regions and directions, which has been manifested in the discrete relaxation mode of a Prony series with the exponentially ascending order of relaxation times. The linear viscoelastic model was previously adopted to replicate the mechanical response of biological material (Qian et al. 2018) with time domain experimental data and can also be applied to reproduce the dynamic response of a viscoelastic material with adaptation of the storage and loss moduli. This constitutive model could improve the variety and accuracy in the brain computational models to develop the prediction of dynamic impact of brain injuries. Although the small dynamic deformation responses of brain tissue were the focus of this study, there is future opportunity to investigate large strain behaviour based on the material parameters derived from dynamic experimental data; this would require further experimental work to investigate the large strain behaviour of the tissue. A recent study showed a numerical approach to support the linear viscoelastic interconversion between the time and frequency dependent material properties of porcine brain tissue, based on the stress relaxation experimental data (Zupančič 2018), even though the conversion of the frequency to the strain rate is inherently limited due to the continuously changing velocity during the oscillation. An optomechanical indentation method was performed with the same testing conditions through both the strain rate and frequency dependent approaches to indicate there is the great correlation between these data of different types (Bartolini et al. 2018). In addition, inverse FFT is able to convert the frequency function to the time function and a

comparison between the frequency and time dependent models becomes available.

A limitation of this study is that a freeze-thawed treatment was applied to prepared specimens. The variation between frozen and fresh tissue was previously studied and the results showed extensive overlap (Clark 1973). In addition, limited changes were shown for mechanical properties on porcine liver (Wex et al. 2014), aortic tissue (O'Leary et al. 2014), and ligaments (Woo et al. 1986).

For sample preparation, the presence of the convolutions within the cerebral cortex, and the pia mater present limitations during the extraction of specimens from the continuum of tissue from the cerebral cortex, additionally it is close to the sulci (i.e. the grooves which give a folded appearance to the brain). Although these factors may have an impact, much cortex tissue was also collected in the circumvoluted area mainly contributing to the testing results, with the magnitude of data measured and trends in this data being broadly in agreement across both these datasets.

4.5 Chapter Summary

In conclusion, bovine brain tissue is viscoelastic with frequency-dependent storage and loss modulus. The dynamic mechanical tests were conducted to characterize the regional and directional properties of the bovine tissue throughout the range of frequencies tested. The viscoelastic storage and loss modulus showed an increasing trend against frequency with a mean value of 12.41 kPa and 5.54 kPa, respectively. In this chapter, the constitutive properties of bovine brain tissue for different regions of corona radiata, corpus callosum, basal ganglia and cortex were determined, and the frequency-dependent compressive behaviour can be captured adequately through a linear viscoelastic model. Applications of the brain viscoelastic properties include the diagnosis of brain injury, complex head computational simulations and the development of protection equipment.

In the next chapter, the compressive viscoelastic properties of brain tissue have been investigated under time and frequency domains. The same physical conditions and theory of viscoelasticity is applied to estimate the prediction of viscoelastic response in the time domain based on frequency-dependent mechanical moduli. Storage and loss modulus were obtained from white and grey matter, of bovine brains, using dynamic mechanical analysis and time domain material functions were derived based on a Prony series representation.

5 Investigation of the compressive viscoelastic properties of brain tissue under time and frequency dependent loading conditions

5.1 Introduction

The mechanical characterization of brain tissue has been analysed in the frequency and time domain. Viscoelastic properties of biological tissue can be effectively obtained in the frequency domain over a wide range of frequencies and using this method with the same testing conditions the mechanical properties can be comprehensively compared (Bartlett et al. 2020). However, some numeric models of brain biomechanics have required the time-dependent relaxation spectrum instead of the available dynamic moduli to analyse the mechanics of brain injury (Forte et al. 2018; Sahoo et al. 2016). Therefore, it is crucial to understand the mechanics of the brain under realistic, dynamic conditions and convert it to enable mathematical modelling in a time domain. Frequency dependent properties and corresponding viscoelastic models of brain tissue have been studied in chapter 3 and chapter 4, but it remains unclear whether such data can be used in computational models to predict mechanical behaviour under various loading conditions such as under time-dependent loading.

Comparison of the mechanical properties of brain tissue in the literature shows that there is a lack of standard testing protocols (Chatelin et al. 2010). Some studies investigated brain tissue in the time domain (Velardi et al. 2006) while dynamic sweep tests on brain tissue in the frequency domain have also been performed (Darvish and Crandall 2001). Although a range of

dynamic mechanical data are available for various materials in the literature, it has rarely been applied in modelling to analyse and design structures, mainly because they are not directly applicable to most of engineering issues and models are often solved in the time domain. Therefore, it is of great practical use to determine time-dependent material properties from frequency-dependent data obtained from mechanical testing.

DMA has been considered as an effective technique for measuring the bulk mechanical properties of viscoelastic materials (Bartlett et al. 2020). This method is flexible and powerful to map frequency-dependent viscoelastic properties of biological tissue over a range of frequencies covering physiological and injury loading conditions. The relaxation modulus which has been widely used in simulations to describe viscous response (Qian et al. 2018) can be determined in the time domain, however, it is limited to the strain rate range used in experiments and it can be time consuming leading to long measurement trials (Zeltmann et al. 2016). Thus, it is of value to characterize viscoelastic properties, such as the Prony series, from dynamic moduli which can be used to predict time-domain phenomena such as stress relaxation when applied to FE models.

With DMA, the testing material should be deformed at an amplitude within the linear stress-strain regime for characterising the bulk mechanical properties. Therefore, to characterize the mechanical behaviour of brain tissue over large strain conditions, using uniaxial compression, is necessary to complement the understanding of compressive properties on various

deformation conditions. Also, different material models are required to capture its mechanical behaviour such as hyperelastic material models. The Prony series can be combined with hyperelasticity to characterize the compressive viscoelastic properties of brain tissue in large strain (Forte et al. 2018).

The purpose of this study was to investigate compressive mechanical properties of brain tissue under various loading conditions covering linear and nonlinear ranges. For linear viscoelastic behaviour, the viscoelastic properties obtained experimentally via dynamic mechanical analysis were transformed to a Prony series, for white and grey brain matter to study the relationship between time and frequency domains. Prony series parameters were determined using a constitutive model and implemented in FE analysis. The FE model was evaluated in both time and frequency domains against relevant experimental data. For nonlinear viscoelastic behaviour, the mechanical properties of brain tissue were studied under large strain, and hyperelastic and quasi-linear viscoelastic models were applied to describe the responses.

5.2 Materials and Methods

5.2.1 Sample Preparation

Eight whole bovine brains were obtained from animals under 12 months of age collected from a supplier (Samples for Schools, Portsmouth, UK), and all of the specimens were free from imperfections. On arrival in the laboratory, the brains were stored at -40°C wrapped in tissue paper soaked in Ringer' solution (Oxoid Ltd, Basingstoke, UK) following the standard procedure (Li et al. 2021; Wilcox et al. 2014). Prior to the mechanical tests, brain samples were thawed in Ringer' solution for 12 hours before dissection. The freeze-thaw process has not been found to adversely affect the mechanical properties of biological tissue (Chan and Titze 2003; Szarko et al. 2010). Slices of cerebrum were collected from brain tissue using a surgical scalpel (Swann-Morton Limited, Sheffield, UK). During the dissection, specimens were immersed in Ringer's solution and a circular trephine of 8 mm diameter was applied to extract white and grey matter samples (Figure 5.1). The specimens of white matter were collected from regions of the corona radiata and corpus callosum, and the specimens of grey matter were collected from regions of the cortex and basal ganglia, which is in agreement with previous studies (Budday et al. 2017; Li et al. 2019). The variability of measured dimensions may be increased due to the soft nature of brain tissue which can cause deformation under its own weight in preparation. Prior to the mechanical tests, geometric dimensions were determined using a Vernier calliper (Draper Tools Ltd, Hampshire, UK). The brain samples obtained were 8 ± 0.1

mm in diameter and 5 ± 0.5 mm (mean ± standard deviation) in thickness.

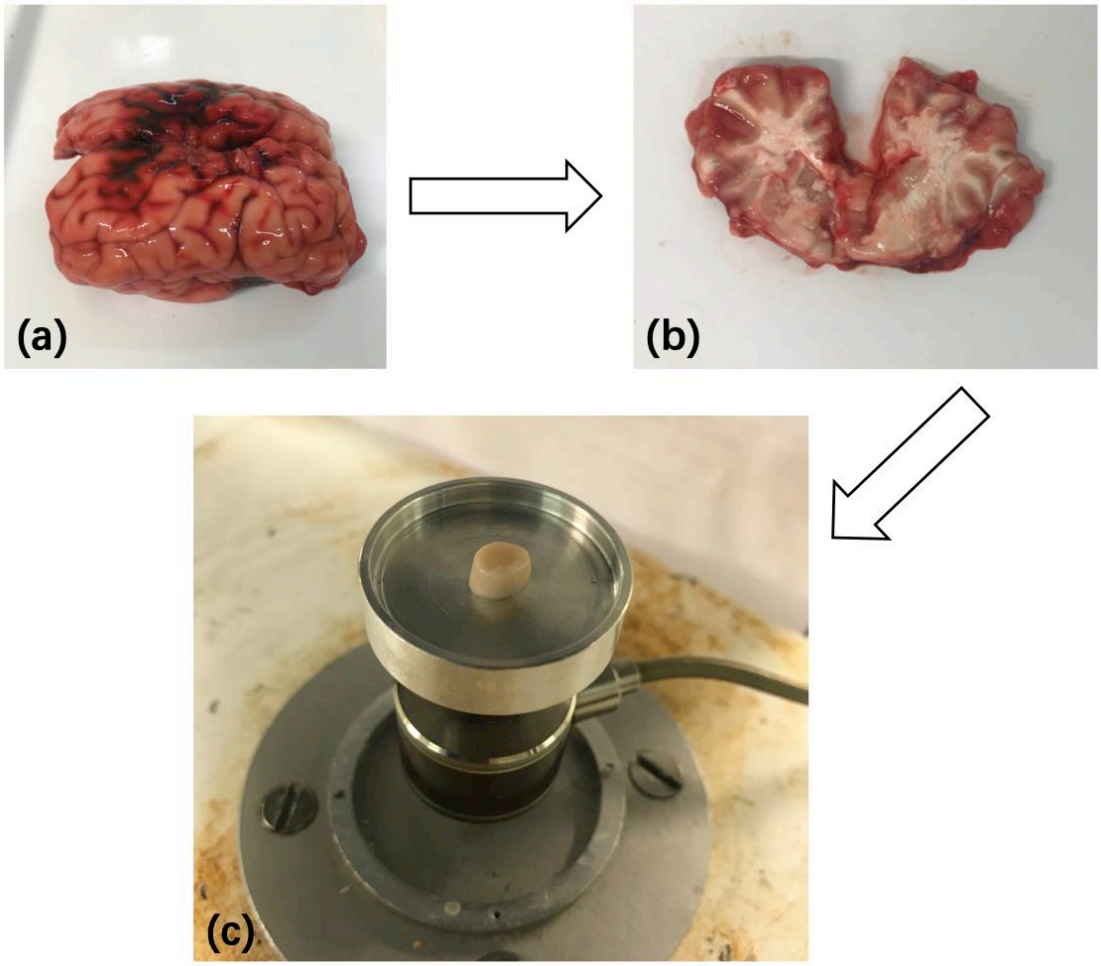

Figure 5.1 – (a) A bovine brain was obtained for dissection and cylindrical specimens were collected from (b) a slice of cerebrum. (c) Representative brain specimen for compressive mechanical testing.

5.2.2 Experimental Setup in Linear Viscoelastic Range

Mechanical testing was conducted using a Bose ElectroForce 3200 (Bose Corporation, ElectroForce Systems Group, Minnesota, USA) testing machine. This approach has been previously used to test many biological and synthetical materials (Barnes et al. 2016; Bartlett et al. 2020; Jannesar et al. 2018). The brain specimens were placed in the sample container; force and displacement values were adjusted to be a zero. Prior to the data collection procedure, an upper flat indenter was lowered onto the specimen until a preload of 10 mN was observed, using the WinTest DMA software (Bose Corporation, ElectroForce Systems Group, Minnesota, USA).

The viscoelastic characterization was investigated both in the time (using stress-relaxation) and the frequency domain (using DMA). To understand the effect of the testing domains on brain tissue, it was essential to keep the samples under the same physical conditions. For DMA, amplitude sweep tests were conducted at 1 Hz to determine the amplitude range within the linear viscoelastic region of the material. Samples were subjected to a pre-strain with a mean displacement of 1 mm (20% of a specimen height) and a 1 Hz pre-conditioning cycle (Cheng et al. 2009; Ohman et al. 2009). A sinusoidally varying displacement was then performed with 1% dynamic amplitude between 0.95 and 1.05 mm (i.e. from peak to trough) across a frequency sweep of 0.5-35 Hz. This frequency range is relevant to the strain rates comparable with previous studies on porcine (Prange and Margulies 2002) and human brain tissue (Forte et al.

2017), and to which the brain might be exposed during physiological and traumatic loading conditions (Laksari et al. 2015). For each frequency, the sinusoidal force and displacement data were recorded and analysed using a Fast Fourier Transform (FFT). The data-set length for force (F^*) and displacement (d^*) at the fundamental frequency were quantified and used to calculate the dynamic stiffness (k^*). The method the software used is described in detail in section 2.3.5. Then, the storage (E') and loss (E'') moduli were calculated by converting from the relevant stiffness through a shape factor from:

$$k^* = \frac{F^*}{d^*} \quad \text{Equation 5.1}$$

$$E' = \frac{k^* cos\delta}{S} \quad \text{Equation 5.2}$$

$$E'' = \frac{k^* sin\delta}{S} \quad \text{Equation 5.3}$$

$$S = \frac{\pi d^2}{4h} \quad \text{Equation 5.4}$$

where h and d are the thickness and diameter of a specimen. The phase angle δ is the phase lag between the applied compressive force and displacement. S is the shape factor for cylindrical samples. Further details on the characterization are provided elsewhere (Wilcox et al. 2014).

For the stress relaxation tests, specimens were subjected to a compressive strain of 0.1 and a relaxation step of 150 s was followed at this compression level. The process of stress relaxation

shows how the stress induced in the material reduces following sudden deformation, from the corresponding stress-strain data and the material's viscoelastic response can be evaluated. The velocity of 180 mm/min was set for the compression step which was consistent with the pre-strain step in DMA. The stress was calculated from the ratio of measured force and sample original cross-sectional area.

Further, samples were subjected to a sinusoidal compression with cyclic loading at a frequency of 35 Hz with 0.05 mm dynamic amplitude for about 2 s to collect hysteresis loops. A lag between the unloading and loading portions of the curve exists for a viscoelastic material. A total of 55 white matter and 41 grey matter samples were tested in the frequency domain through DMA, and 8 white matter and 10 grey matter samples were tested through stress relaxation and cyclic loading measurements. All samples were tested at room temperature and hydrated with Ringer's solution during the testing. The collected experimental data were initially used to determine the viscoelastic parameters (from frequency domain tests) and compared with FE models under both testing domains for validation. For clarity, a schematic showing the experimental design is outlined in Figure 5.2.

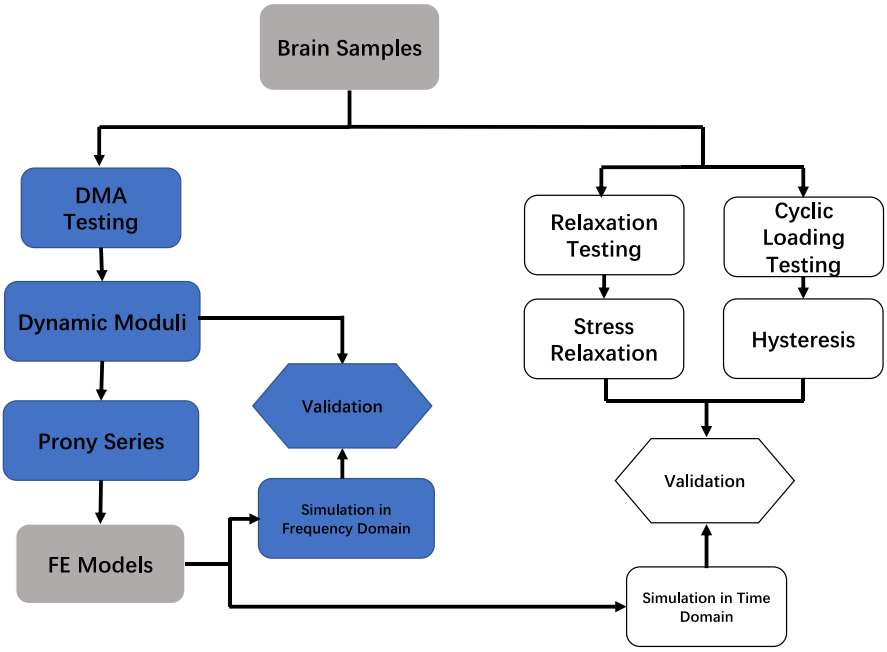

Figure 5.2 – Outline of the experimental design for this chapter in the linear range. Blue boxes denote workflow linked to frequency domain and white boxes denote the workflow linked to time domain. The number of specimens tested in DMA was 55 white matter and 41 grey matter. For stress relaxation and cyclic loading measurements, 8 white matter and 10 grey matter samples were tested.

Sigmaplot version 14.5 (Systat Software Inc., London, UK) was used for statistical analysis. A two-way analysis of variance (ANOVA) was performed accounting for anatomical region and frequency with Tukey post-hoc analysis. Statistical tests were assumed to be significant at the 5% level. The statistical approach was used to determine whether there were significant differences between regions of brain white and grey matter over tested frequencies which is consistent to a previous study (Bartlett et al. 2020) and no interactions were found for the factors of region and frequency.

5.2.3 Experimental Setup in Nonlinear Range

To investigate the compressive properties of brain tissue in large strain, the upper plate compressed the specimen to the displacement of 30% of the height of the sample (i.e. 0.3 strain) for pre-set deformation velocity of 50 mm/min. Afterwards, a relaxation step of 150 seconds was applied by holding the upper plate. Engineering stress (force over the undeformed area) and strain (deformation over the sample initial height) were calculated for each test. The relaxation time indicates how fast the brain specimens dissipate stress after a sudden deformation and it was used to describe the viscous parts of a material. For the large strain tests, samples were only obtained from white matter, which can provide enough testing specimens with a larger area. A total of 8 brain tissue samples were tested in this method. All the stress-strain curves with the same testing conditions were averaged to show the final trend.

5.2.4 Constitutive Modelling

5.2.4.1 Linear Viscoelastic Model

Linear viscoelastic theory has been used in computational studies to analyse the patterns of brain injuries and the relationship between strain and stress (Budday et al. 2017; Cheng and Bilston 2007). In addition, this model can be effectively applied in commercial FE software. The time dependent response of the material is applied in the model determining the stress relaxation ($\tau(t)$) for a viscoelastic model:

$$\tau(t) = \int_0^t \mu(t - t')\dot{\gamma}(t')dt' \qquad \text{Equation 5.5}$$

where $\dot{\gamma}$ is the strain rate tensor and $\mu(t)$ is the time-dependent relaxation modulus. The generalized Maxwell model is widely used to characterize the modulus function for linear viscoelastic materials with a main elastic branch and *N* spring-dashpot pair branch shown in Figure 5.3. Using the Prony series, the constitutive relation of the viscoelastic response in the time domain is as follows:

$$\mu(t) = G_\infty + \sum_{i=1}^{N} g_i \exp\left(-\frac{t}{t_i'}\right) \qquad \text{Equation 5.6}$$

where G_∞ is the equilibrium modulus, g_i and t_i' are the relative moduli and the relaxation time of the Prony series for *N* relaxation modes where $t_i' = \eta_i/g_i$; η_i is the corresponding viscosity. The initial stress modulus can be obtained from the sum of G_∞ and g_i.

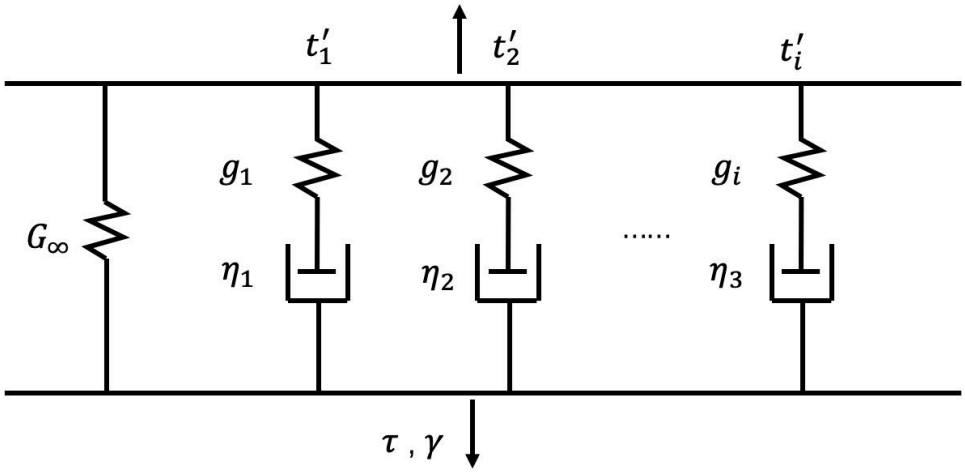

Figure 5.3 – A schematic interpretation of the generalized Maxwell model. G_∞ is the stiffness of the main elastic branch, g_i and η_i represents the stiffness of the spring and viscosity in branch *i*. t_i' is the relaxation time constant of the spring-dashpot pair in branch *i*.

In the frequency domain, Equation 5.5 can be transferred to the Laplace form by considering a pure imaginary variable *s* to $j\omega$ as:

$$u^*(j\omega) = s\tilde{u}(s) = \frac{\tilde{\tau}(s)}{\tilde{\gamma}(s)} = \frac{\tilde{\tau}(j\omega)}{\tilde{\gamma}(j\omega)} \quad \text{Equation 5.7}$$

where $\tilde{u}$ is the relaxation modulus, $\tilde{\tau}$ is the stress tensor and $\tilde{\gamma}$ is the strain tensor in the Laplace form. ω is an angular frequency and $j = \sqrt{-1}$. The complex modulus u^* can be expressed from the dynamic storage modulus u' and loss modulus u'' as:

$$u^* = u' + ju'' \quad \text{Equation 5.8}$$

A discrete relaxation spectrum is considered in physical models. The relaxation modulus $\mu(t)$ expressed above is in the form of a discrete set of exponential decays. Using this discrete function, the complex modulus u^* can then be defined as:

$$u^*(j\omega) = G_\infty + \sum_{i=1}^{N} g_i \frac{t_i' j\omega}{1 + t_i' j\omega} \quad \text{Equation 5.9}$$

Thus, the Prony series representations of dynamic storage and loss modulus in the generalized Maxwell model can be obtained as functions of frequency:

$$u'(j\omega) = G_\infty + \sum_{i=1}^{N} g_i \frac{(t_i'\omega)^2}{1 + (t_i'\omega)^2} \quad \text{Equation 5.10}$$

$$u''(j\omega) = \sum_{i=1}^{N} g_i \frac{t_i'\omega}{1 + (t_i'\omega)^2} \quad \text{Equation 5.11}$$

The dynamic modulus and relaxation modulus shared the coefficients. The parameters of

discrete frequency dependent relaxation modulus are estimated using the non-linear least squares fit algorithm by calibrating the constitutive models with the average experimental data based on the average square of deviation between the measured dynamic modulus from the mechanical tests and the predicted values via Equation 5.12.

$$\sum_{j=1}^{m}\left(\left(\frac{u'(\omega_j)}{\bar{u}_j'}-1\right)^2+\left(\frac{u''(\omega_j)}{\bar{u}_j''}-1\right)^2\right)=\text{minimized} \qquad \text{Equation 5.12}$$

where $\bar{u}_j'$, $\bar{u}_j''$ are the measured dynamic modulus at m frequencies ω_j with $u'(\omega_j)$ and $u''(\omega_j)$ the predicted values calculated from Equation 5.10 and Equation 5.11, respectively.

From here, the relaxation times t_i' are expected to be prescribed and the coefficients g_i are subsequently calculated. The resulting constants are considered all positive. The spacing of relaxation times has been suggested around 1 logarithmic time (i.e. $\log_{10}$ of relaxation time) (Park and Schapery 1999) and negative coefficients may appear when the interval is too small (Friedrich and Hofmann 1983). In addition, the number N of Maxwell elements is an important issue for the success of the nonlinear method. A large number of relaxation modes generally leads to higher accuracy, but more complexity is generated and negative constants start to occur with ill-posed issues (Tian et al. 2015). In this study, the initial number of relaxation elements was empirically chosen at around ten for transmission and redundant elements can be merged or eliminated. From the preliminary studies, an eight term Prony series was chosen for these linear viscoelastic models. The goodness of fit of data to the given model was assessed using the coefficient of determination R^2.

5.2.4.2 Quasi-linear Viscoelastic Model

A quasi-linear viscoelastic (QLV) model can describe the high strain experimental data for brain tissue. The QLV allows the material behaviour to be divided into two responses: a time-independent elastic response and a linear viscoelastic response. The parameters of these models can be obtained separately from the mechanical experiments.

For the time-independent behaviour, a hyperelastic model was applied to describe the brain tissue compressive response for large deformation. The brain tissue was considered as an isotropic and incompressible material, which is generally characterized by a strain-energy function W. The strain energy density and stresses are expressed in terms of the stretch ratio λ. The stretch ratio in a uniaxial experiment is defined as the ratio between the deformed length of the specimen (L) and its original length (L_0).

$$\lambda = \frac{L}{L_0} \qquad \text{Equation 5.13}$$

Three commonly established incompressible isotropic hyperelastic models (Table 5-1) were fitted to average stress-strain experimental data respectively to obtain the material parameters used in the simulations. The constitutive models of hyperelastic models applied are described in detail in section 2.3.4.

Table 5-1 – Incompressible strain energy functions and the uniaxial stress response for each hyperelastic model. μ_0, J_m and α are the material parameters.

Hyperelastic model	Strain energy function	Uniaxial stress response
Neo-Hookean	$W = \frac{\mu_0}{2}(I_1 - 3)$	$S_{11} = \mu_0(\lambda - \lambda^{-2})$
Gent	$W = -\frac{\mu_0}{2} J_m \ln\left(1 - \frac{I_1 - 3}{J_m}\right)$	$S_{11} = \frac{\mu_0 J_m}{J_m - \lambda^2 - 2\lambda^{-1} + 3}(\lambda - \lambda^{-2})$
Ogden	$W = \frac{2\mu_0}{\alpha^2}(\lambda_1^\alpha + \lambda_2^\alpha + \lambda_3^\alpha - 3)$	$S_{11} = \frac{2\mu_0}{\alpha}\left\{\lambda^{\alpha-1} - \lambda^{-\left(\frac{\alpha}{2}+1\right)}\right\}$

The parameters from these three material models can be determined by fitting the compressive stress-strain data using the least-square method.

For the viscoelastic behaviour, the Prony series expansion of the dimensionless relaxation modulus was combined with the strain energy function (Miller and Chinzei 1997):

$$\psi(t) = \int_0^t \left\{ g_d(t-\tau) \frac{dw}{d\tau} \right\} \qquad \text{Equation 5.14}$$

where ψ is time dependent strain energy, W is the hyperelastic strain energy from Table 5-1 and $g_d(t)$ is the dimensionless relaxation modulus function:

$$g_d(t) = 1 - \sum_{p=1}^{N} g_p \left(1 - e^{-t/\tau_p}\right) \qquad \text{Equation 5.15}$$

where g_p and τ_p are material parameters of pth term in the number N Prony series and determined by fitting $g_d(t)$ with experimental values obtained from the relaxation test. In

order to describe the viscoelastic response adequately, a minimum of 3 terms (g_p) were needed.

5.2.5 FE Analysis

The average mechanical behaviour of brain tissue for white and grey matter was simulated, separately, both in the frequency and time domain using COMSOL Multiphysics 5.5 (COMSOL, Stockholm, Sweden). For simulations in both domains, an axisymmetric model was used with a cylindrical geometry representing the average tested brain specimen of 4 mm in radius and 5 mm in thickness. The bottom surface was restrained vertically while it was free to move and expand horizontally. A linear viscoelastic model was applied under the COMSOL solid mechanics module. To avoid ill-conditioning for incompressible materials in the FE simulation, a Poisson's ratio of 0.49 was chosen (Maikos et al. 2008). The viscoelastic parameters obtained from dynamic modulus of white and grey brain tissue (derived from section 5.2.2) were inputted into the general Maxwell material constitutive model with eight viscoelastic branches, under the material setting to represent the mechanical behaviour for time and frequency testing methods in linear viscoelastic region. A mapped 4 node was employed for brain tissue to create an axisymmetric quadrilateral mesh on boundaries and an element ratio node was applied to specify the element size in the distribution (Figure 5.4). The applied mesh density was validated by a mesh convergence analysis.

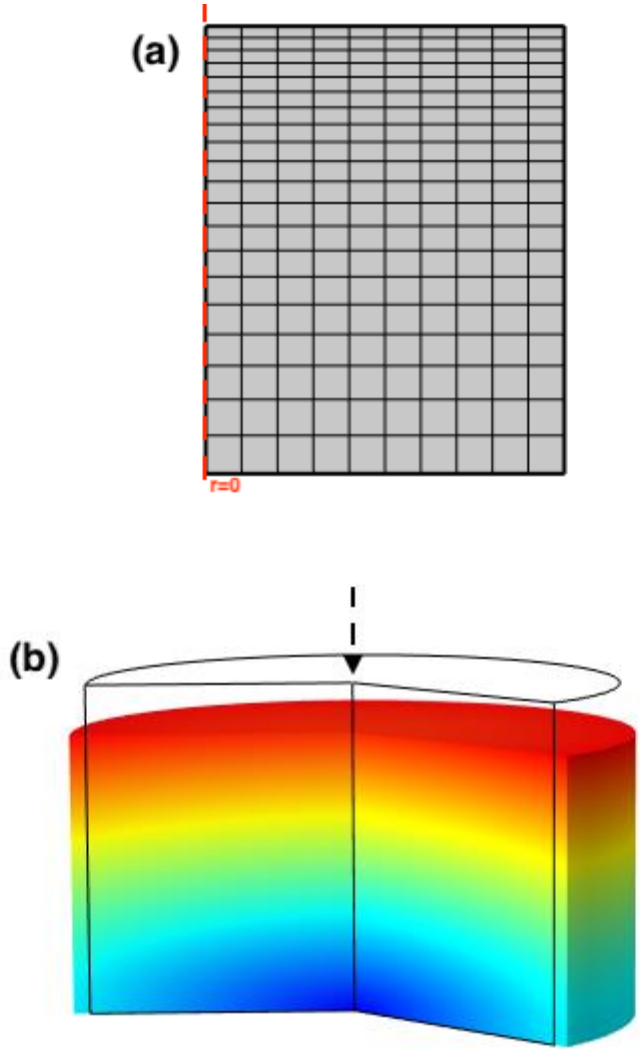

Figure 5.4 – Finite element simulation used for the uniaxial compression of brain tissue in (a) axisymmetric and (b) deformed 2D revolution configurations.

In the frequency domain analysis, the top surface of brain tissue was displaced by 1 mm in the vertical direction, followed by a harmonic perturbation of 0.05 mm over a range of frequencies from 0.5-35 Hz. These models were solved under conditions which mimicked the experimental conditions of DMA tests.

In the time domain analysis, the brain tissue was compressed to 0.1 strain and held for a

relaxation step consistent to the experimental conditions to obtain simulated stress relaxation results. In addition, a sinusoidal prescribed displacement was set under the time dependent solver at 35 Hz for 2 s in the form $\sin(2\pi ft)$, where f is the testing frequency and t is the time, to obtain the force displacement viscoelastic hysteresis loops. The comparison between the FE models and physical tests were used for validation.

For the simulation of brain tissue experiencing the large strain loading condition, an hyperelastic material model was applied instead of a linear elastic material model where Neo-Hookean, Gent and Ogden models were selected to describe the elastic response under the assumption of incompressibility for brain tissue. The viscoelastic model was then selected under the hyperelastic material mode to describe the time-dependent relaxation response. The FE models were analysed in the time domain and the brain sample was compressed to 0.3 strain with deformation velocity of 50 mm/min, followed by a relaxation step of 150 s by holding the upper plate. The boundary conditions in the simulations were consistent with the experiments. The simulant results from the quasi-linear viscoelastic model for brain tissue, where Neo-Hookean, Gent and Ogden hyperelastic models were applied respectively as its elastic part were compared to the experimental data.

5.3 Results

5.3.1 Frequency Dependency of Viscoelasticity

The frequency dependent mechanical behaviours of brain white and grey matter were characterized using dynamic mechanical testing, and the results show that the storage modulus is greater than the loss modulus over all tested frequencies. Figure 5.5(a) illustrates an increasing trend with frequency for white matter storage and loss modulus with average values of 15.72 kPa and 7.97 kPa, respectively. Figure 5.5(b) illustrates the significantly lower storage and loss modulus ($p < 0.05$) for grey matter by performing statistical analysis with average values of 7.97 kPa and 3.45 kPa, respectively. The mean results of the experimental dynamic moduli of brain tissue tested from various regions were used to determine the optimized parameters of the discrete relaxation spectrum with an eight term Prony series (Table 5-2) and the equilibrium modulus was 0.48 kPa. The number of eight pairs of relaxation modes was adequate to simulate the mechanical behaviour converted from the frequency-domain and redundant modes were merged. The FE models in the frequency domain were capable of capturing the trend for both storage and loss moduli across the frequencies investigated (lines in Figure 5.5).

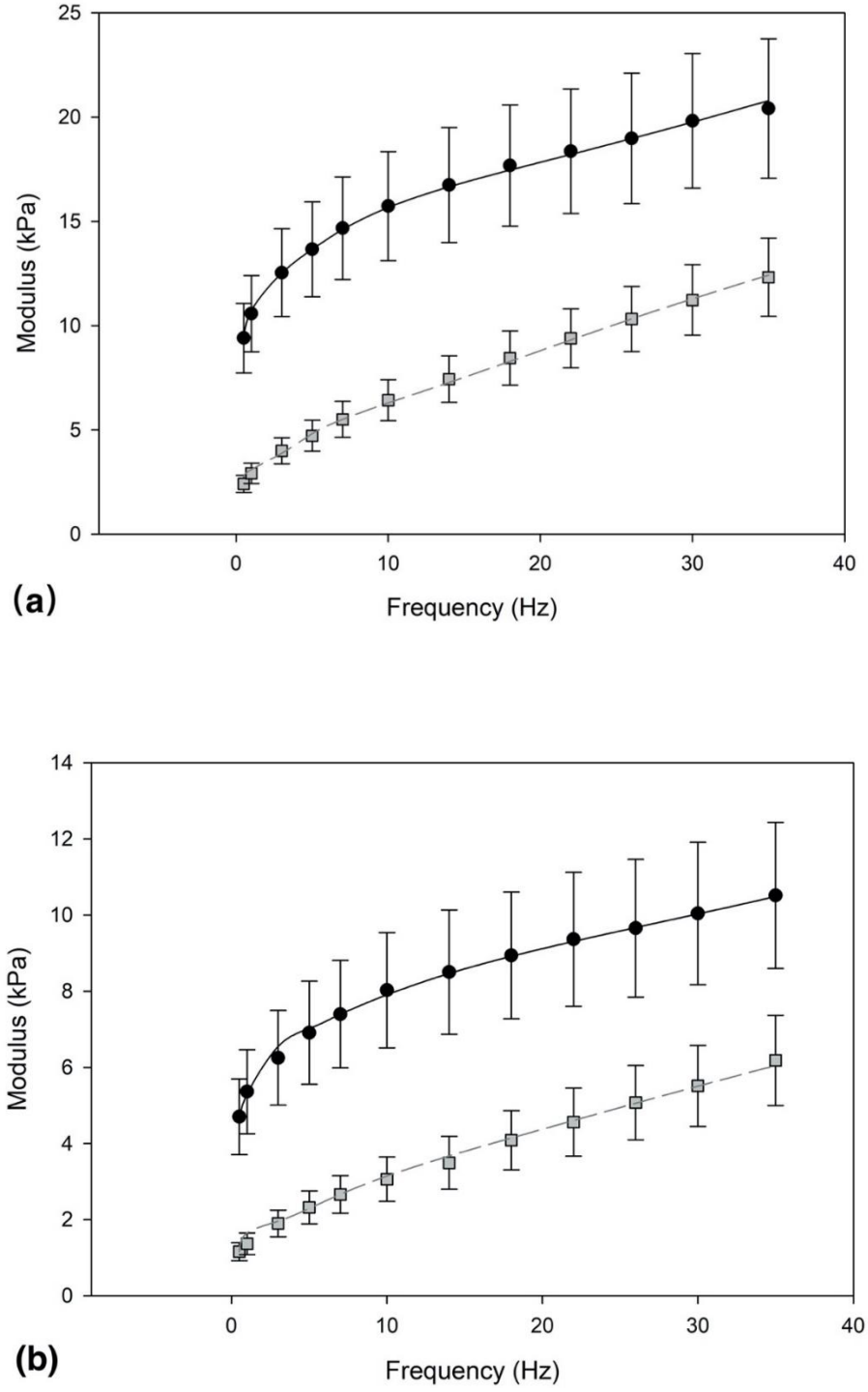

Figure 5.5 – Variation of mean storage (circle) and loss (squares) moduli against frequency for (a) white and (b) grey matter tissue obtained using DMA. Error bars represent 95% confidence intervals. Predictions of dynamic properties from FE simulations, in the frequency domain, are shown as the lines for dynamic storage (full black line) and loss (dashed grey line) modulus.

5.3.2 Time Dependency of Viscoelasticity

The mean stress relaxation behaviours were obtained and the material relaxation for both white and grey matter (Figure 5.6) showed immediately a drop after the compression platen was held. The stress drop for white matter is higher than that of grey matter. The viscoelastic parameters converted from dynamic modulus were applied in the time dependent simulations and the models were able to approximate the trend of stress relaxation responses. For the white matter, the prediction of the stress relaxed slower at the beginning compared to the experimental results. This was followed by a faster relaxation and with a longer relaxation process, the viscoelastic response was more closely approximated with a difference of less than 19% between model and experimental data. For the grey matter, the predicted results appeared to relax faster at first and then exhibited similar relaxation behaviour with a difference of up to 13%. The viscoelastic response in prediction of models was mostly approximated within the 95% confidence intervals through the measured relaxation process.

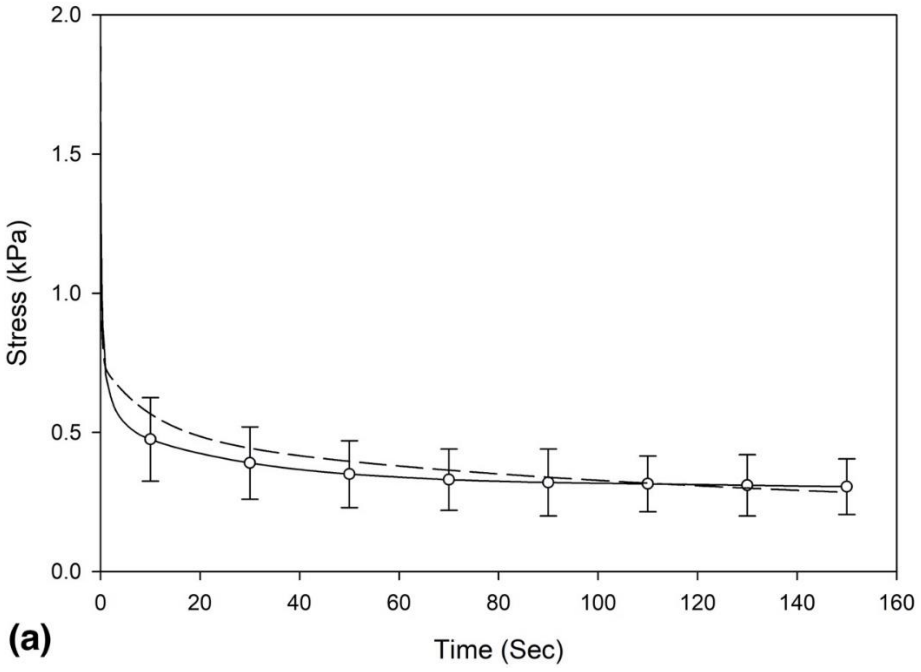

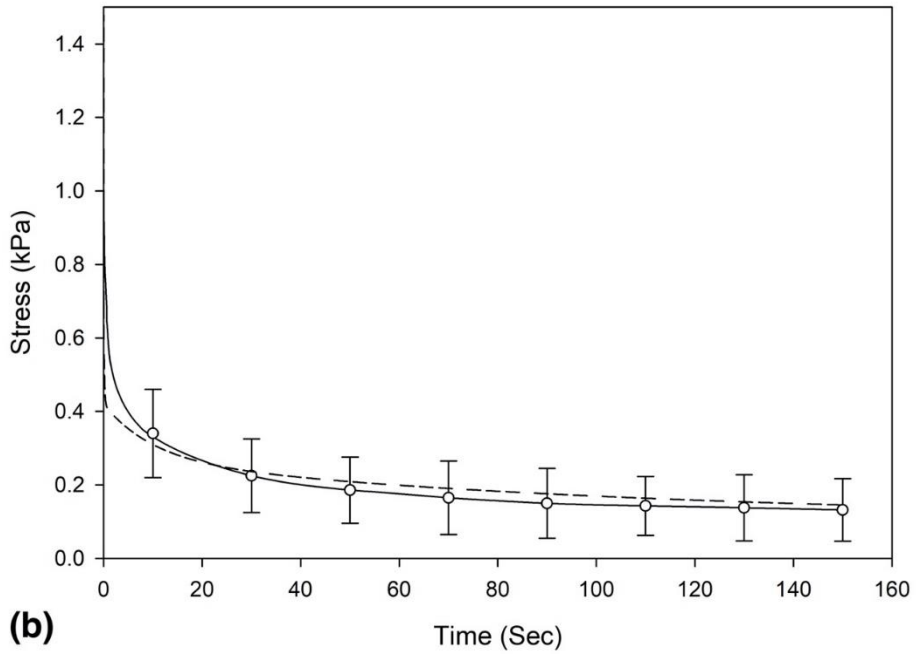

Figure 5.6 – Relaxation response of (a) white and (b) grey matter tissue obtained from the stress relaxation tests (full line) with 95% confidence intervals shown as error bars, and the prediction of stress relaxation (dash line) based on frequency domain derived parameters from FE simulations in the time domain.

The hysteresis loops for white and grey matter tissue are shown in Figure 5.7 as a measure of observing the dissipated energy of the material. Under the same testing protocols, samples from white matter exhibited a larger hysteresis area than samples from grey matter, meaning the greater amount of energy dissipated for white matter tissue. The curves for both white and grey matter were approximately elliptical. This indicated the tested specimens showed linear viscoelastic mechanical behaviour. In simulations, the viscoelastic parameters converted from dynamic modulus were applied in the time dependent models and used to predict the stress strain relationship; the ranges of stress (from minimum to maximum stress) in the simulations were estimated well for both white and grey matter which were similar to experimental results. The hysteresis behaviour for white matter was closely approximated by model prediction with a difference in the area enclosed by hysteresis loops of up to 18%. For grey matter the predicted area was larger than the experimental results, with up to a 34% area difference.

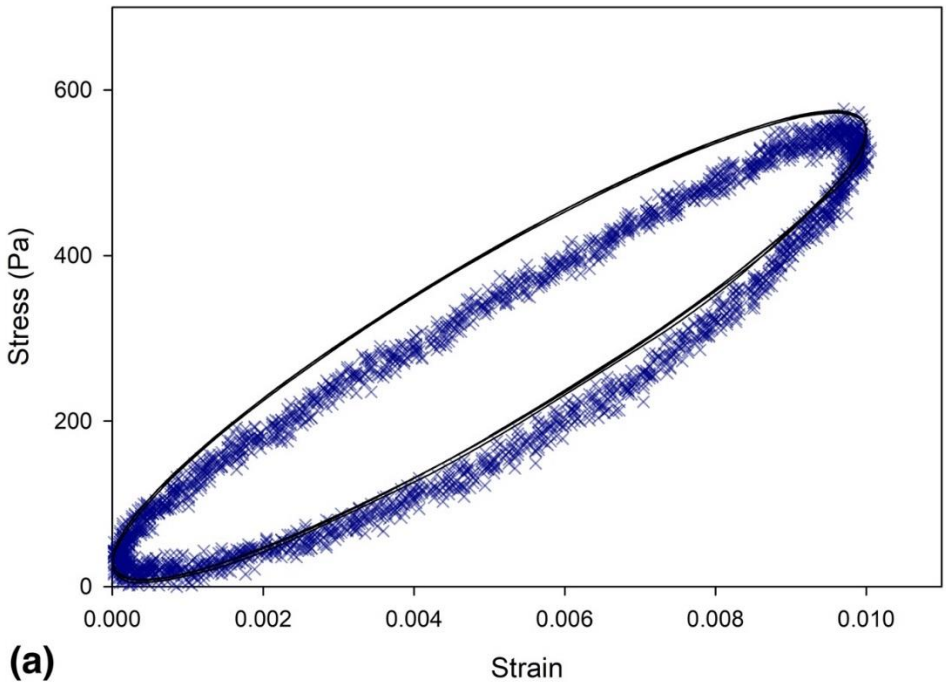

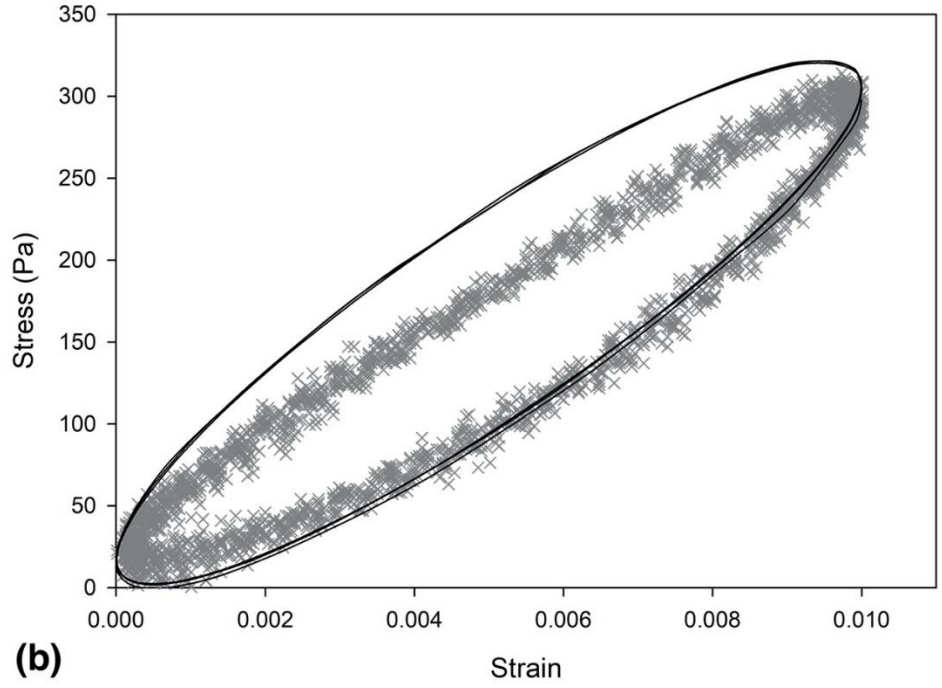

Figure 5.7 – Representative hysteresis loops of stress against strain for (a) white matter and (b) grey matter tissue obtained from cyclic loading tests with model prediction results (black line) based on frequency domain derived parameters following FE simulations in the time analysis.

Table 5-2 – Material parameters of relaxation moduli obtained from the mean dynamic viscoelastic properties for white and grey brain matter.

	Linear viscoelastic model parameter			
	White matter		Grey matter	
i	$g_i(kPa)$	$t_i'(s)$	$g_i(kPa)$	$t_i'(s)$
1	24.33	7.36×10^{-4}	7.30	1.00×10^{-4}
2	19.37	2.23×10^{-3}	17.88	1.45×10^{-3}
3	4.87	2.51×10^{-2}	2.43	1.55×10^{-2}
4	4.46	2.73×10^{-1}	2.43	1.45×10^{-1}
5	2.43	1.00×10^{1}	1.46	1.00×10^{1}
6	2.43	1.00×10^{2}	1.46	1.00×10^{2}
7	1.46	1.00×10^{3}	0.49	1.00×10^{3}
8	0.49	1.00×10^{4}	0.29	1.00×10^{4}

5.3.3 Large Strain Behaviour of Viscoelasticity

The mean compressive stress-strain behaviour for brain tissue compressed to 30% strain showed a nonlinear trend (Figure 5.8), this mechanical behaviour could be observed when the strain exceeded 0.1 and the mean stress increased to approximately 1.5 kPa. For the loading condition with large strain, the linear elastic model was not able to predict the brain tissue's nonlinear response. This elastic response was represented more effectively using hyperelastic models. For the time-dependent relaxation response (Figure 5.9), the viscoelastic behaviour was represented by the Prony series of the relaxation modulus, described in section 5.2.4.2 and the viscoelastic parameters were obtained by fitting the material models (Table 5-3) with mean experimental data.

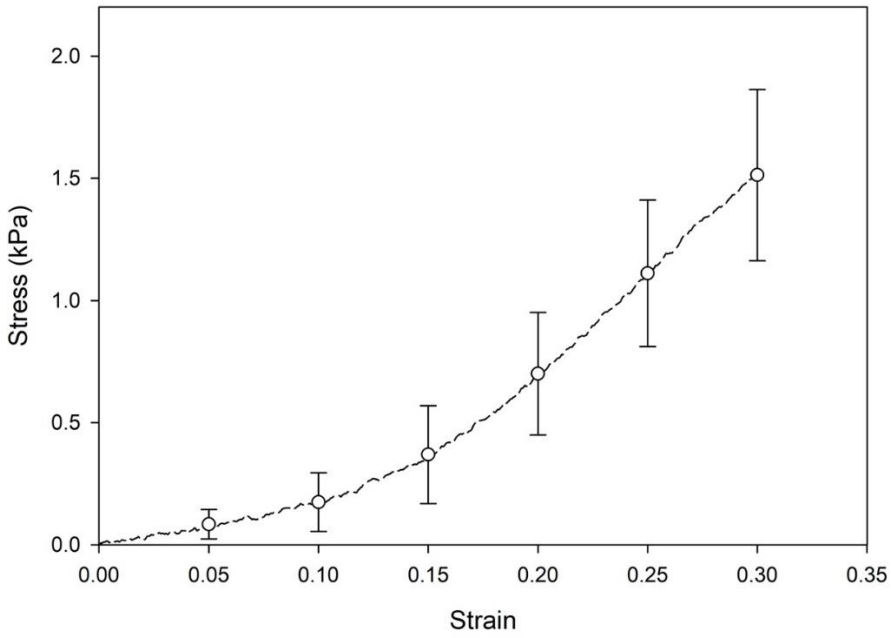

Figure 5.8 –Mean engineering stress-strain curves for eight white matter tissue under 0.3 strain level with 95% confidence intervals shown as error bars.

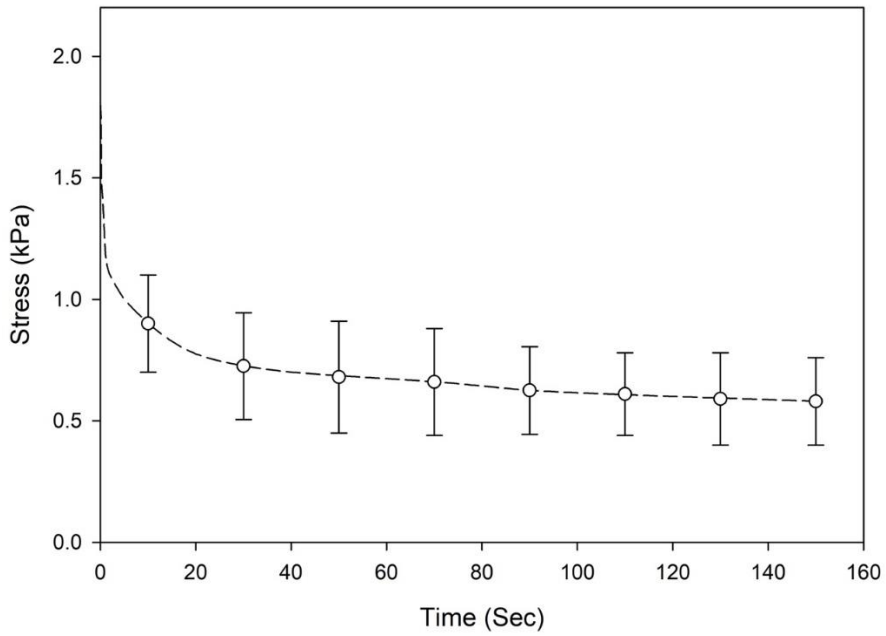

Figure 5.9 – Mean relaxation response of eight white matter tissue obtained from the stress relaxation tests after 0.3 strain compression with 95% confidence intervals shown as error bars.

A quasi-linear viscoelastic model was represented with hyperelastic models as an elastic response to capture brain tissue behaviour under large strain. Neo-Hookean, Gent and Ogden models were defined, as noted in Table 5-1, as an instantaneous effect and the elastic response was fitted with mean experimental data to obtain relevant parameters (Table 5-4). Figure 5.10 showed the response of quasi-linear viscoelastic models with different hyperelastic components and compared the results to experimental data. It can be observed that the Neo-Hookean model only predicted an increasing trend, without the accuracy of the other two models which instead predicted a similar response. The Ogden model fitted the experimental behaviour more accurately than the Gent model where the loading response fitted within the 95% confidence intervals. And the models fitted well the experimental data for strain up to 0.2 and the stress in the simulation for Gent model was higher than in the test as the strain was close to 0.3, which indicated it overestimated the actual experimental result at this strain level.

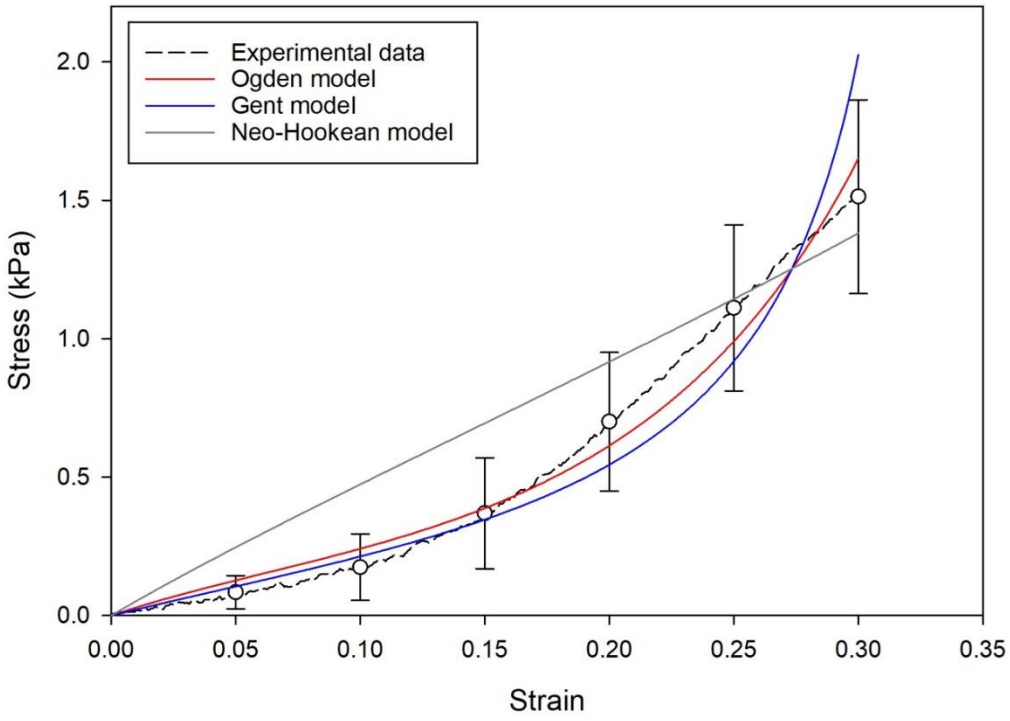

Figure 5.10 – Quasi-linear viscoelastic predictions of simulation were performed in the time domain analysis where hyperelasticity is accounted for using Neo-Hookean, Gent and Ogden models, for the elastic response at 0.3 strain. A Prony series has been derived from stress-relaxation behaviour and accounts for time-dependent viscous response. The mean experimental stress-strain response (black dash line) for eight white matter is shown with 95% confidence intervals shown as error bars.

Table 5-3 – Material coefficients of Prony series representing time-dependent viscoelastic response.

i	τ_{pi} (s)	g_{pi}
1	0.421	0.389
2	10.26	0.217
3	163.7	0.154

Table 5-4 – Material coefficients of hyperelastic models representing elastic response.

Ogden	Gent	Neo-Hookean
$\mu_0 = 646.8\ Pa$	$\mu_0 = 418.2\ Pa$	
		$\mu_0 = 994.7\ Pa$
$\alpha = 14.7$	$J_m = 0.5$	

5.4 Discussion

This chapter has investigated the viscoelastic properties of brain tissue under time and frequency testing domains and computational models were developed to predict the mechanical behaviour based on the parameters of a discrete relaxation spectrum from dynamic moduli. In addition, hyperelastic models were applied in simulation combined with viscoelastic material model to describe brain tissue under large strain loading conditions. Dynamic mechanical experiments are effective for measuring the viscoelastic properties of biological tissue over a range of frequency and the dynamic properties of brain tissue measured can be converted in the time domain data which are applicable in engineering analysis. Frequency-dependent storage and loss moduli were collected from brain white and grey matter tissue in compression. Stress relaxation tests were performed to obtain the time-dependent viscoelastic behaviour and brain samples were subjected to a sinusoidal compressive displacement in the time domain to obtain the hysteresis loops. For different testing protocols, the brain samples were kept under the same physical conditions. The time-dependent experimental results were compared to the predictions from simulations based on the constitutive linear viscoelastic, converting frequency to time-domain data. This validated the use of viscoelastic data of brain tissue, derived from the frequency-domain, for use in FE models in the time-domain. The brain tissue were modelled further under large strain loading conditions, using a quasi-linear viscoelastic model with Ogden, Gent and Neo-Hookean hyperelastic models.

The dynamic mechanical properties of brain tissue showed an increasing trend over tested frequencies from DMA measurements, which is in agreement with previous studies on porcine brains (Hrapko et al. 2008) as well as other biological materials, including human bladder tumours (Barnes et al. 2016). Frequency-dependent dynamic moduli showed brain white matter is stiffer. A similar trend for the regional difference was found on human brain tissue (Jin et al. 2013). A wide range of loading conditions has been applied to determine the frequency-dependent viscoelastic properties. Human brain tissue has been studied in shear (Fallenstein et al. 1969) and the frequency-dependent behaviour of porcine bladder was characterized in tensile (Barnes et al. 2015). Further, brain tissue has been investigated in the frequency domain through magnetic resonance elastography (MRE) (Clayton et al. 2012). However, the dynamic compressive properties of brain tissue are still not fully understood (Chatelin et al. 2010). The compressive force is important in the analysis of brain injuries where the brain could be exposed to compressive waves during the course of head impact (Morse et al. 2014). Even though potential differences exist in the various testing methods compared, the general trends for the dynamic storage and loss modulus versus frequency on these biological tissues were consistent across these.

The standard mechanical models have been applied in this study to capture the linear viscoelastic material functions of brain tissue with Prony series representations, and the fitting of dynamic moduli from experiments and the time domain material functions are subsequently obtained. There are other mathematical models available to describe the linear viscoelastic

response of a material (Tschoegl 2012). The fractional derivative models with a fractional order 'spring-dashpot' element were used to determine the viscoelastic behaviour in relaxation tests on brain tissue (Zhang et al. 2019). The modified power law, derived from the phenomenology of polymers, was applied on soft and biological materials to describe their power law viscoelastic response from a wide range of test conditions (Bonfanti et al. 2020). These models are able to characterize viscoelastic properties using model coefficients, the determination of the constants from experimental results generally is less efficient due to the complicated mathematical expressions and it is limited for the conversion of parameters across material functions (Park 2001).

The parameters in the simulations for linear viscoelastic models were determined by fitting the dynamic storage and loss modulus from experiments. There are various techniques for the fitting described in the literature. A simple collocation method has been applied on polymethylmethacrylate to fit the viscoelastic behaviour from dynamic shear and tensile relaxation tests (Schapery 1962). A least squares method was widely used to obtain model coefficients on brain tissue viscoelastic properties and has the benefits of being easily implemented in commercial software (Budday et al. 2017; Cheng and Bilston 2007). In this study, the frequency dependent responses of brain white and grey matter tissue were evident from the discrete relaxation mode with the exponentially ascending order of relaxation times and positive constraints, which is consistent to a previous study which analysed dynamic mechanical data (Baumgaertel and Winter 1989). The technique presented in this chapter can

have wider applications for other biological tissues such as coronary arteries (Burton et al. 2017) and mitral valve (Wilcox et al. 2014), where the frequency dependent properties have been investigated and described using simple fitting equations obtained through regression analysis. It enables the viscoelastic properties of the brain to be measured under realistic, dynamic conditions and makes this information available for brain models which predict trauma (Madouh and Ramesh 2019; Townsend et al. 2019; Wu et al. 2019).

The viscoelastic characterization of brain tissue in the time domain was studied through stress relaxation tests and the hysteresis loops were obtained to characterize the dissipated energy. The experimental results show that the behaviour of brain tissue is not only frequency-dependent, but also time-dependent. Further, the viscous relaxation for white and grey matter was similar with a stress relaxation of around 85% which is in agreement with a previous study on human brain tissue (Budday et al. 2017). Hysteresis loops for white matter showed a larger area than that for grey matter. A similar trend was found for bovine brain tissue indicating that the white matter with larger dissipated energy shows more viscous than grey matter (Van et al. 2010).

In FE simulations, the models with linear viscoelasticity were able to well capture the dynamic storage and loss modulus for both brain white and grey matter in the frequency domain with the FE responses within the 95% confidence intervals. The model viscoelastic parameters were collected from dynamic mechanical tests and time domain material functions were derived

based on the Prony series representation. Although mild brain traumatic loading conditions were the focus of this study, there is future opportunity to investigate the applicability of the model at higher loading rates, such as blast brain impacts (Singh and Cronin 2019; Unnikrishnan et al. 2019; Vogel et al. 2020). A previous study investigated the differences of converting dynamic modulus to relaxation modulus, however, there was no direct experimental data for validation (Zhang et al. 2018). The simulated results of the time domain in this study showed the general trends for stress relaxation behaviour on brain tissue which is comparable to the experimental data. Despite the initial difference between the predicted and measured results, the viscoelastic response in prediction of models was mostly approximated within the 95% confidence intervals which indicated the prediction of models was considered reliable. The hysteresis area for both brain white and grey matter was predicted to be larger in simulations and the simulated hysteresis area for white matter was larger than that of grey matter which is consistent to the experimental trends. The approach presented in this study of converting material properties between frequency and time domains enables brain modelling in the time domain based on the mechanics of brain tissue measured under dynamic loading conditions.

Brain tissue was modelled with the FE method using a quasi-linear viscoelastic model, which can represent accurately the tissue behaviour for large strain loading conditions. The Ogden model as the elastic part of a QLV was considered to more accurately capture the mechanical behaviour of brain tissue as compared to the Gent or the Neo-Hookean. This was because all

predictions fell within the 95% confidence intervals of the experimental data obtained. In previous studies on soft biological tissue, it has been suggested that a QLV model was insufficient to describe the viscoelastic behaviour of a material and that purely nonlinear models should be applied (Provenzano et al. 2001; Shetye et al. 2014). However, the material behaviour in these studies was only investigated at low strain levels of less than 0.1 and not analysed under large strain loading conditions. For the small strain behaviour of viscoelastic materials, linear viscoelastic model is more suitable as discussed above in this chapter. To avoid the instabilities of fitting hyperelastic properties, the mean experimental data was fitted instead of using the individual test results. The proposed QLV model presented in this chapter is available in commercial FE software (e.g. COMSOL) and, therefore, further related FE analysis can be easily implemented. Further, various mechanical testing on brain tissue with various peak strains representative of physiological and injurious loading conditions as well as creep and stress relaxation will be performed to determine if a more advanced material model is needed to capture the soft tissue under more general loading conditions. However, the quasi-linear viscoelastic model was able to simulate the large strain mechanical properties.

5.5 Chapter Summary

To conclude, the viscoelastic behaviour of brain tissue was investigated under both time and frequency domains. Frequency-dependent storage and loss moduli were collected for both white and grey matter through dynamic mechanical tests which can be represented accurately by the linear viscoelastic models. The time-domain material functions were obtained through the corresponding frequency-domain material functions based on a Prony series representation. The stress relaxation and hysteresis characterizations were studied and compared to the predictions from model simulations. The outcomes provide a better understanding of the material viscoelastic behaviour and the linear viscoelasticity between the time and frequency dependent material functions of biological tissues. The quasi-linear viscoelastic model was applied in simulation with various hyperelastic parts to describe the large strain response of brain tissue obtained from experiments. This analysis is of importance for a number of applications, for brain tissue it enables various loading conditions to be simulated, including traumatic loading.

6 Discussion and Conclusions

6.1 Discussion

This thesis has presented the investigation of the viscoelastic properties of brain tissue under various loading conditions. The compressive frequency-dependent behaviour of brain tissue was, for the first time, quantitatively measured and the viscoelastic material model was applied in the numerical simulations to describe its behaviour and enable the feasibility of deriving time-domain viscoelastic properties from frequency-domain based experiments.

Chapter 3 of this thesis used compressive dynamic mechanical analysis to quantify general viscoelastic properties of porcine brain tissue under different testing conditions. The viscoelastic storage and loss stiffness are dependent on the indentation mean displacement and the indenter size, increasing with higher mean displacement and larger indenter diameters. The mean displacement was considered having a greater effect on the frequency-dependent trend of stiffness as compared to the indenter size. The viscoelastic properties with regards to different indentation depth and indenter size were investigated previously in quasi-static loading conditions (Budday et al. 2015; Liu et al. 2009b). However, the understanding of mechanical behaviour for various testing conditions on brain tissue is not clear in the frequency domain. These frequency-dependent viscoelastic properties are also important for brain injury analysis. Confined compression was selected in this work because the general mechanical characterization of brain tissue was investigated in the macroscope where the brain is

considered as the soft tissue constrained by the skull. The confined testing is thus the nature of the boundary conditions at skull/brain interface. The brain tissue was tested at frequencies of 0.1 to 35 Hz in 14 steps. For mild traumatic brain injuries (mTBI), oscillatory force at around 20 Hz with low acceleration could be a possible cause (Laksari et al. 2015). The conversion of a frequency to a constant strain is inherently limited, because the strain-rate is continuously changing during the oscillation. From the recent literature, the conversion was calculated from the quasi-linear portion of the oscillation (Bartolini et al. 2018). Based on this, the strain rate is estimated from frequency, strain amplitude and the tip diameter and in chapter 3, the maximum strain rate is estimated between 7 and 14 s^{-1}, which is comparable to TBI (Rashid et al. 2013). The dynamic stiffness was dependent on the indenter size while the storage and loss moduli from three indenters were constant with a mean value of 8.09 kPa and 4.85 kPa, respectively.

Chapter 4 of this thesis investigated the compressive frequency-dependent viscoelastic properties of bovine brain extensively and presented a mathematical model in the frequency domain to capture the tissue behaviour based on the experimental results. The brain samples were generally obtained from white and grey matter to determine the regional properties. Brain samples from corpus callosum region were extracted in the two orientations to determine the directional properties. The viscoelastic characterization of brain tissue can improve the fidelity of the computational models of the head and provide essential information to the prediction and analysis of brain injuries in clinical treatment. Even though the compressive loading plays a significant role in head trauma (Bar-Kochba et al. 2016; Young et al. 2015), the dynamic

compressive characterization of brain tissue has not been understood completely (Chatelin et al. 2010). The effect of brain regions and testing directions on the frequency-dependent viscoelastic properties was studied in compression using DMA. The compressive dynamic properties of bovine brain tissue were heterogenous for regions of corona radiata, corpus callosum, basal ganglia and cortex but not sensitive to orientation showing frequency dependent statistical results, with viscoelastic properties increasing with frequency. Due to the lack of experimental data for compressive frequency-dependent properties of brain tissue, most simulations were applied in the time domain with viscoelastic models to describe brain mechanical behaviour (Li et al. 2019; Samadi-Dooki et al. 2018). This chapter has outlined a linear viscoelastic model which can be applied in simulations to reproduce the compressive dynamic response of brain tissue with adaption of experimental moduli for different regions and directions.

Chapter 5 of this thesis investigated the viscoelastic properties of brain tissue under time and frequency testing domains. This chapter presented a technique, for deriving time-domain viscoelastic parameters from frequency-dependent compressive data of brain tissue, as validated by comparing experimental tests with computational simulations. Although dynamic mechanical experiments are effective for measuring the viscoelastic properties of biological tissue over a range of frequency (Bartlett et al. 2020; Kohandel et al. 2005; Pattison et al. 2015), the dynamic properties are not always applicable in engineering, where analysis is performed using a time-dependent domain. This is the first study to validate the use of viscoelastic data of

brain tissue, derived from the frequency-domain, for use in FE models in the time-domain. It can provide wider applications for other biological tissues (Burton et al. 2017; Wilcox et al. 2014), where the frequency dependent properties have been investigated and described using simple fitting equations obtained through regression analysis. In this chapter, brain white and grey matter samples were tested through DMA, stress relaxation and cyclic loading tests with the same physical conditions and the theory of viscoelasticity was applied to estimate the prediction of viscoelastic response in the time domain based on frequency-dependent mechanical moduli through Finite Element models. In addition, large strain behaviour of brain tissue was also studied experimentally and analysed in simulations using a quasi-linear viscoelastic model with Ogden, Gent and Neo-Hookean hyperelastic models. The QLV model with Ogden model being the elastic response can best describe the brain tissue when the large deformation is considered.

6.2 Conclusions

The overall conclusions from this thesis are outlined below:

1) Brain tissue shows frequency dependent-viscoelastic properties. As the indenter size increased, the storage and loss stiffness of porcine brain tissue significantly increased ($p < 0.05$). The storage stiffness decreased significantly as the mean displacement decreased ($p < 0.05$). The average storage modulus of porcine brain tissue was found to be 8.09 kPa and the average loss modulus was found being 4.85 kPa.

2) The dynamic properties of bovine brain tissue were heterogenous for regions including white matter (corona radiata and corpus callosum) and grey matter (cortex and basal ganglia). Generally, the dynamic storage and loss moduli of white matter (15.72 kPa and 7.09 kPa) were greater than that of grey matter (7.97 kPa and 3.45 kPa). The brain tissue from the corpus callosum showed the greatest mean storage and loss modulus (18.19 kPa and 7.82 kPa) over frequencies, followed by the corona radiata (12.28 kPa and 6.08 kPa). The bovine brain tissue from the cortex had marginally higher mean storage and loss modulus (8.86 kPa and 3.85 kPa) than from the basal ganglia with a lowest value of 7.05 kPa and 3.02 kPa.

3) For the dynamic viscoelastic behaviour of bovine brain tissue, no significant directional dependency on the storage modulus was revealed over all frequencies tested while the loss

modulus was found significantly larger at 1.8 to 1.6 times for brain specimens tested aligned to the fibre tracts below the frequency of 7 Hz ($p < 0.05$).

4) The linear viscoelastic model in the frequency domain can be used to characterize the compressive mechanical behaviour of bovine brain tissue in numerical models across a range of frequencies. The quasi-linear viscoelastic model used with a hyperelastic component can describe the large strain response of brain tissue.

5) The time-domain material functions can be obtained through the corresponding frequency-domain material functions based on a Prony series representation. The approach of converting material properties between frequency and time domains enables brain modelling in the time domain based on the mechanics of brain tissue measured under dynamic loading conditions.

6.3 Limitations and Future Work

The overall limitations from this thesis are outlined below:

1) The use of animal brain tissue (i.e. porcine and bovine brains) in place of human brain tissue for all experiments presented in this thesis as the limitation. Although there are similarities on mechanical response of brain tissue between human and porcine, human brain tissue would still be ideal due to the differences in size and morphology.

2) For all mechanical testing in this thesis, the brain tissue was tested *in vitro*. Directly measuring brain tissue properties in the body would be ideal, however, current technologies are insufficient for isolating brain tissue properties at various loading conditions. The variation in mechanical characterization may be due to the difference between *in vivo* and *in vitro* properties of tissue.

3) All tests were conducted at room temperature. Although a slight influence of temperature on the mechanical properties of the tissue, the main purpose of this thesis was to understand the dynamic mechanical characterization of brain tissue under various loading conditions.

4) Although all tested brain specimens were hydrated with Ringer's solution during the testing process to make the contact surface relatively smooth, the effect of the friction on compressive mechanical properties acts as a further limitation.

5) The scalpel used in Chapter 3 to obtain brain specimens may contribute to a small amount of variability in the sample size and shape. However, the diameter of samples was measured using callipers in different directions and the moduli account for the variability.

6) The material constitutive model presented in Chapter 4 and 5 was characterized based on the compressive response of the brain tissue. Therefore, the accuracy of the presented constitutive model is limited to compressive loading conditions.

For all experimental chapters presented in this thesis, it would be of value to test human brain tissue under the same testing methods. The implementation of human brain tissue would assess the feasibility of animal brain tissue as a model for human brain tissue. In addition, the use of human brain tissue can provide valuable clinical information and act directly as a benchmark for matching a potential clinical-grade biomaterial suitable for regenerative medicine. All mechanical tests in this thesis were conducted at room temperature. A future development considers the influence of temperature on the mechanical properties of the brain tissue.

Further tensile or shear experimental tests could be applied on brain tissue in the future under the same testing conditions (e.g. the frequency range) to develop a general constitutive model which is able to capture tissue dynamic mechanical behavior under combined shear, tension and compression loading cases. The material constitutive model could be further developed when considering the biphasic theory where the brain tissue is considered to be saturated with cerebrospinal fluid, enabling to capture the behaviour caused by the movement of the fluid in

the solid matrix.

The testing conditions applied on brain samples were associated with brain injuries such as mild brain trauma and diffuse axonal injury. The dynamic mechanical properties and viscoelastic modelling of brain tissue presented in this thesis could be further applied in the analysis of accident-related scenarios with the head subjected to falls and automotive accidents. In addition, the loading conditions on brain tissue could be extended in the future with larger frequency range or strain level to investigate dynamic mechanical behaviour of brain tissue under non-penetrating ballistic and traffic road impacts.

With regards to Chapter 5, the time-dependent mechanical properties on brain tissue could be further investigated at a range of peak strains and strain rates representative of physiological and injurious loading conditions. It could provide important information if a more complicated material model is required to describe the tissue behavior under arbitrary loading cases. Further, it would be of value to use the inverse FE modelling for optimization to obtain the material parameters. The advanced optimization method could directly incorporate FE models in the parameter optimization and provide an accurate FE-adoptable model for the material.

References

Aidulis, D., D. E. Pegg, C. J. Hunt, Y. A. Goffin, A. Vanderkelen, B. Van Hoeck, T. Santiago, T. Ramos, E. Gruys, and W. Voorhout. 2002. 'Processing of Ovine Cardiac Valve Allografts: 1. Effects of Preservation Method on Structure and Mechanical Properties'. *Cell Tissue Bank* 3(2):79–89. doi: 10.1023/A:1022873513040.

Alexander, Stephen L., C. Allan Gunnarsson, Karin Rafaels, and Tusit Weerasooriya. 2020. 'Multiscale Response of the Human Skull to Quasi-Static Compression'. *Journal of the Mechanical Behavior of Biomedical Materials* 102(May 2019):103492. doi: 10.1016/j.jmbbm.2019.103492.

Arbogast, K. B., K. L. Thibault, B. S. Pinheiro, K. I. Winey, and S. S. Margulies. 1997. 'A High-Frequency Shear Device for Testing Soft Biological Tissues'. *Journal of Biomechanics* 30(7):757–59.

Arbogast, Kristy B., and Susan S. Margulies. 1997. 'Regional Differences in Mechanical Properties of the Porcine Central Nervous System'.

Arbogast, Kristy B., and Susan S. Margulies. 1999. 'A Fiber-Reinforced Composite Model of the Viscoelastic Behavior of the Brainstem in Shear'. *Journal of Biomechanics* 32(8):865–70. doi: https://doi.org/10.1016/S0021-9290(99)00042-1.

Aspden, R. M. 1991. 'Aliasing Effects in Fourier-Transforms of Monotonically Decaying Functions and the Calculation of Viscoelastic Moduli by Combining Transforms over Different Time Periods'. *Journal of Physics D-Applied Physics* 24(6):803–8. doi: Doi 10.1088/0022-3727/24/6/002.

Bar-Kochba, Eyal, Mark T. Scimone, Jonathan B. Estrada, and Christian Franck. 2016. 'Strain and Rate-Dependent Neuronal Injury in a 3D in Vitro Compression Model of Traumatic Brain Injury'. *Scientific Reports* 6:30550. doi: 10.1038/srep30550.

Barnes, S. C., B. M. Lawless, D. E. T. Shepherd, D. M. Espino, G. R. Bicknell, and R. T. Bryan. 2016. 'Viscoelastic Properties of Human Bladder Tumours'. *Journal of the Mechanical Behavior of Biomedical Materials* 61:250–57. doi: 10.1016/j.jmbbm.2016.03.012.

Barnes, S. C., D. E. Shepherd, D. M. Espino, and R. T. Bryan. 2015. 'Frequency Dependent Viscoelastic Properties of Porcine Bladder'. *Journal of the Mechanical Behavior of Biomedical Materials* 42:168–76. doi: 10.1016/j.jmbbm.2014.11.017.

Bartlett, Richard D., Despoina Eleftheriadou, Rachael Evans, David Choi, and James B. Phillips. 2020. 'Mechanical Properties of the Spinal Cord and Brain: Comparison with Clinical-Grade Biomaterials for Tissue Engineering and Regenerative Medicine'. *Biomaterials* 120303. doi: https://doi.org/10.1016/j.biomaterials.2020.120303.

Bartolini, L., D. Iannuzzi, and G. Mattei. 2018. 'Comparison of Frequency and Strain-Rate Domain Mechanical Characterization'. *Scientific Reports* 8. doi: ARTN 1369710.1038/s41598-018-31737-3.

Baumgaertel, M., and H. H. Winter. 1989. 'Determination of Discrete Relaxation and Retardation Time Spectra from Dynamic Mechanical Data'. *Rheologica Acta* 28(6):511–19. doi: Doi 10.1007/Bf01332922.

Baxter, J., K. G. Buchan, and D. M. Espino. 2017. 'Viscoelastic Properties of Mitral Valve Leaflets: An Analysis of Regional Variation and Frequency-Dependency'. *Proceedings of the Institution of Mechanical Engineers Part H-Journal of Engineering in Medicine* 231(10):938–44. doi: 10.1177/0954411917719741.

Bayly, Philip V, Erik H. Clayton, and Guy M. Genin. 2012. 'Quantitative Imaging Methods for the Development and Validation of Brain Biomechanics Models'. *Annual Review of Biomedical Engineering* 14:369–96. doi: 10.1146/annurev-bioeng-071811-150032.

Blum, M. M., and T. C. Ovaert. 2012. 'Experimental and Numerical Tribological Studies of a Boundary Lubricant Functionalized Poro-Viscoelastic PVA Hydrogel in Normal Contact and Sliding'. *Journal of the Mechanical Behavior of Biomedical Materials* 14:248–58. doi: 10.1016/j.jmbbm.2012.06.009.

Boltzmann, Ludwig. 1878. 'Zur Theorie Der Elastischen Nachwirkung'. *Annalen Der Physik* 241(11):430–32. doi: doi:10.1002/andp.18782411107.

Bonfanti, A., J. L. Kaplan, G. Charras, and A. Kabla. 2020. 'Fractional Viscoelastic Models for Power-Law Materials'. *Soft Matter* 16(26):6002–20. doi: 10.1039/d0sm00354a.

Boudjema, F., B. Khelidj, and M. Lounis. 2017. 'Dynamical Properties of the Brain Tissue under Oscillatory Shear Stresses at Large Strain Range'. *Journal of Physics: Conference Series* 790:12002. doi: 10.1088/1742-6596/790/1/012002.

Brands, D. W. A., P. H. M. Bovendeerd, Gerrit Peters, Jac Wismans, MHJW Paas, and Bree JLMJ. 1999. 'Comparison of the Dynamic Behaviour of Brain Tissue and Two Model Materials'. *The Visual Computer - VC*.

Bruns Jr, John, and W. Allen Hauser. 2003. 'The Epidemiology of Traumatic Brain Injury: A Review'. *Epilepsia* 44:2–10.

Budday, S., R. Nay, R. de Rooij, P. Steinmann, T. Wyrobek, T. C. Ovaert, and E. Kuhl. 2015. 'Mechanical Properties of Gray and White Matter Brain Tissue by Indentation'. *Journal of the Mechanical Behavior of Biomedical Materials* 46:318–30. doi: 10.1016/j.jmbbm.2015.02.024.

Budday, S., G. Sommer, C. Birkl, C. Langkammer, J. Haybaeck, J. Kohnert, M. Bauer, F. Paulsen, P. Steinmann, E. Kuhl, and G. A. Holzapfel. 2017. 'Mechanical Characterization of Human Brain Tissue'. *Acta Biomaterialia* 48:319–40. doi: 10.1016/j.actbio.2016.10.036.

Budday, S., G. Sommer, G. A. Holzapfel, P. Steinmann, and E. Kuhl. 2017. 'Viscoelastic Parameter Identification of Human Brain Tissue'. *Journal of the Mechanical Behavior of Biomedical Materials* 74:463–76. doi: 10.1016/j.jmbbm.2017.07.014.

Burton, H., J. Freij, and D. M. Espino. 2017. 'Dynamic Viscoelasticity and Surface Properties of Porcine Left Anterior Descending Coronary Arteries'. *Cardiovascular Engineering and Technology* 8(1):41–56. doi: 10.1007/s13239-016-0288-4.

Capizzi, Allison, Jean Woo, and Monica Verduzco-Gutierrez. 2020. 'Traumatic Brain Injury: An Overview of Epidemiology, Pathophysiology, and Medical Management'. *Medical Clinics* 104(2):213–38.

Carrillo, F., S. Gupta, M. Balooch, S. J. Marshall, G. W. Marshall, L. Pruitt, and C. M. Puttlitz. 2005. 'Nanoindentation of Polydimethylsiloxane Elastomers: Effect of Crosslinking, Work of Adhesion, and Fluid Environment on Elastic Modulus'. *Journal of Materials Research* 20(10):2820–30. doi: 10.1557/Jmr.2005.0354.

Chan, Roger W., and Ingo R. Titze. 2003. 'Effect of Postmortem Changes and Freezing on the Viscoelastic Properties of Vocal Fold Tissues.' *Annals of Biomedical Engineering* 31(4):482–91. doi: 10.1114/1.1561287.

Chatelin, S., A. Constantinesco, and R. Willinger. 2010. 'Fifty Years of Brain Tissue Mechanical Testing: From in Vitro to in Vivo Investigations'. *Biorheology* 47(5–6):255–76. doi: 10.3233/BIR-2010-0576.

Cheng, L., X. Xia, W. Yu, L. E. Scriven, and W. W. Gerberich. 2000. 'Flat-Punch Indentation of Viscoelastic Material'. *Journal of Polymer Science Part B-Polymer Physics* 38(1):10–22. doi: Doi 10.1002/(Sici)1099-0488(20000101)38:1<10::Aid-

Polb2>3.0.Co;2-6.

Cheng, S., and L. E. Bilston. 2007. 'Unconfined Compression of White Matter'. *Journal of Biomechanics* 40(1):117–24. doi: 10.1016/j.jbiomech.2005.11.004.

Cheng, Shaokoon, Elizabeth C. Clarke, and Lynne E. Bilston. 2009. 'The Effects of Preconditioning Strain on Measured Tissue Properties'. *Journal of Biomechanics* 42(9):1360–62. doi: https://doi.org/10.1016/j.jbiomech.2009.03.023.

Chow, M. J., and Y. Zhang. 2011. 'Changes in the Mechanical and Biochemical Properties of Aortic Tissue Due to Cold Storage'. *The Journal of surgical research* 171(2):434–42. doi: 10.1016/j.jss.2010.04.007.

Christ, Andreas F., Kristian Franze, Helene Gautier, Pouria Moshayedi, James Fawcett, Robin J. M. Franklin, Ragnhildur T. Karadottir, and Jochen Guck. 2010. 'Mechanical Difference between White and Gray Matter in the Rat Cerebellum Measured by Scanning Force Microscopy'. *Journal of Biomechanics* 43(15):2986–92. doi: 10.1016/j.jbiomech.2010.07.002.

Clark, R. E. 1973. 'Stress-Strain Characteristics of Fresh and Frozen Human Aortic and Mitral Leaflets and Chordae Tendineae - Implications for Clinical Use'. *Journal of Thoracic and Cardiovascular Surgery* 66(2):202–8.

Clayton, Erik H., Guy M. Genin, and Philip V. Bayly. 2012. 'Transmission, Attenuation and Reflection of Shear Waves in the Human Brain'. *Journal of the Royal Society Interface* 9(76):2899–2910. doi: 10.1098/rsif.2012.0325.

Darvish, K. K., and J. R. Crandall. 2001. 'Nonlinear Viscoelastic Effects in Oscillatory Shear Deformation of Brain Tissue'. *Medical Engineering & Physics* 23(9):633–45. doi: Doi 10.1016/S1350-4533(01)00101-1.

Delaine-Smith, R. M., S. Burney, F. R. Balkwill, and M. M. Knight. 2016. 'Experimental Validation of a Flat Punch Indentation Methodology Calibrated against Unconfined Compression Tests for Determination of Soft Tissue Biomechanics'. *Journal of the Mechanical Behavior of Biomedical Materials* 60:401–15. doi: https://doi.org/10.1016/j.jmbbm.2016.02.019.

Dempster, Wilfrid T. 1967. 'Correlation of Types of Cortical Grain Structure with Architectural Features of the Human Skull'. *American Journal of Anatomy* 120(1):7–31. doi: 10.1002/aja.1001200103.

van Dommelen, J. A. W., T. P. J. van der Sande, M. Hrapko, and G. W. M. Peters. 2010. 'Mechanical Properties of Brain Tissue by Indentation: Interregional Variation'. *Journal of the Mechanical Behavior of Biomedical Materials* 3(2):158–66. doi: https://doi.org/10.1016/j.jmbbm.2009.09.001.

Elinder, Goran, Anders Eriksson, Boubou Hallberg, Niels Lynoe, Pia Maly Sundgren, Mans Rosen, Ingemar Engstrom, and Bjorn-Erik Erlandsson. 2018. 'Traumatic Shaking: The Role of the Triad in Medical Investigations of Suspected Traumatic Shaking.' *Acta Paediatrica (Oslo, Norway : 1992)* 107 Suppl:3–23. doi: 10.1111/apa.14473.

Elkin, B. S., A. Ilankova, and B. Morrison. 2011. 'Dynamic, Regional Mechanical Properties of the Porcine Brain: Indentation in the Coronal Plane'. *Journal of Biomechanical Engineering-Transactions of the Asme* 133(7).

Endo, B. 1966. 'A Biomechanical Study of the Human Facial Skeleton by Means of Strain-Sensitive Lacquer.' *Okajimas Folia Anatomica Japonica* 42(4):205–17. doi: 10.2535/ofaj1936.42.4_205.

Espino, D. M., D. E. T. Shepherd, and D. W. L. Hukins. 2014. 'Viscoelastic Properties of Bovine Knee Joint Articular Cartilage: Dependency on Thickness and Loading Frequency'. *Bmc Musculoskeletal Disorders* 15. doi: Artn 20510.1186/1471-2474-15-205.

Fallenstein, G. T., V. D. Hulce, and J. W. Melvin. 1969. 'Dynamic Mechanical Properties of Human Brain Tissue'. *Journal of Biomechanics* 2(3):217-+. doi: Doi 10.1016/0021-9290(69)90079-7.

Fallenst.Gt, V. D. Hulce, and J. W. Melvin. 1969. 'Dynamic Mechanical Properties of Human Brain Tissue'. *Mechanical Engineering* 91(9):77-.

Faridmehr, Iman, Mohd Hanim Osman, Azlan Bin Adnan, Ali Farokhi Nejad, Reza Hodjati, and Mohammadamin Azimi. 2014. 'Correlation between Engineering Stress-Strain and True Stress-Strain Curve'. *American Journal of Civil Engineering and Architecture* 2(1):53–59. doi: 10.12691/ajcea-2-1-6.

Feng, Y., C. H. Lee, L. Sun, S. Ji, and X. Zhao. 2017. 'Characterizing White Matter Tissue in Large Strain via Asymmetric Indentation and Inverse Finite Element Modeling'. *Journal of the Mechanical Behavior of Biomedical Materials* 65:490–501. doi: 10.1016/j.jmbbm.2016.09.020.

Feng, Y., R. J. Okamoto, R. Namani, G. M. Genin, and P. V Bayly. 2013. 'Measurements of Mechanical Anisotropy in Brain Tissue and Implications for Transversely Isotropic

Material Models of White Matter'. *Journal of the Mechanical Behavior of Biomedical Materials* 23:117–32. doi: 10.1016/j.jmbbm.2013.04.007.

Finan, J. D., S. N. Sundaresh, B. S. Elkin, G. M. McKhann 2nd, and B. Morrison 3rd. 2017. 'Regional Mechanical Properties of Human Brain Tissue for Computational Models of Traumatic Brain Injury'. *Acta Biomaterialia* 55:333–39. doi: 10.1016/j.actbio.2017.03.037.

Forte, A. E., S. Galvan, and D. Dini. 2018. 'Models and Tissue Mimics for Brain Shift Simulations'. *Biomechanics and modeling in mechanobiology* 17(1):249–61. doi: 10.1007/s10237-017-0958-7.

Forte, A. E., S. M. Gentleman, and D. Dini. 2017. 'On the Characterization of the Heterogeneous Mechanical Response of Human Brain Tissue'. *Biomechanics and modeling in mechanobiology* 16(3):907–20. doi: 10.1007/s10237-016-0860-8.

Friedrich, Chr, and B. Hofmann. 1983. 'Nichtkorrekte Aufgaben in Der Rheometrie'. *Rheologica Acta* 22(5):425–34.

Fulcher, G. R., D. W. L. Hukins, and D. E. T. Shepherd. 2009. 'Viscoelastic Properties of Bovine Articular Cartilage Attached to Subchondral Bone at High Frequencies'. *Bmc Musculoskeletal Disorders* 10. doi: Artn 6110.1186/1471-2474-10-61.

Galford, J. E., and J. H. Mcelhaney. 1970. 'A Viscoelastic Study of Scalp, Brain, and Dura'. *Journal of Biomechanics* 3(2):211-+. doi: Doi 10.1016/0021-9290(70)90007-2.

Galgano, Michael, Gentian Toshkezi, Xuecheng Qiu, Thomas Russell, Lawrence Chin, and Li-Ru Zhao. 2017. 'Traumatic Brain Injury: Current Treatment Strategies and Future Endeavors'. *Cell Transplantation* 26(7):1118–30. doi: 10.1177/0963689717714102.

Gent, A. N. 1996. 'A New Constitutive Relation for Rubber'. *Rubber Chemistry and Technology* 69(1):59–61. doi: 10.5254/1.3538357.

Gidde, R. R., and P. M. Pawar. 2017. 'On Effect of Viscoelastic Characteristics of Polymers on Performance of Micropump'. *Advances in Mechanical Engineering* 9(2). doi: Artn 168781401769121110.1177/1687814017691211.

Goh, K. L., Y. Chen, S. M. Chou, A. Listrat, D. Bechet, and T. J. Wess. 2010. 'Effects of Frozen Storage Temperature on the Elasticity of Tendons from a Small Murine Model'. *Animal* 4(9):1613–17. doi: 10.1017/S1751731110000698.

Goriely, A., M. G. Geers, G. A. Holzapfel, J. Jayamohan, A. Jerusalem, S. Sivaloganathan, W. Squier, J. A. van Dommelen, S. Waters, and E. Kuhl. 2015. 'Mechanics of the Brain: Perspectives, Challenges, and Opportunities'. *Biomech Model Mechanobiol* 14(5):931–65. doi: 10.1007/s10237-015-0662-4.

Guertler, C. A., R. J. Okamoto, J. L. Schmidt, A. A. Badachhape, C. L. Johnson, and P. V Bayly. 2018. 'Mechanical Properties of Porcine Brain Tissue in Vivo and Ex Vivo Estimated by MR Elastography'. *J Biomech* 69:10–18. doi: 10.1016/j.jbiomech.2018.01.016.

Hohmann, Erik, Natalie Keough, Vaida Glatt, Kevin Tetsworth, Reinhard Putz, and Andreas Imhoff. 2019. 'The Mechanical Properties of Fresh versus Fresh/Frozen and Preserved (Thiel and Formalin) Long Head of Biceps Tendons: A Cadaveric Investigation'. *Annals of Anatomy* 221:186–91. doi: 10.1016/j.aanat.2018.05.002.

Holmes, M. H. 1986. 'Finite Deformation of Soft Tissue: Analysis of a Mixture Model in Uni-Axial Compression'. *Journal of biomechanical engineering*, *108*(4), 372–381. https://doi.org/10.1115/1.3138633

Hrapko, M., J. A. W. van Dommelen, G. W. M. Peters, and J. S. H. M. Wismans. 2006. 'The Mechanical Behaviour of Brain Tissue: Large Strain Response and Constitutive Modelling'. *Biorheology* 43(5):623–36.

Hrapko, M., J. A. W. van Dommelen, G. W. M. Peters, and J. S. H. M. Wismans. 2008. 'The Influence of Test Conditions on Characterization of the Mechanical Properties of Brain Tissue'. *Journal of Biomechanical Engineering-Transactions of the Asme* 130(3). doi: Artn 03100310.1115/1.2907746.

Hyder, Adnan A., Colleen A. Wunderlich, Prasanthi Puvanachandra, G. Gururaj, and Olive C. Kobusingye. 2007. 'The Impact of Traumatic Brain Injuries: A Global Perspective'. *NeuroRehabilitation* 22(5):341–53.

Jannesar, S., M. Allen, S. Mills, A. Gibbons, J. C. Bresnahan, E. A. Salegio, and C. J. Sparrey. 2018. 'Compressive Mechanical Characterization of Non-Human Primate Spinal Cord White Matter'. *Acta Biomaterialia* 74:260–69. doi: 10.1016/j.actbio.2018.05.002.

Jiang, Jiali, and Jianxiong Lu. 2009. 'Impact of Temperature on the Linear Viscoelastic Region of Wood'. *Canadian Journal of Forest Research* 39(11):2092–99.

Jin, Xin, Feng Zhu, Haojie Mao, Ming Shen, and King H. Yang. 2013. 'A Comprehensive Experimental Study on Material Properties of Human Brain Tissue'. *Journal of Biomechanics* 46(16):2795–2801. doi: https://doi.org/10.1016/j.jbiomech.2013.09.001.

Johnson, Victoria E., William Stewart, and Douglas H. Smith. 2013. 'Axonal Pathology in Traumatic Brain Injury'. *Experimental Neurology* 246:35–43. doi: 10.1016/j.expneurol.2012.01.013.

Kaboorani, Alireza, and Pierre Blanchet. 2014. 'Determining the Linear Viscoelastic Region of Sugar Maple Wood by Dynamic Mechanical Analysis'. *BioResources* 9(3):4392–4409.

Kohandel, M., S. Sivaloganathan, G. Tenti, and K. Darvish. 2005. 'Frequency Dependence of Complex Moduli of Brain Tissue Using a Fractional Zener Model'. *Physics in Medicine and Biology* 50(12):2799–2805. doi: 10.1088/0031-9155/50/12/005.

Kohn, J. C., and D. M. Ebenstein. 2013. 'Eliminating Adhesion Errors in Nanoindentation of Compliant Polymers and Hydrogels'. *Journal of the Mechanical Behavior of Biomedical Materials* 20:316–26. doi: 10.1016/j.jmbbm.2013.02.002.

Koncan, David, Michael Gilchrist, Michael Vassilyadi, and Thomas Blaine Hoshizaki. 2019. 'A Three-Dimensional Finite Element Model of a 6-Year-Old Child for Simulating Brain Response from Physical Reconstructions of Head Impacts'. *Proceedings of the Institution of Mechanical Engineers, Part P: Journal of Sports Engineering and Technology*. doi: 10.1177/1754337118822940.

Kushner, D. 1998. 'Mild Traumatic Brain Injury: Toward Understanding Manifestations and Treatment.' *Archives of Internal Medicine* 158(15):1617–24. doi: 10.1001/archinte.158.15.1617.

Laksari, K., L. C. Wu, M. Kurt, C. Kuo, and D. C. Camarillo. 2015. 'Resonance of Human Brain under Head Acceleration'. *Journal of the Royal Society Interface* 12(108). doi: ARTN 20150331 10.1098/rsif.2015.0331.

Lapeer, Rudy J., Paul D. Gasson, and Vasudev Karri. 2010. 'A Hyperelastic Finite-Element Model of Human Skin for Interactive Real-Time Surgical Simulation'. *IEEE Transactions on Biomedical Engineering* 58(4):1013–22.

Law, S. K. 1993. 'Thickness and Resistivity Variations over the Upper Surface of the Human Skull'. *Brain Topogr* 6(2):99–109.

Lawless, B. M., H. Sadeghi, D. K. Temple, H. Dhaliwal, D. M. Espino, and D. W. L. Hukins. 2017. 'Viscoelasticity of Articular Cartilage: Analysing the Effect of Induced Stress and the Restraint of Bone in a Dynamic Environment'. *Journal of the Mechanical Behavior of Biomedical Materials* 75:293–301.

Li, Weiqi, Duncan E.T. Shepherd, and Daniel M. Espino. 2020. 'Dynamic Mechanical Characterization and Viscoelastic Modeling of Bovine Brain Tissue'. *Journal of the Mechanical Behavior of Biomedical Materials* 114(October 2020):104204. doi: 10.1016/j.jmbbm.2020.104204.

Li, Weiqi, Duncan E. T. Shepherd, and Daniel M. Espino. 2020. 'Frequency Dependent Viscoelastic Properties of Porcine Brain Tissue'. *Journal of the Mechanical Behavior of Biomedical Materials* 102:103460. doi: 10.1016/j.jmbbm.2019.103460.

Li, Weiqi, Duncan E. T. Shepherd, and Daniel M. Espino. 2021. 'Investigation of the Compressive Viscoelastic Properties of Brain Tissue Under Time and Frequency Dependent Loading Conditions'. *Annals of Biomedical Engineering*. doi: 10.1007/s10439-021-02866-0.

Li, Zhigang G., Haifeng F. Yang, Guangliang L. Wang, Xiaoqiang Q. Han, and Shaopeng P. Zhang. 2019. 'Compressive Properties and Constitutive Modeling of Different Regions of 8-Week-Old Pediatric Porcine Brain under Large Strain and Wide Strain Rates'. *Journal of the Mechanical Behavior of Biomedical Materials* 89:122–31. doi: 10.1016/j.jmbbm.2018.09.010.

Liu, Bin, Lixian Zhang, and Huajian Gao. 2006. 'Poisson Ratio Can Play a Crucial Role in Mechanical Properties of Biocomposites'. *Mechanics of Materials* 38(12):1128–42. doi: https://doi.org/10.1016/j.mechmat.2006.02.002.

Liu, Kaifeng, Mark R. VanLandingham, and Timothy C. Ovaert. 2009a. 'Mechanical Characterization of Soft Viscoelastic Gels via Indentation and Optimization-Based Inverse Finite Element Analysis'. *Journal of the Mechanical Behavior of Biomedical Materials* 2(4):355–63. doi: https://doi.org/10.1016/j.jmbbm.2008.12.001.

Liu, Kaifeng, Mark R. VanLandingham, and Timothy C. Ovaert. 2009b. 'Mechanical Characterization of Soft Viscoelastic Gels via Indentation and Optimization-Based Inverse Finite Element Analysis'. *Journal of the Mechanical Behavior of Biomedical Materials* 2(4):355–63. doi: https://doi.org/10.1016/j.jmbbm.2008.12.001.

Maas, Andrew I. R., Nino Stocchetti, and Ross Bullock. 2008. 'Moderate and Severe Traumatic Brain Injury in Adults.' *The Lancet. Neurology* 7(8):728–41. doi: 10.1016/S1474-4422(08)70164-9.

MacManus, D B, B. Pierrat, J. G. Murphy, and M. D. Gilchrist. 2017. 'A Viscoelastic Analysis of the P56 Mouse Brain under Large-Deformation Dynamic Indentation'. *Acta Biomaterialia* 48:309–18. doi: 10.1016/j.actbio.2016.10.029.

MacManus, David B., Baptiste Pierrat, Jeremiah G. Murphy, and Michael D. Gilchrist. 2017. 'Region and Species Dependent Mechanical Properties of Adolescent and Young Adult Brain Tissue'. *Scientific Reports* 7(1):1–12. doi: 10.1038/s41598-017-13727-z.

Madouh, Fatma A., and K. T. Ramesh. 2019. 'The Influence of Shear Anisotropy in MTBI: A White Matter Constitutive Model'. *Annals of Biomedical Engineering* 47(9):1960–70. doi: 10.1007/s10439-019-02321-1.

Mahmood, H., D. E. T. Shepherd, and D. M. Espino. 2018. 'Surface Damage of Bovine Articular Cartilage-off-Bone: The Effect of Variations in Underlying Substrate and Frequency'. *BMC Musculoskelet Disord* 19(1):384. doi: 10.1186/s12891-018-2305-2.

Maikos, Jason T., Ragi A. I. Elias, and David I. Shreiber. 2008. 'Mechanical Properties of Dura Mater from the Rat Brain and Spinal Cord'. *Journal of Neurotrauma* 25(1):38–51. doi: 10.1089/neu.2007.0348.

McElhaney, James H., John L. Fogle, John W. Melvin, Russell R. Haynes, Verne L. Roberts, and Nabih M. Alem. 1970. 'Mechanical Properties of Cranial Bone'. *Journal of Biomechanics* 3(5):495IN5497-496511.

Mckee, Ann C., and Daniel H. Daneshvar. 2015. 'Chapter 4 - The Neuropathology of Traumatic Brain Injury'. Pp. 45–66 in *Traumatic Brain Injury, Part I*. Vol. 127, edited by J. Grafman and A. M. B. T.-H. of C. N. Salazar. Elsevier.

McKeen, Laurence W. 2016. '1 - Introduction to Fatigue of Plastics and Elastomers'. Pp. 1–26 in, edited by L. W. B. T.-F. and T. P. of P. and E. (Third E. McKeen. William Andrew Publishing.

McPherson, Gregg K., and Timothy J. Kriewall. 1980. 'The Elastic Modulus of Fetal Cranial Bone: A First Step towards an Understanding of the Biomechanics of Fetal Head Molding'. *Journal of Biomechanics* 13(1):9–16. doi: 10.1016/0021-9290(80)90003-2.

Meaney, David F., and Douglas H. Smith. 2011. 'Biomechanics of Concussion'. *Clinics in Sports Medicine* 30(1):19–vii. doi: 10.1016/j.csm.2010.08.009.

Menard, Kevin P., and Noah R. Menard. 2020. *Dynamic Mechanical Analysis*. CRC press.

Mendizabal, A., I. Aguinaga, and E. Sánchez. 2015. 'Characterisation and Modelling of Brain Tissue for Surgical Simulation'. *Journal of the Mechanical Behavior of Biomedical Materials* 45:1–10. doi: https://doi.org/10.1016/j.jmbbm.2015.01.016.

Miller, K., and K. Chinzei. 1997. ‘Constitutive Modelling of Brain Tissue: Experiment and Theory’. *Journal of Biomechanics* 30(11–12):1115–21.

Miller, K., K. Chinzei, G. Orssengo, and P. Bednarz. 2000. ‘Mechanical Properties of Brain Tissue In-Vivo: Experiment and Computer Simulation’. *Journal of Biomechanics* 33(11):1369–76. doi: Doi 10.1016/S0021-9290(00)00120-2.

Miller, Karol. 1999. ‘Constitutive Model of Brain Tissue Suitable for Finite Element Analysis of Surgical Procedures’. *Journal of Biomechanics* 32(5):531–37. doi: https://doi.org/10.1016/S0021-9290(99)00010-X.

Morse, Justin D., Jennifer A. Franck, Bethany J. Wilcox, Joseph J. Crisco, and Christian Franck. 2014. ‘An Experimental and Numerical Investigation of Head Dynamics Due to Stick Impacts in Girls’ Lacrosse.’ *Annals of Biomedical Engineering* 42(12):2501–11. doi: 10.1007/s10439-014-1091-8.

Mow, Van C., S. C. Kuei, W. Michael Lai, and Cecil G. Armstrong. 1980. ‘Biphasic Creep and Stress Relaxation of Articular Cartilage in Compression: Theory and Experiments’. *Journal of Biomechanical Engineering* 102(1):73–84.

Muhr, A. H. 2005. ‘Modeling the Stress-Strain Behavior of Rubber’. *Rubber Chemistry and Technology* 78(3):391–425. doi: 10.5254/1.3547890.

Nguyen, Rita, Kirsten M. Fiest, Jane McChesney, Churl-Su Kwon, Nathalie Jette, Alexandra D. Frolkis, Callie Atta, Sarah Mah, Harinder Dhaliwal, Aylin Reid, Tamara Pringsheim, Jonathan Dykeman, and Clare Gallagher. 2016. ‘The International Incidence of Traumatic Brain Injury: A Systematic Review and Meta-Analysis’. *Canadian Journal of Neurological Sciences / Journal Canadien Des Sciences Neurologiques* 43(6):774–85. doi: DOI: 10.1017/cjn.2016.290.

Nicolle, S, M. Lounis, and R. Willinger. 2004. ‘Shear Properties of Brain Tissue over a Frequency Range Relevant for Automotive Impact Situations: New Experimental Results’. *Stapp car crash journal* 48:239–58.

Nicolle, Stéphane, Mourad Lounis, and Rémy Willinger. 2004. ‘Shear Properties of Brain Tissue over a Frequency Range Relevant for Automotive Impact Situations: New Experimental Results’. *SAE Technical Papers* 2004-Novem(November):239–58. doi: 10.4271/2004-22-0011.

Ning, Xinguo, Qiliang Zhu, Yoram Lanir, and Susan S. Margulies. 2006. ‘A Transversely Isotropic Viscoelastic Constitutive Equation for Brainstem Undergoing Finite

Deformation.' *Journal of Biomechanical Engineering* 128(6):925–33. doi: 10.1115/1.2354208.

Ogden, Raymond W. 1997. *Non-Linear Elastic Deformations*. Courier Corporation.

Ohman, Caroline, Massimiliano Baleani, and Marco Viceconti. 2009. 'Repeatability of Experimental Procedures to Determine Mechanical Behaviour of Ligaments.' *Acta of Bioengineering and Biomechanics* 11(1):19–23.

O'Leary, S. A., B. J. Doyle, and T. M. McGloughlin. 2014. 'The Impact of Long Term Freezing on the Mechanical Properties of Porcine Aortic Tissue'. *Journal of the Mechanical Behavior of Biomedical Materials* 37:165–73. doi: 10.1016/j.jmbbm.2014.04.015.

Pan, C., F. Chen, J. Zhou, X. Li, F. Zhao, and X. Zhang. 2018. 'Multiregional Viscoelastic Characterization of the Corona Radiata in the Sagittal Plane of the Porcine Brain'. *Medical & biological engineering & computing*. doi: 10.1007/s11517-018-1891-3.

Park, S. W. 2001. 'Analytical Modeling of Viscoelastic Dampers for Structural and Vibration Control'. *International Journal of Solids and Structures* 38(44):8065–92. doi: https://doi.org/10.1016/S0020-7683(01)00026-9.

Park, SW, and RA Schapery. 1999. 'Methods of Interconversion between Linear Viscoelastic Material Functions. Part I--a Numerical Method Based on Prony Series'. *International Journal of Solids and Structures* 36(11):1653–75.

Pattison, A. J., M. McGarry, J. B. Weaver, and K. D. Paulsen. 2015. 'A Dynamic Mechanical Analysis Technique for Porous Media'. *IEEE transactions on bio-medical engineering* 62(2):443–49. doi: 10.1109/TBME.2014.2357771.

Pervin, F., and W. N. W. Chen. 2011. 'Effect of Inter-Species, Gender, and Breeding on the Mechanical Behavior of Brain Tissue'. *Neuroimage* 54 Suppl 1:S98-102. doi: 10.1016/j.neuroimage.2010.03.077.

Pervin, F., and W. W. Chen. 2009. 'Dynamic Mechanical Response of Bovine Gray Matter and White Matter Brain Tissues under Compression'. *Journal of Biomechanics* 42(6):731–35. doi: 10.1016/j.jbiomech.2009.01.023.

Pfister, B. J., T. P. Weihs, M. Betenbaugh, and G. Bao. 2003. 'An in Vitro Uniaxial Stretch Model for Axonal Injury'. *Annals of Biomedical Engineering* 31(5):589–98. doi: 10.1114/1.15666445.

Prange, M. T., and S. S. Margulies. 2002. 'Regional, Directional, and Age-Dependent Properties of the Brain Undergoing Large Deformation'. *Journal of Biomechanical Engineering-Transactions of the Asme* 124(2):244–52. doi: 10.1115/1.1449907.

Prange, M. T., D. F. Meaney, and S. S. Margulies. 2000. 'Defining Brain Mechanical Properties: Effects of Region, Direction, and Species'. *Stapp car crash journal* 44:205–13.

Provenzano, Paolo, Roderic Lakes, Thomas Keenan, and Ray vanderby. 2001. 'Nonlinear Ligament Viscoelasticity'. *Annals of Biomedical Engineering* 29(10):908–14. doi: 10.1114/1.1408926.

Qian, L., H. Zhao, Y. Guo, Y. Li, M. Zhou, L. Yang, Z. Wang, and Y. Sun. 2018. 'Influence of Strain Rate on Indentation Response of Porcine Brain'. *Journal of the Mechanical Behavior of Biomedical Materials* 82:210–17. doi: 10.1016/j.jmbbm.2018.03.031.

Rashid, B, M. Destrade, and M. D. Gilchrist. 2012. 'Mechanical Characterization of Brain Tissue in Compression at Dynamic Strain Rates'. *Journal of the Mechanical Behavior of Biomedical Materials* 10:23–38. doi: 10.1016/j.jmbbm.2012.01.022.

Rashid, B., M. Destrade, and M. D. Gilchrist. 2014. 'Mechanical Characterization of Brain Tissue in Tension at Dynamic Strain Rates'. *Journal of the Mechanical Behavior of Biomedical Materials* 33:43–54. doi: 10.1016/j.jmbbm.2012.07.015.

Rashid, Badar, Michel Destrade, and Michael D. Gilchrist. 2012. 'Temperature Effects on Brain Tissue in Compression'. *Journal of the Mechanical Behavior of Biomedical Materials* 14:113–18. doi: https://doi.org/10.1016/j.jmbbm.2012.04.005.

Rashid, Badar, Michel Destrade, and Michael D. Gilchrist. 2013. 'Mechanical Characterization of Brain Tissue in Simple Shear at Dynamic Strain Rates'. *Journal of the Mechanical Behavior of Biomedical Materials* 28:71–85. doi: https://doi.org/10.1016/j.jmbbm.2013.07.017.

Rodriguez, Sara Russell, Sue Mallonee, Pam Archer, and Jeffery Gofton. 2006. 'Evaluation of Death Certificate-Based Surveillance for Traumatic Brain Injury—Oklahoma 2002'. *Public Health Reports* 121(3):282–89.

Sahoo, D., C. Deck, and R. Willinger. 2014. 'Development and Validation of an Advanced Anisotropic Visco-Hyperelastic Human Brain FE Model'. *Journal of the Mechanical Behavior of Biomedical Materials* 33:24–42. doi: 10.1016/j.jmbbm.2013.08.022.

Sahoo, D., C. Robbe, C. Deck, F. Meyer, A. Papy, and R. Willinger. 2016. 'Head Injury

Assessment of Non-Lethal Projectile Impacts: A Combined Experimental/Computational Method'. *Injury-International Journal of the Care of the Injured* 47(11):2424–41. doi: 10.1016/j.injury.2016.09.004.

Samadi-Dooki, A., G. Z. Voyiadjis, and R. W. Stout. 2018. 'A Combined Experimental, Modeling, and Computational Approach to Interpret the Viscoelastic Response of the White Matter Brain Tissue during Indentation'. *Journal of the Mechanical Behavior of Biomedical Materials* 77:24–33. doi: 10.1016/j.jmbbm.2017.08.037.

Schapery, Richard Allan. 1962. 'A Simple Collocation Method for Fitting Viscoelastic Models to Experimental Data'.

Shaw, Nigel A. 2002. 'The Neurophysiology of Concussion'. *Progress in Neurobiology* 67(4):281–344. doi: https://doi.org/10.1016/S0301-0082(02)00018-7.

Shepherd, D. E. T., B. B. Seedhom, and R. W. Mann. 1999. 'A Technique for Measuring the Compressive Modulus of Articular Cartilage under Physiological Loading Rates with Preliminary Results'. *Proceedings of the Institution of Mechanical Engineers Part H-Journal of Engineering in Medicine* 213(H3):291–92.

Shetye, Snehal S., Kevin L. Troyer, Femke Streijger, Jae H. T. Lee, Brian K. Kwon, Peter A. Cripton, and Christian M. Puttlitz. 2014. 'Nonlinear Viscoelastic Characterization of the Porcine Spinal Cord'. *Acta Biomaterialia* 10(2):792–97. doi: https://doi.org/10.1016/j.actbio.2013.10.038.

Singh, Dilaver, and Duane Cronin. 2019. 'Multi-Scale Modeling of Head Kinematics and Brain Tissue Response to Blast Exposure'. *Annals of Biomedical Engineering* 47(9):1993–2004. doi: 10.1007/s10439-018-02193-x.

Smith, Douglas H., and David F. Meaney. 2000. 'Axonal Damage in Traumatic Brain Injury'. *The Neuroscientist* 6(6):483–95.

Szarko, M., K. Muldrew, and J. E. A. Bertram. 2010. 'Freeze-Thaw Treatment Effects on the Dynamic Mechanical Properties of Articular Cartilage'. *Bmc Musculoskeletal Disorders* 11. doi: Artn 23110.1186/1471-2474-11-231.

Takhounts, E. G., J. R. Crandall, and K. Darvish. 2003. 'On the Importance of Nonlinearity of Brain Tissue under Large Deformations'. *Stapp car crash journal* 47:79–92.

Tamura, Atsutaka, Sadayuki Hayashi, Isao Watanabe, Kazuaki Nagayama, and Takeo Matsumoto. 2007. 'Mechanical Characterization of Brain Tissue in High-Rate

Compression'. *Journal of Biomechanical Science and Engineering* 2(3):115–26. doi: 10.1299/jbse.2.115.

Taylor, C A, J. M. Bell, M. J. Breiding, and L. K. Xu. 2017. 'Traumatic Brain Injury-Related Emergency Department Visits, Hospitalizations, and Deaths - United States, 2007 and 2013'. *Mmwr Surveillance Summaries* 66(9):1–18.

Taylor, Christopher A, Jeneita M. Bell, Matthew J. Breiding, and Likang Xu. 2017. 'Traumatic Brain Injury-Related Emergency Department Visits, Hospitalizations, and Deaths - United States, 2007 and 2013.' *Morbidity and Mortality Weekly Report. Surveillance Summaries (Washington, D.C. : 2002)* 66(9):1–16. doi: 10.15585/mmwr.ss6609a1.

Thibault, Lawrence E., Thomas A. Gennarelli, Susan S. Margulies, Jeffrey Marcus, and Rolf Eppinger. 1990. 'The Strain Dependent Pathophysiological Consequences of Inertial Loading on Central Nervous System Tissue'. in *International Conference on the Biomechanics of Impacts, Bron*.

Tian, Xiao-ge, Liang-jun Liu, Fa-mei Yu, and Lin He. 2015. 'Relaxation Modulus Model of Aged Asphalt Mixture'. *Journal of Highway and Transportation Research and Development (English Edition)* 9(3):1–6. doi: 10.1061/JHTRCQ.0000449.

Townsend, Molly T., Eren Alay, Maciej Skotak, and Namas Chandra. 2019. 'Effect of Tissue Material Properties in Blast Loading: Coupled Experimentation and Finite Element Simulation'. *Annals of Biomedical Engineering* 47(9):2019–32. doi: 10.1007/s10439-018-02178-w.

Tschoegl, Nicholas W. 2012. *The Phenomenological Theory of Linear Viscoelastic Behavior: An Introduction*. Springer Science & Business Media.

Unnikrishnan, Ginu, Haojie Mao, Aravind Sundaramurthy, E. David Bell, Stewart Yeoh, Kenneth Monson, and Jaques Reifman. 2019. 'A 3-D Rat Brain Model for Blast-Wave Exposure: Effects of Brain Vasculature and Material Properties'. *Annals of Biomedical Engineering* 47(9):2033–44. doi: 10.1007/s10439-019-02277-2.

Velardi, F., F. Fraternali, and M. Angelillo. 2006. 'Anisotropic Constitutive Equations and Experimental Tensile Behavior of Brain Tissue'. *Biomechanics and Modeling in Mechanobiology* 5(1):53–61. doi: 10.1007/s10237-005-0007-9.

Vicente, Naoki Sasaki ED1-Juan de. 2012. 'Viscoelastic Properties of Biological Materials'. P. Ch. 5 in. Rijeka: IntechOpen.

Vogel, Edward W., Matthew B. Panzer, Fatima N. Morales, Nevin Varghese, Cameron R. Bass, David F. Meaney, and Barclay Morrison. 2020. 'Direct Observation of Low Strain, High Rate Deformation of Cultured Brain Tissue During Primary Blast'. *Annals of Biomedical Engineering* 48(4):1196–1206. doi: 10.1007/s10439-019-02437-4.

Wang, R. Z., and M. Sarntinoranont. 2019. 'Biphasic Analysis of Rat Brain Slices under Creep Indentation Shows Nonlinear Tension-Compression Behavior'. *Journal of the Mechanical Behavior of Biomedical Materials* 89:1–8.

Weickenmeier, J., M. Kurt, E. Ozkaya, M. Wintermark, K. B. Pauly, and E. Kuhl. 2018. 'Magnetic Resonance Elastography of the Brain: A Comparison between Pigs and Humans'. *Journal of the Mechanical Behavior of Biomedical Materials* 77:702–10. doi: 10.1016/j.jmbbm.2017.08.029.

Weickenmeier, J., P. Saez, C. A. M. Butler, P. G. Young, A. Goriely, and E. Kuhl. 2017. 'Bulging Brains'. *Journal of Elasticity* 129(1):197–212. doi: 10.1007/s10659-016-9606-1.

Wex, C., A. Stoll, M. Frohlich, S. Arndt, and H. Lippert. 2014. 'Mechanics of Fresh, Frozen-Thawed and Heated Porcine Liver Tissue'. *International Journal of Hyperthermia* 30(4):271–83. doi: 10.3109/02656736.2014.924161.

Wilcox, A. G., K. G. Buchan, and D. M. Espino. 2014. 'Frequency and Diameter Dependent Viscoelastic Properties of Mitral Valve Chordae Tendineae'. *Journal of the Mechanical Behavior of Biomedical Materials* 30:186–95. doi: 10.1016/j.jmbbm.2013.11.013.

Woo, S. L. Y., C. A. Orlando, J. F. Camp, and W. H. Akeson. 1986. 'Effects of Postmortem Storage by Freezing on Ligament Tensile Behavior'. *Journal of Biomechanics* 19(5):399–404. doi: Doi 10.1016/0021-9290(86)90016-3.

Wu, John Z., Christopher S. Pan, Bryan M. Wimer, and Charles L. Rosen. 2017. 'Finite Element Simulations of the Head-Brain Responses to the Top Impacts of a Construction Helmet: Effects of the Neck and Body Mass'. *Proceedings of the Institution of Mechanical Engineers. Part H, Journal of Engineering in Medicine* 231(1):58–68. doi: 10.1177/0954411916678017.

Wu, Taotao, Ahmed Alshareef, J. Sebastian Giudice, and Matthew B. Panzer. 2019. 'Explicit Modeling of White Matter Axonal Fiber Tracts in a Finite Element Brain Model'. *Annals of Biomedical Engineering* 47(9):1908–22. doi: 10.1007/s10439-019-02239-8.

Young, Leanne, Gregory T. Rule, Robert T. Bocchieri, Timothy J. Walilko, Jennie M. Burns, and Geoffrey Ling. 2015. 'When Physics Meets Biology: Low and High-Velocity

Penetration, Blunt Impact, and Blast Injuries to the Brain.' *Frontiers in Neurology* 6:89. doi: 10.3389/fneur.2015.00089.

Zeltmann, Steven Eric, B. R. Bharath Kumar, Mrityunjay Doddamani, and Nikhil Gupta. 2016. 'Prediction of Strain Rate Sensitivity of High Density Polyethylene Using Integral Transform of Dynamic Mechanical Analysis Data'. *Polymer* 101:1–6. doi: https://doi.org/10.1016/j.polymer.2016.08.053.

Zhang, Ling, William J. Jackson, and Sarah A. Bentil. 2019. 'The Mechanical Behavior of Brain Surrogates Manufactured from Silicone Elastomers'. *Journal of the Mechanical Behavior of Biomedical Materials* 95(April):180–90. doi: 10.1016/j.jmbbm.2019.04.005.

Zhang, Weiguang, Bingyan Cui, Xingyu Gu, and Qiao Dong. 2018. 'Comparison of Relaxation Modulus Converted from Frequency- and Time-Dependent Viscoelastic Functions through Numerical Methods'. *Applied Sciences (Switzerland)* 8(12). doi: 10.3390/app8122447.

Zou, H., and J. P. Schmiedeler. 2008. 'Predicting Brain Injury under Impact with a Strain Measure from Analytical Models'. *International Journal of Crashworthiness* 13(3):337–48. doi: 10.1080/13588260801943047.

Zupančič, Barbara. 2018. 'Application of the Time-Strain Superposition – Part II: Prediction of the Frequency-Dependent Behaviour of Brain Tissue'. *Journal of the Mechanical Behavior of Biomedical Materials* 86:325–35. doi: 10.1016/j.jmbbm.2018.07.007.